Antifungal and Antiparasitic Activity of Novel Metallocene-containing Fluconazole Derivatives

Yan Lin,[a] Gonzalo Scalese,[b] Christina A Bulman,[c] Robin Vinck,[a] Olivier Blacque,[d] Margot Paulino,[e] Andres Ballesteros-Casallas,[e] Leticia Pérez Díaz,[f] Gustavo Salinas,[g,h] Makedonka Mitreva,[i,*] Tobias Weil,[j,*] Kevin Cariou,[a,*] Judy A. Sakanari,[c,*] Dinorah Gambino,[b,*] and Gilles Gasser[a,*]

a) Chimie ParisTech, PSL University, CNRS, Institute of Chemistry for Life and Health Sciences, Laboratory for Inorganic Chemical Biology, 75005 Paris, France. WWW: www.gassergroup.com.
b) Área Química Inorgánica, Facultad de Química, Universidad de la República, 11800 Montevideo, Uruguay.
c) University of California, San Francisco, Department of Pharmaceutical Chemistry, San Francisco, CA 94158, USA.
d) Department of Chemistry, University of Zurich, Winterthurerstrasse 190, 8057 Zurich, Switzerland.
e) Área Bioinformática, Departamento DETEMA, Facultad de Química, Universidad de la República, 11600 Montevideo, Uruguay.
f) Sección Genómica Funcional, Facultad de Ciencias, Universidad de la República, 11400 Montevideo , Uruguay
g) Worm Biology Lab, Institut Pasteur de Montevideo, 11400 Montevideo, Uruguay.
h) Departamento de Biociencias, Facultad de Química, Universidad de la República, 11800 Montevideo, Uruguay.
i) Department of Medicine, Washington University School of Medicine, St. Louis, MO 63108, USA.
j) Research and Innovation Centre, Fondazione Edmund Mach Via E. Mach 1, 38010 San Michele all'Adige, Italy.

*Corresponding Authors:

Email: mmitreva@wustl.edu; tobias.weil@fmach.it; kevin.cariou@chimieparistech.psl.eu; judy.sakanari@ucsf.edu; dgambino@fq.edu.uy; gilles.gasser@chimieparistech.psl.eu.

Keywords: Antifungal Agents; Bioorganometallic Chemistry; Fluconazole; Metals in Medicine; Chagas disease; Parasitic helminths; Neglected Tropical Diseases (NTDs).

Abstract

The search for new anti-infectives based on metal complexes is gaining momentum. Among the different options taken by researchers, the one involving the use of organometallic complexes is probably the most successful one with a compound, namely ferroquine, already in clinical trial against malaria. In this study, we describe the preparation and in-depth characterization of 10 new (organometallic) derivatives of the approved antifungal drug fluconazole. Our rationale is that the sterol 14α-demethylase is an enzyme part of the ergosterol biosynthesis route in *Trypanosoma* and is similar to the one in pathogenic fungi. To demonstrate our postulate, docking experiments to assess the binding of our compounds with the enzyme were also performed. Our compounds were then tested on a range of fungal strains and parasitic organisms, including the protozoan parasite *Trypanosoma cruzi* (*T. cruzi*) responsible for Chagas disease, an endemic disease in Latin America and ranked as the third most prevalent parasitic disease after malaria and schistosomiasis. Of high interest, the most two potent compounds of the study on *T. cruzi* that contain a ferrocene or cobaltocenium were found to be harmless for an invertebrate animal model, namely *Caenorhabditis elegans* (*C. elegans*), without affecting motility, viability or development.

Introduction

Chagas disease, caused by protozoan parasite *Trypanosoma cruzi* (*T. cruzi*), is endemic in Latin America and ranked as the third most prevalent parasitic disease after malaria and schistosomiasis. It spread to non-endemic regions due to population mobility, urbanization and emigration, and currently affects 7 million people worldwide with 10,000 annual deaths.[1,2] *T. cruzi* is principally transmitted through the feces of triatomine bugs (commonly known as kissing bugs) at the site of the bite or mucous membranes. Alternative transmission routes include blood transfusion, congenital transmission, organ transplantation, laboratory accidents and less commonly orally through contaminated food.[3] The life cycle of *T. cruzi* is complex with distinct morphological and functional forms passing through triatomine vectors and mammalian hosts. Non-replicative blood stream trypomastigotes and replicative intracellular amastigotes are the typical forms of the organism in mammalian hosts, whereas replicative epimastigotes and infective metacyclic trypomastigotes are identified in the triatomine vector.[4] Triatomine vector ingests circulating trypomastigotes in a blood meal from an infected mammalian host. They transform into epimastigotes in the digestive tract of the vector and then differentiate into metacyclic trypomastigotes at the end of the intestine, which are excreted with the feces of the vector. Metacyclic trypomastigotes are deposited into the mammalian host through the bite wound or mucous membranes. After invading mammalian host cells, trypomastigotes differentiate into the intracellular amastigote form that replicate by binary fission before re-differentiating into trypomastigotes. Trypomastigotes are released upon cell lysis into the circulation, then infect other host cells or are transmitted to the insects during their blood meal, restarting the life cycle.[5] Current available chemotherapy for Chagas disease is limited to two old drugs, nifurtimox and benznidazole (**Figure 1**), which were discovered more than 50 years ago. These compounds are effective during the acute phase of the disease but their effectiveness in the chronic phase is unsatisfactory. Additionally, several adverse effects ranging from digestive manifestations to neurological disturbances and high resistance levels have been associated to long-term treatments with these drugs. In the last two decades, drug discovery of new drugs for Chagas disease has been a major challenge for researchers. Despite many natural and synthetic compounds that have been assayed against *T. cruzi*, only allopurinol (mainly used to prevent gout) and a few sterol biosynthesis inhibitors (SBI´s) have advanced to clinical trial.[6,7] The sterol 14α-demethylase is an enzyme part of the ergosterol biosynthesis route in *Trypanosoma* and is similar to the one in pathogenic fungi. Antifungal azole agents such as imidazoles (ketoconazole) and triazoles

(itraconazole, posaconazole and ravuconazole), were therefore seemingly the most promising repurposed drugs for inhibiting the growth of trypanosomes.[8–11] However, currently available SBIs, such as ketoconazole and itraconazole, are not potent enough to eradicate the parasite from human patients or experimentally infected animals.[12–14]

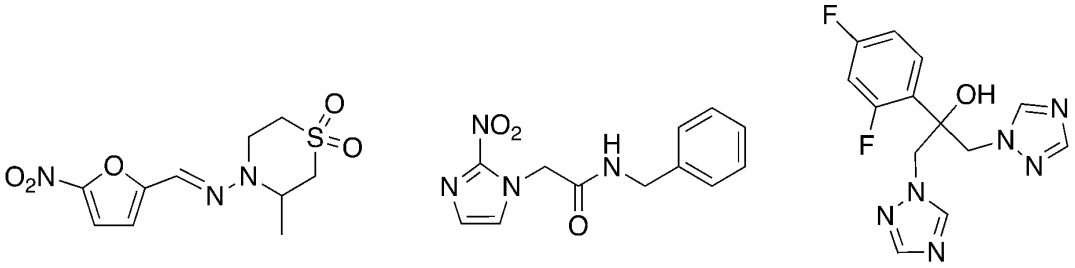

Figure 1. Structures of Nifurtimox, Benznidazole, and Fluconazole.

Fluconazole (**Figure 1**) is a first-generation triazole, which is extensively used in the treatment of various superficial and systemic fungal infections. Its half-life is longer than other second- and third- generation triazoles and its bioavailability is superior to them as well.[15] The spectrum of antifungal activities includes most *Candida* species (e.g., *C. albicans*, *C. parapsilosis*, and *C. tropicalis*), *Cryptococcus neoformans*, and dermatophytes. However, *Candida krusei*, hyphomycetes, and *Aspergillus* species are intrinsically resistant to fluconazole.[16,17] On the other hand, widespread drug exposure in prophylaxis and long-term therapy have given rise to acquired drug resistance in some species, e.g. *Candida glabrata*.[18] The increasing number of drug resistance and clinical failure treatment clearly states the urgent need for new and effective drugs. Interestingly, it was recently demonstrated by some of us that organometallic derivatives of fluconazole were highly potent *in vitro* against the parasitic nematodes, *Brugia pahangi* and *Trichuris muris*. Although these parasites do not possess 14α-demethylase, the derivatives were effective in reducing the reproductive output and fecundity of *B. pahangi in vivo* and hold much promise as novel anthelmintics to treat human diseases.[19]

Organometallic compounds such as metallocene, metal-carbene, and metal-carbonyl have recently been found to be alternative chemotherapeutic agents due to their specific and unique physicochemical properties.[20–31] The most two famous examples were ferrocenyl derivatives of known organic drugs, the antimalarial drug chloroquine and the anticancer drug tamoxifen, namely ferroquine and ferrocifen, which were reported by the Biot and Jaouen's group, respectively.[32,33] In both examples, the incorporation of the ferrocenyl moiety into the organic drug led to superior activities compared to their

parent drugs. The additional activities was shown to be caused, among others, by the generation of reactive oxygen species via the reversible ferrocene/ferrocenium redox couple.[34] In this article, we use a similar strategy replacing one of the two identical triazoles in fluconazole by metallocenyl moieties (ferrocene (Fc), ruthenocene (Rc), cobaltocenium (Cc)) aiming to improve its bioactivities as antifungal and antiparasitic agents (**Figure 2**). The remarkable physicochemical properties of ferrocene (e.g., not-toxic, stable, robust, lipophilic, and redox reversible) are no doubtful made it the most popular substitutes in medicinal organometallic chemistry.[25] In contrast to the well-developed ferrocene-containing bioactive molecules, the incorporation of the isoelectronic cobaltocenium into known drugs has only been explored to a much lesser extent.[35] Cobaltocenium is a stable, 18-electron cationic structure that can undergo a reversible monoelectronic reduction to yield the uncharged 19-electron cobaltocene, which also acts as internal reference redox couple as ferrocene/ferrocenium.[36,37] In contrast to ferrocenyl donor substituents, cobaltocenium acceptor substituents possess opposite electronic properties due to its cationic charge and reversible cobaltocenium/cobaltocene redox couple. Furthermore, the intrinsically positive charged structure of cobaltocenium is highly soluble in polar solvents, e.g., water, leading to desirable drug delivery for targeting to cells, tissues, and selected organs.[38] Additionally, we prepared ruthenocene (Rc), adamantane (Am), and benzene (Ph) analogs to help us further understand the effect of the metallocene moiety. Ruthenocene is isoelectronic to ferrocene, and they have very similar geometry and steric demand, yet Rc displays vastly different redox properties than Fc.[39] Adamantane, due to its three-dimensional structure, is worth investigating in this setting, as a fully organic non-aromatic bulky 3D moiety. It was shown in the past to have excellent activity when used as a surrogate for ferrocene/ruthenocene.[40] In comparison, a phenyl group is aromatic but lacks the third-dimensionality of adamantane.

In this work, we present the synthesis and complete characterization of ten new (organometallic) fluconazole derivatives (**Figure 2**) and their in-depth biological activity on a range of fungal strains and parasitic organisms. Of note, toxicity studies on *Caenorhabditis elegans (C. elegans)* and docking experiments to assess the binding of our compounds with 14α-demethylase were also performed.

This work:

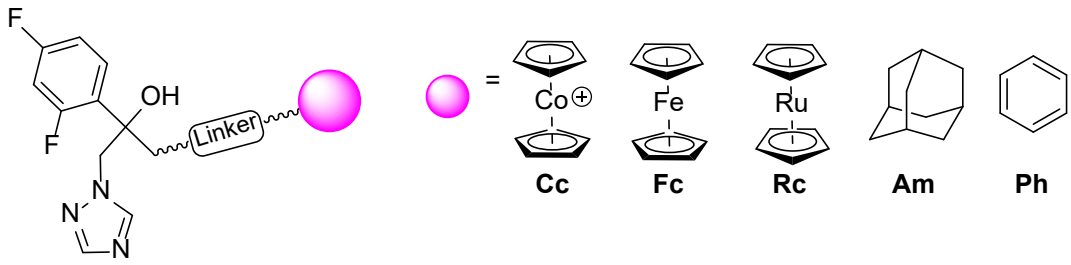

Fluconazole derivatives Linker: 1,2,3-triazole or amide

Figure 2. Schematic representation of the compounds synthesized in this study.

Results and Discussion

Synthesis and characterization

Two synthetic approaches were applied to synthesize FCZ analogues depending on the linker, 1,2,3-triazole or amide, between the organometallic group and the FCZ core. (**Scheme 1**) Triazoles can be viewed as bioisostere of various groups, most prominently amides.[41,42] It was thus interesting to synthesize FCZ analogues through two powerful ligation methods and investigate the roles of these linkers. Of note, in order to obtain initial insights into their biological activity, we synthesized these FCZ analogues as racemic mixtures to avoid any tedious asymmetric synthesis.[43] In the first strategy, fluconazole derivatives (**A1**-**5**) were prepared by convenient synthetic methodologies of copper-catalyzed azide-alkyne cycloaddition (CuAAC) reaction, active Cu(I) species were generated *in situ* by reduction of $CuSO_4$ with 2 folds sodium ascorbate in degassed THF/H_2O (3:2) mixture (**Scheme 1A**).[44] 1,4-disubstitutied 1,2,3-triazole were obtained upon cycloaddition of azide **SS1** with a set ofterminal alkynes, with yield ranging from 50% to 94%. In the second strategy, compounds **B1**-**5** with amide linker were prepared by *N*-acylation of amine **SS2** (**Scheme 1B**) with various acyl chlorides. The latter can be readily obtained from thecarboxylic acids **SB1**-**5** by reaction with thionyl chloride (**SB1**) or oxalyl chloride (**SB2-5**) in dichloromethane (see Supporting Information for synthetic details). Both cobaltocenium compounds **A1** and **B1** were initially isolated as their PF_6^- salts (by recrystallization and by column chromatography on neutral aluminium oxide, respectively). **A1-PF$_6$** and **B1-PF$_6$**, were then converted to their chloride (Cl^-) salts. Several reasons were considered for this metathesis, notably solubility and potency as chlorides are generally preferable counterions for *in vivo* testing of drug candidates.[45] The ion-exchange was performed with Amberlite IRA-402 (chloride form) in methanol according to the reported literature.[46] The addition of resin induced yellowish solid to subsequently dissolve in solvent after 15 min vigorous stirring, further stirring was needed for sufficient ion exchange. The disappearance of characteristic signals around -70 ppm in the ^{19}F NMR spectrum afford evidence of complete removal of PF_6^-. All newly synthesized compounds were unambiguously characterized by ^1H, ^{13}C and ^{19}F NMR spectroscopy, HR-MS and IR, while their purities were confirmed by microanalysis. Details on synthesis and characterization of the complexes can be found in the Supporting Information.

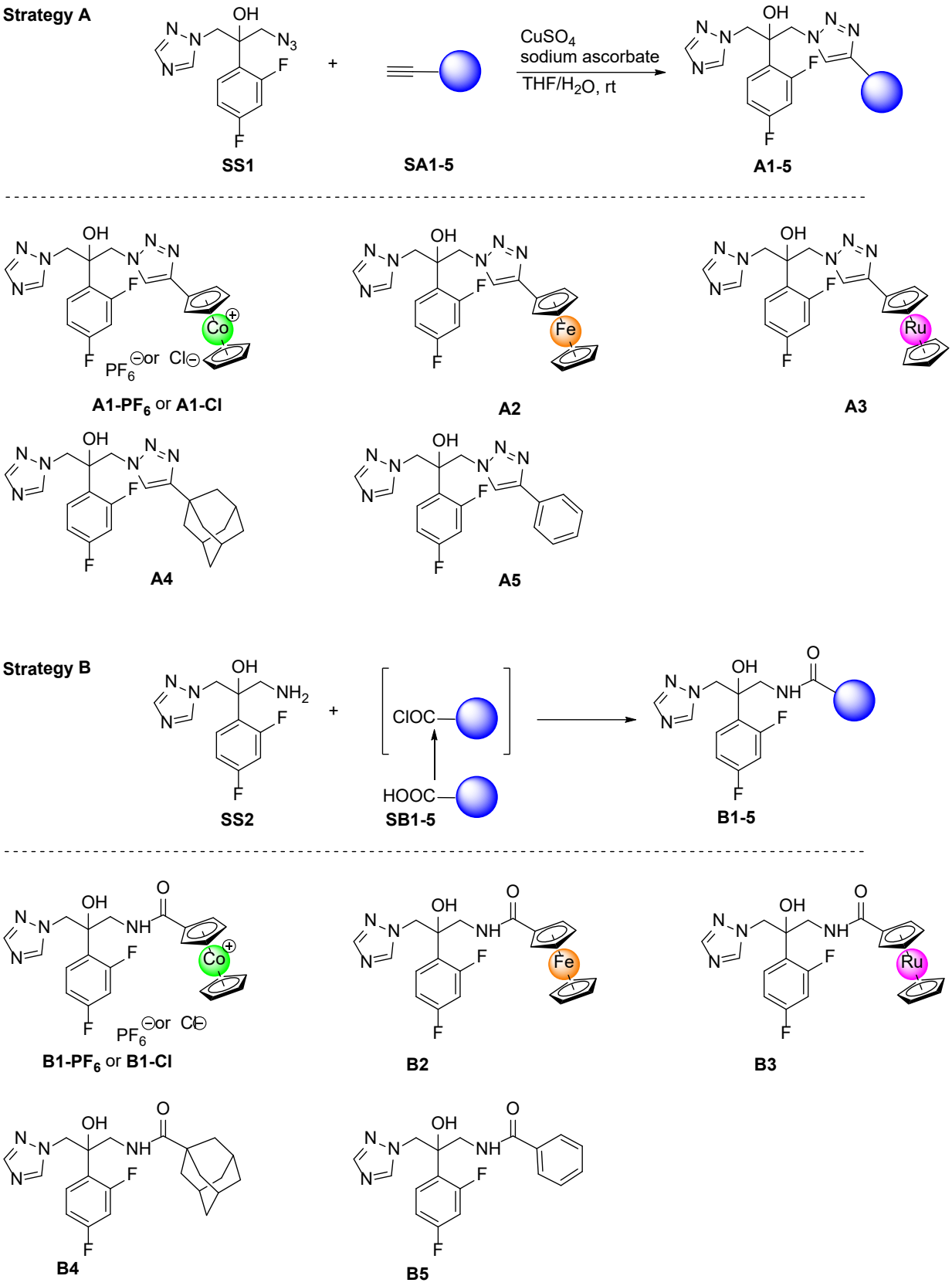

Scheme 1. **A**. Synthesis of the FCZ analogues with 1,2,3-triazole as a linker; **B**. Synthesis of the FCZ analogues with amide as a linker.

X-ray Crystallography

Single crystal structure determinations were carried out for eleven fluconazole derivatives synthesized in this study (**A1-PF$_6$**, **A1-Cl**, **A2-A5**, **B1-PF$_6$**, **B1-Cl**, and **B3-B5**, **Figure 3**). Details on the acquisition of the structures can be found in Supporting Information. In all cases, the crystal structures confirmed the identity of the complexes. The crystal structures also show that the metallocenes exhibit the standard sandwich geometry with nearly parallel cyclopentadienyl rings. Since all the complexes contain a stereogenic center, it is worth to note that the crystal structure space groups are not chiral which means that both enantiomers are present in the crystal in equal amount (racemate), except complex **A5** that crystallized in the chiral space group $P4_3$ in the (R) configuration only.

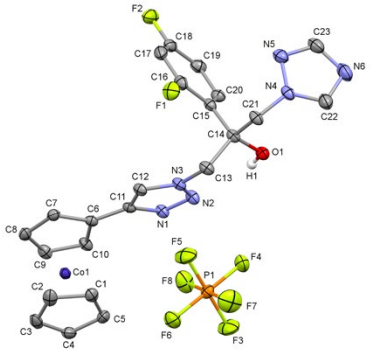

A1-PF$_6$

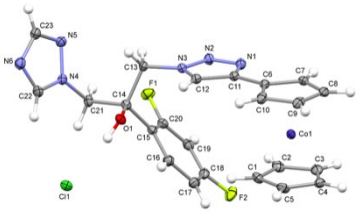

A1-Cl

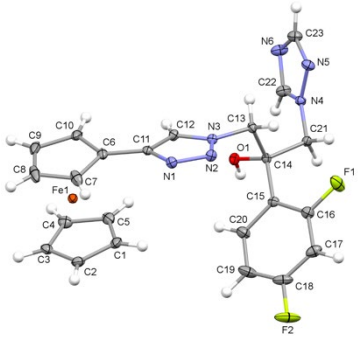

A2

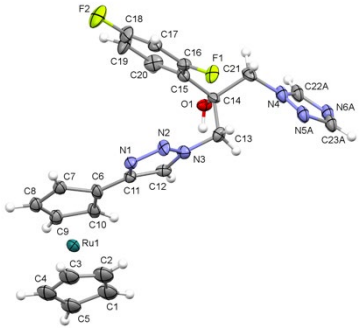

A3

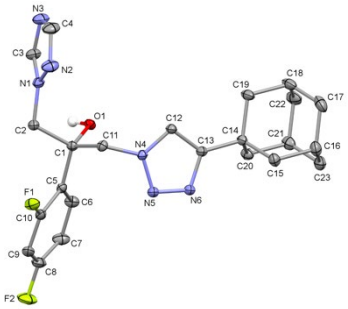

A4

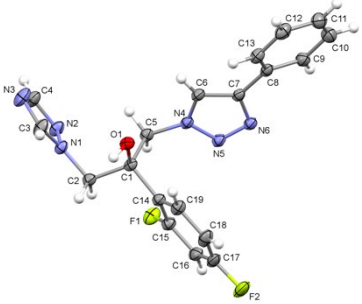

A5

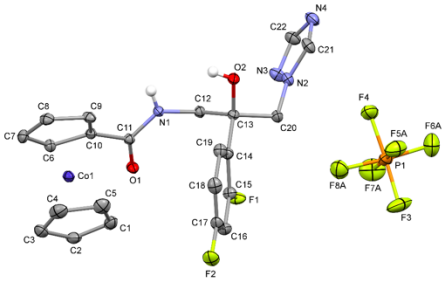

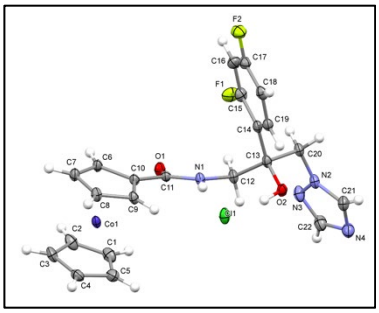

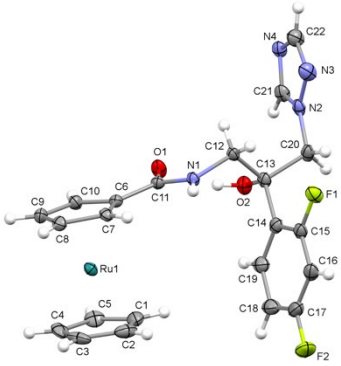

B1-PF_6 **B1-Cl** **B3**

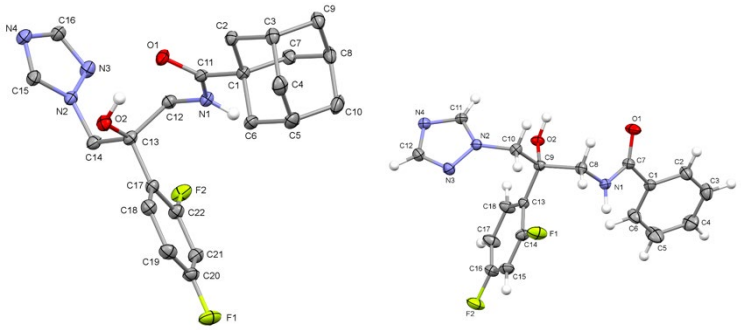

B4 **B5**

Figure 3. ORTEP drawing depicting the structures of **A1-PF6**, **A1-Cl**, **A2-A5**, **B1-PF6**, **B1-Cl**, and **B3-B5** showing displacement ellipsoids at the 30% probability level.

Stability of compounds in DMSO

DMSO is the most widely used storage solvent in bioassay due to its powerful solvating ability and low toxicity.[47] As potential drug candidates, their stability in DMSO is an important parameter needed to be investigated. We dissolved all the newly synthesized FCZ derivatives in DMSO-d_6 and monitored by ^{1}H NMR spectroscopy every 24 h. No shifted peaks or new peaks (which would be sign of some degradation of the compounds) were found for all the tested compounds over 3 days, showing that they are stable in DMSO-d_6. The NMR spectra of these studies can be found in Supporting Information Figures S9 - S32.

Cytotoxicity on VERO cells

In order to evaluate the potential cytotoxicity of the compounds, they were screened on VERO cells (ATCC CCL81) as mammalian cell model. Cell viability was assessed using the MTT (3-(4, 5-dimethylthiazolyl-2)-2, 5-diphenyltetrazolium bromide) assay, where MTT is reduced by metabolically active cells to generate reducing equivalents such as NADH and NADPH, resulting in the formation of an intracellular purple formazan whose absorbance is measured at 570 nm. The compounds showed low toxicity on the mammalian model with IC_{50} values in the range 68.5-476.4 µM and good selectivity index values (Table 1).

Toxicity on *C. elegans*

C. elegans, a nematode model organism, has been used as a simplified proxy of animal toxicity for drug discovery as well as in ecotoxicological studies since it allows acute toxicity and developmental and reproductive toxicity (DART) to be examined.[48] **A1Cl** and **A2** were selected as representative of the series of new compounds to perform this study due to their high activity, particularly against *T. cruzi* (Table 1). The results showed that compounds **A1Cl** and **A2** were harmless for this invertebrate animal model without affecting motility, viability or development. More specifically, compounds **A1Cl** and **A2** did not affect worm motility after 18 h incubation at a concentration as high as 100 µM (**Figure 4**). In contrast, the known anthelmintic ivermectin used as a positive control reduced motility to zero at 2 µM (**Figure 4**). The worms treated with compounds **A1Cl** and **A2** at 100 µM or with vehicle only were recovered from wells and seeded on NGM (nematode growth media) plates and food to assess development. Worms treated at 100 µM showed normal development (L4 - adult worm – egg - L1). In addition, development was also assessed after a 5 h incubation with 100 µM **A1Cl** and **A2** or vehicle of 100 synchronized L1 larval worms. After treatment L1 were seeded on NGM plates and food and in all cases developed from L1 to adult worms in 72 hours.

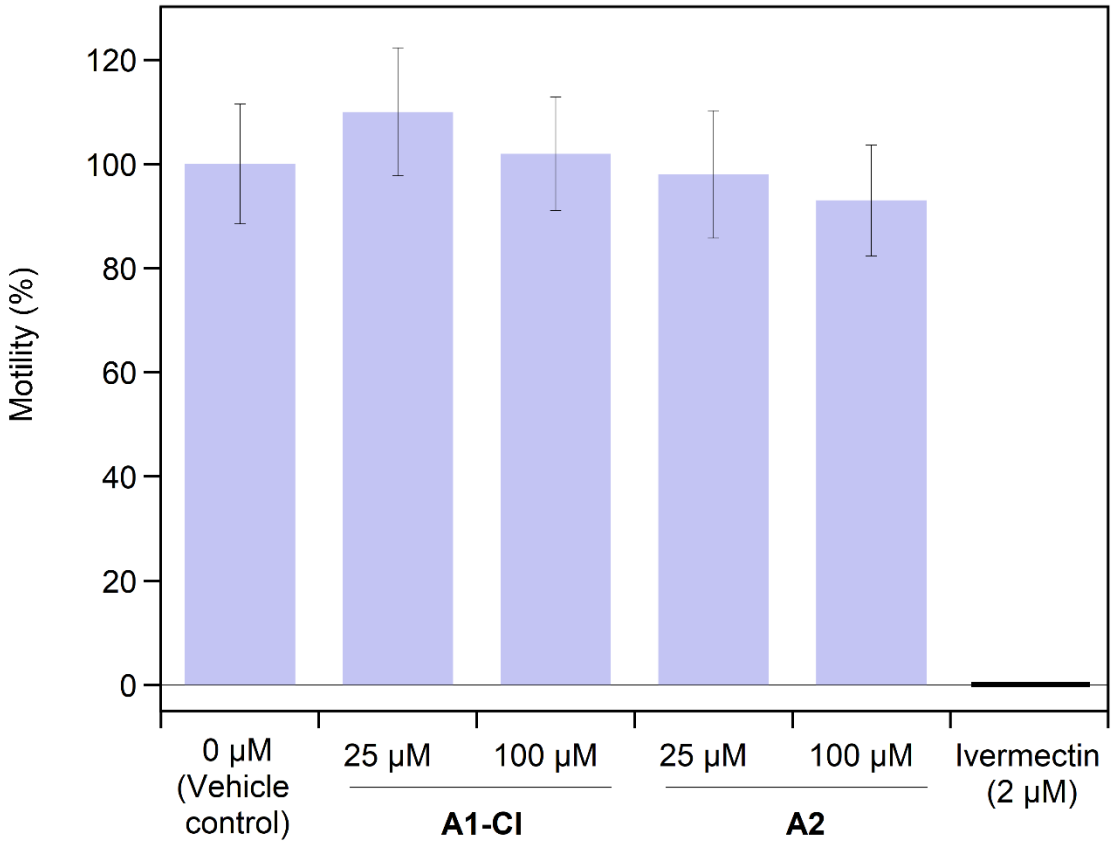

Figure 4. Effect of **A1Cl** and **A2** on *C. elegans* motility at a dose of up to 100 µM. Seventy L4 adult worms per well were incubated in M9 buffer, 1% DMSO and compounds **A2** and **A1Cl** at 25 and 100 µM concentrations. Vehicle control (without compound) was used as a reference of normal motility in 1% DMSO. Ivermectin was used as a positive control at 2 µM. In each experiment, four replicas were performed for each concentration. One representative experiment of three biological replicates is shown. Error bars correspond to standard deviations.

In vitro activity against *T. cruzi* and selectivity towards the parasites

With the compounds in hand, we then tested their activity on *T. cruzi* trypomastigotes, CL Brener strain. Freshly DMSO solutions of the compounds were diluted in culture medium to obtain the different concentrations tested. After incubation of the parasites with increasing concentrations of the compounds for 24 h, viability of the trypomastigotes was tested using alamar Blue^{TM}, where resazurin is reduced to resofurin, a compound that is red in color and highly fluorescent. Dose-response curves were recorded and the IC_{50} values were determined. Most of the compounds showed IC_{50} values in the micromolar range and lower than that of the reference antitrypanosomal drug nifurtimox and of fluconazole. In addition, they showed good selectivity towards the parasite (Selectivity index: IC_{50} VERO cells /IC_{50} *T. cruzi*) (Table 1). The ferrocene derivative **A2** and the cobaltcenium compound **A1-Cl** showed the lower IC_{50} values and the higher selectivity index values. As expected, **A1-Cl** showed higher activity than its hexafluorophosphate analogue.

Table 1. *In vitro* activity on *T. cruzi* (trypomastigotes CL Brener strain), cytotoxicity on mammalian cells (VERO cells) and selectivity towards the parasites (SI values).

Compounds	IC_{50} VERO ± SD (µM)	IC_{50} *T. cruzi* ± SD (µM)	SI[a]
A1-PF_6	194.7 ± 12.4	**7.79 ± 0.82**	**25.0**
A1-Cl	109.7 ± 12.2	**4.88 ± 0.77**	**22.5**
A2	68.5 ± 7.9	**2.47 ± 1.20**	**27.7**
A3	171.0 ± 10.5	14.4 ± 2.1	11.9
A4	> 200	> 96	ND
A5	167.1 ± 20.1	13.1 ± 1.34	12.8
B1-Cl	476.4 ± 58.7	17.6 ± 1.9	27.0
B2	> 200	92.49 ± 9.09	>2.2
B3	> 200	10.6 ± 2.7	> 18.8

B4	188.8 ± 19.7	14.8 ± 5.8	12.8
B5	160.5 ± 18.0	23.2 ± 4.3	6.9
FCZ	173.0 ± 30.2	23.6 ± 2.0	7.3
NFX	998.5 ± 90.6[b]	20.1 ± 2.86[c]	**49.6**

SI[a]: Selectivity index: IC_{50} mammalian cells /IC_{50} *T. cruzi;* [b] data from reference [2]; [c] data from reference [48]; ND: not determined.

Compounds efficacy against clinical fungal isolates

The antifungal activity of the compounds was then tested towards *Candida albicans* and non *albicans* strains (Table 2). Compounds **A5** and **B5** in particular displayed strong activities (even submicromolar for the latter) towards all but one of the investigated strains, including fluconazole-resistant (MIC_{50} FCZ >100) clinical isolates, at concentrations evaluated as safe on human embryonic kidney cells (<25 µM, see Figure 3). Compounds **B2**, **B3** and **B4** showed good antifungal properties as well, yet when compared to **B5** their activity was less pronounced against FCZ resistant *C. albicans* and *C. tropicalis* clinical isolates. Only the FCZ resistant *C. glabrata* clinical isolate was highly resistant to all tested compounds.

Table 2. MIC_{50} values on a panel of clinical *Candida* isolates (µM)

Strains	$A1_{PF6}$	A1Cl	A2	A3	A4	A5	B1Cl	B2	B3	B4	B5	FCZ
C. albicans SC5314	100	100	**32.6**	**30**	**16.5**	**5.2**	100	**2.1**	**2**	**1.2**	**0.7**	**0.8**
C. albicans MFB005.FS3	100	100	65.3	**30**	**33**	**5.2**	100	**8.6**	**7.8**	**2.4**	**1.4**	**0.4**
C. albicans YMS 102.2	100	100	100	60.1	100	**10.5**	100	100	100	**19.2**	**22.3**	100
C. parapsilosis MFB005.FS5	100	100	65.3	**30**	**16.5**	**5.2**	100	**17.2**	**7.8**	**2.4**	**0.7**	**0.4**
C. parapsilosis MFB070.N1	100	100	100	100	100	**10.5**	100	**8.6**	**7.8**	**2.4**	**0.7**	100
C. tropicalis RTT35.1	100	100	100	100	100	**10.5**	100	**17.2**	**15.6**	**38.4**	**2.8**	100
C. tropicalis RTT35.3	100	100	100	100	100	**20.9**	100	**34.3**	**15.6**	**19.2**	**2.8**	100
C. glabrata MFB005.FS4	100	100	65.3	**30**	**16.5**	**5.2**	100	**8.6**	**7.8**	**2.4**	**0.7**	**0.4**
C. glabrata RTT 199.3	100	100	100	100	100	100	100	100	100	100	100	100

Compounds efficacy against *B. pahangi* and *T. muris*

The percent inhibition of motility was determined for two species of parasitic helminths, *B. pahangi* and *T. muris in vitro* using the fluconazole analogs.[49–53] Both **A2** and **A3** were effective in inhibiting *B. pahangi* and *T. muris* worm motility by >70% using concentrations of 50 µm and 100 µM, respectively (Table 3). Compound **A4** was the most potent analog against *B. pahangi* (90% inhibition of worm motility) but it

did not affect *T. muris* worms. Since the B series were not potent against *B. pahangi*, they were not assessed further with *T. muris* since these latter worms are considerably more difficult to eliminate.

In this worm assay, **A2** was effective in causing worm death against both *Brugia* and *Trichuris* using 50 and 100 µm, respectively. Although the concentrations used in the worm assay were high (>10 µm), **A2** was not toxic to the free-living nematode, *C. elegans* in the DART assay, even at 100 µm. Results of the *C. elegans* toxicity assay showed that **A2** had no detrimental effect on the adult worms nor did it cause any developmental or reproductive toxicity which bodes well for the future development of a more potent series of derivatives against the two parasitic nematode species or other parasitic helminths.

Table 3. Percent inhibition of motility using compounds against *B. pahangi* for 6 days and *T. muris* for 3 days.

	Brugi pahangi females (50 µM)					*Trichuris muris males & females (100 µM)*			
Compounds	**Day 0**	**Day 1**	**Day 2**	**Day 3**	**Day 6**	**Day 0**	**Day 1**	**Day 2**	**Day 3**
A1-PF_6	29	20	14	14	55	30	25	28	52
A1-Cl	22	16	6	2	19	37	16	29	15
A2	13	1	0	7	**83**	21	58	**89**	**77**
A3	17	22	29	17	**73**	7	22	53	**84**
A4	13	32	40	58	**90**	0	7	4	23
A5	0	7	8	13	29	21	41	55	37
B1-Cl	0	0	0	0	0				
B2	28	27	34	34	49				
B3	2	8	8	4	52				
B4	0	0	6	7	56				
B5	0	4	6	2	17				

Computational evaluation of putative action mechanisms based on biomolecular models

Computational (*in silico*) strategies have long been recognized as excellent tools for investigating and proposing possible mechanisms of action of bioactive molecules.[50] A sequences alignment of *T. cruzi* and *H. sapiens* sterol 14α-demethylase sequences and a 3D protein alignment were performed to conjecture about the specificity of designed compounds. The study of putative binding sites of both sterol 14 α-demethylases followed by molecular docking of the *T. cruzi* enzyme and the putative ligands were carried out (see Supplementary Information for details). The analysis of the resulting docked complexes was

accomplished with graphical revision. This final step could provide the knowledge of 1) how the fluconazole derivatives bind to the biomolecule; 2) which are the main contacts that can occur in such interaction; 3) as well as an estimation of the binding energy, provided as the Score value in molecular docking.

The *T. cruzi* crystallographic structure of sterol 14-alpha-demethylase co-crystallized with fluconazole was obtained from Protein Data Bank with the id code 2WX2. After docking with the eleven molecular models of compound under study (Fluconazole, A and B series), the interaction energies resulted all with negative values, indicating attractive interaction between the compounds and the enzyme.

It is observed that the complexes (both A and B series) orient the fluconazole moiety part facing the heme moiety (Figure 5). Some less populated poses of the docking reverse the position and the heme moiety interacts with ferrocene, cobaltocene or ruthenocene, respectively, but they resulted mostly with lower scores.

As can be seen in Table S7, all derivatives resulted with improved scores with respect to the fluconazole, and presented a higher number of interactions. As an example, it could be interesting to mention the interaction of compounds A1, A2 and A3 with the residue M360, suggesting that this residue could be important to understand the effect of compounds on the 14-alpha-demethylase. The same cannot be said for the B series whose components, in addition to showing a tendency to lower scores, also show no contact with M360. An animated gif of A2 complex poses is available in Figure S100.

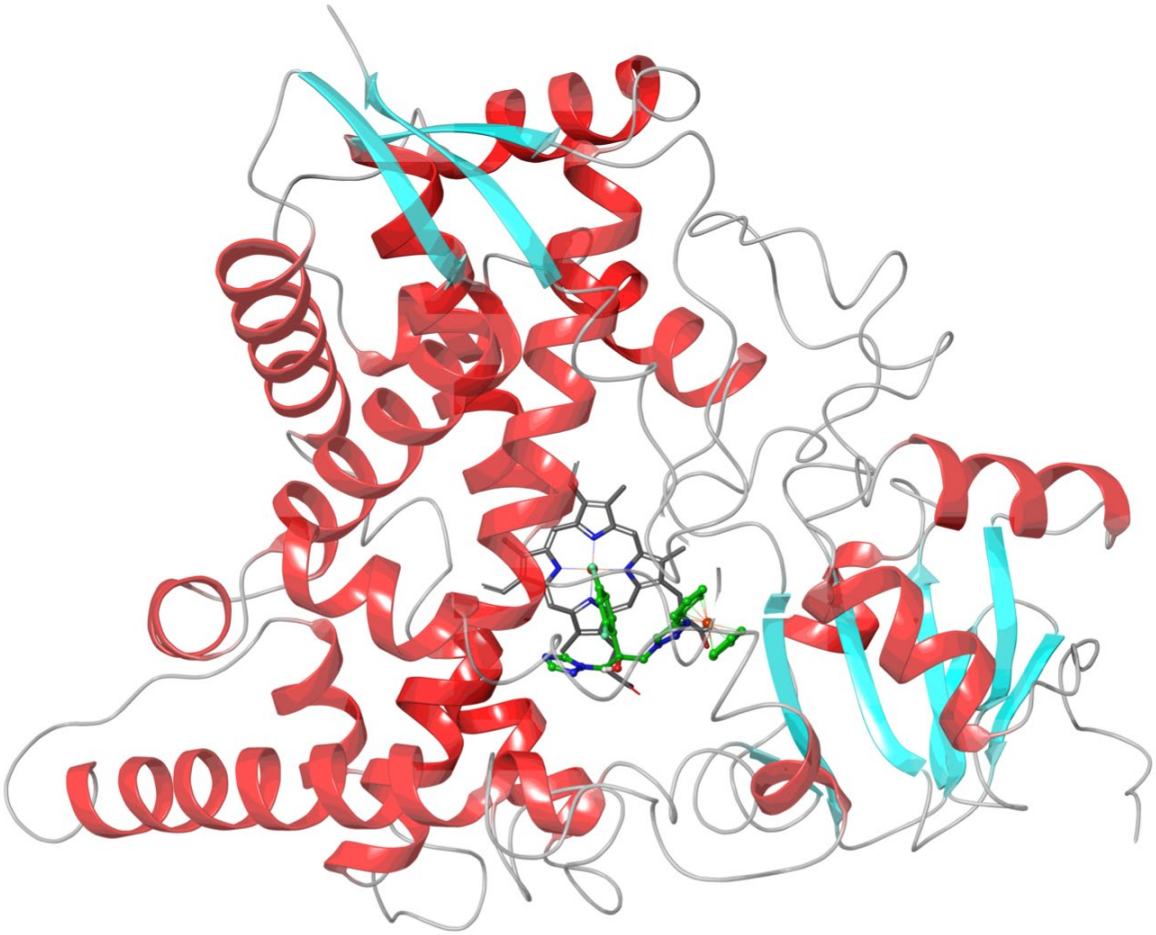

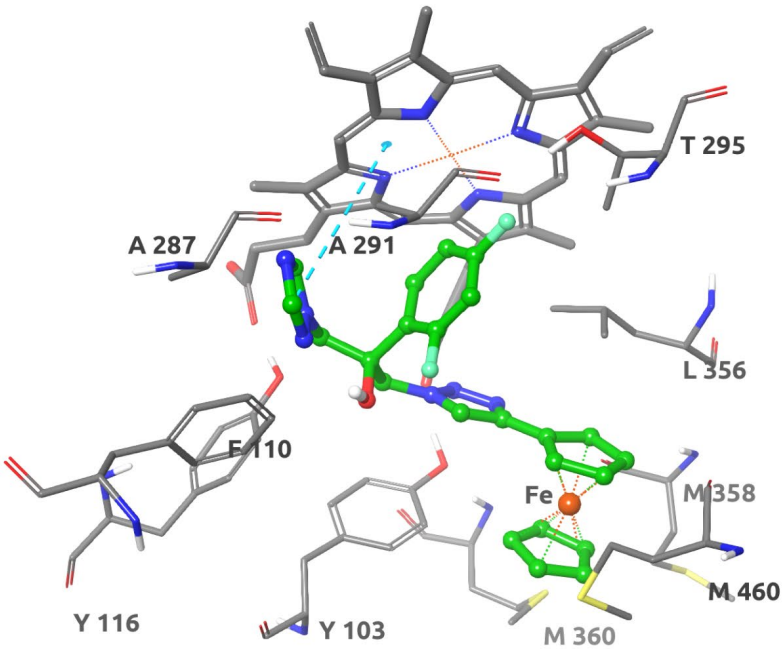

Figure 5. ***Up:*** *T. cruzi* ribbons of enzyme. HEME is atom type colored, **A2** molecule stick model is green colored. ***Bottom:*** Close-up view of complex of **A2** with CYP51 3D structure in the docked site. The **A2** is shown in green sticks. All other side chain and HEMO docked conformations are shown in stick colored in gray (carbon atoms), red (oxygen atoms or blue (nitrogen atoms). Hydrogen atoms are not shown. The interaction region is conformed by HEMO moiety and Y103, F110, Y116, A287, A291, T295, L356, M358, M360 and M460 sterol 14-alpha-demethylase residues. The fluor phenyl moiety is always oriented towards the HEMO in all best docked molecules. Beyond the clear result expressed in the anchored structures obtained, the small difference in the anchoring energies can be explained by the lack of sensitivity of the methods used in the evaluation of organometallic complexes. In that sense, this in silico work has allowed to clearly define which structures of enzyme-ligand complexes to use for further studies involving quantum mechanics (QM and QM/MM).

Conclusion

In this work, 10 new (organometallic) derivatives of the antifungal agent fluconazole were synthesized and characterized using a range of different analytical techniques, including by X-ray crystallography. Their antifungal and antiparasitic activities were then tested, revealing that the ferrocene derivative **A2** and the cobaltcenium compound **A1-Cl** had the lower IC_{50} values and the higher selectivity index values against *T. cruzi.* The toxicity of these two compounds was tested on *C. elegans*. They were found to be harmless for this invertebrate animal model without affecting motility, viability or development. Interestingly, when the series of our compounds were tested against fungal infections, other compounds than **A1-Cl** and **A2** were found to be the most active, namely compounds **A5** and **B5** that do not contain an organometallic moiety but a phenyl moiety. They displayed strong activities (even submicromolar for the latter) towards all but one of the investigated strains, including fluconazole-resistant (MIC_{50} FCZ >100) clinical isolates, at concentrations evaluated as safe on human embryonic kidney cells. Since azole derivatives were recently found to be active on two species of parasitic helminths, *B. pahangi* and *T. muris in vitro*, we also tested the activity of our compounds on these parasites. The ferrocenyl and ruthenocenyl derivatives **A2** and **A3**, respectively were found to be effective in inhibiting *B. pahangi* and *T. muris* worm motility by >70% using concentrations of 50 µm and 100 µM, respectively. Overall, this study further demonstrates that the organometallic derivatization of known antifungal drug can produce new, easy-to-synthesize compounds with high biological activity. The computational studies indicated that there is a preferred site for the compounds studied, close to the HEMO group and similar to the binding site of fluconazole. Furthermore, the binding mode of fluconazole, with its fluoromethyl group always oriented towards the HEMO group is the same adopted for all best scored conformations. Differences justifying the best obtained IC_{50} values may be associated with increased scored energies evaluated with further QM/MM studies.

Supporting Information

Synthetic pathways (Scheme S1-S8), procedures and characterization of the compounds, Selected crystal data and structure refinement parameters (Table S1-S5), NMR (Fig. S1–S73) spectra, copies of the IR (Fig. S74–S84) and Stability studies (Fig. S85-S95), Computational studies (Fig. S96-S99), the results of docking analysis (Table S7), animate version of the best docked conformation for the A2 molecule (Fig. S100).

Author Contributions: M.Mi., T.W., K.C, J.A.S., D.G. and G.G. conceived the project. Y.L. prepared and characterized the compounds. O.B. undertook the crystallographic studies. C.A.B. and H.J. performed *in vitro* experiments on *T. muris* and *B. pahangi*. R.V. undertook cytotoxic studies on non-cancerous and cancerous cells. T.W. performed *in vitro* studies on fungi. G.Sc., L.P.D. and G.Sa. performed toxicity on *C. elegans* and *T. cruzi*. M.P and A.B.-C. performed computational studies. M.Mi., T.W., K.C, J.A.S., D.G. and G.G wrote the manuscript. All authors edited the manuscript.

Acknowledgments

This work was funded by the Swiss National Science Foundation (Grant Sinergia CRSII5_173718). This work has also received support from an ERC Consolidator Grant PhotoMedMet to G.G. (GA 681679) and by the program «Investissements d'Avenir » launched by the French Government and implemented by the ANR with the reference ANR-10-IDEX-0001-02 PSL (G.G.). This research was supported by the Autonomous Province of Trento (Accordo di Programma P1611051I (M.M.), by the FOCEM (MERCOSUR Structural Convergence Fund, [COF 03/11]), by the France-Uruguay ECOS-SUD project U20E02 and by the University of California San Francisco Quantitative Biosciences Institute and Paris Sciences et Lettres University QLife grant (J.A.S. and G.G). The following reagent was provided by the NIH/NIAID Filariasis Research Reagent Resource Center for distribution through BEI Resources, NIAID, NIH: Adult Female *Brugia pahangi* (Live), NR-48903. N2 *C. elegans* and OP50 bacterial strains were kindly provided by the Caenorhabditis Genetics Center (CGC

Competing Interests: The authors declare that they have no competing interests.

Data and materials Availability: All data associated with this study are present in the paper or the Supporting Information.

References

(1) WHO. *Chagas disease (American trypanosomiasis)*. https://www.who.int/westernpacific/health-topics/chagas-disease (accessed 2022-01-02).

(2) Scalese, G.; Machado, I.; Salinas, G.; Pérez-Díaz, L.; Gambino, D. Heteroleptic Oxidovanadium(V) Complexes with Activity against Infective and Non-Infective Stages of Trypanosoma Cruzi. *Molecules* **2021**, *26* (17), 5375. https://doi.org/10.3390/molecules26175375.

(3) Field, M. C.; Horn, D.; Fairlamb, A. H.; Ferguson, M. A. J.; Gray, D. W.; Read, K. D.; De Rycker, M.; Torrie, L. S.; Wyatt, P. G.; Wyllie, S.; Gilbert, I. H. Anti-Trypanosomatid Drug Discovery: An Ongoing Challenge and a Continuing Need. *Nat Rev Microbiol* **2017**, *15* (4), 217–231. https://doi.org/10.1038/nrmicro.2016.193.

(4) Paucar, R.; Moreno-Viguri, E.; Pérez-Silanes, S. Challenges in Chagas Disease Drug Discovery: A Review. *CMC* **2016**, *23* (28), 3154–3170. https://doi.org/10.2174/0929867323999160625124424.

(5) Bern, C. Chagas' Disease. *N Engl J Med* **2015**, *373* (5), 456–466. https://doi.org/10.1056/NEJMra1410150.

(6) J, B.; M, B. M.; Chanda, K. An Overview on the Therapeutics of Neglected Infectious Diseases—Leishmaniasis and Chagas Diseases. *Front. Chem.* **2021**, *9*, 622286. https://doi.org/10.3389/fchem.2021.622286.

(7) Scarim, C. B.; Jornada, D. H.; Chelucci, R. C.; de Almeida, L.; dos Santos, J. L.; Chung, M. C. Current Advances in Drug Discovery for Chagas Disease. *European Journal of Medicinal Chemistry* **2018**, *155*, 824–838. https://doi.org/10.1016/j.ejmech.2018.06.040.

(8) Lepesheva, G. I.; Villalta, F.; Waterman, M. R. Targeting Trypanosoma Cruzi Sterol 14α-Demethylase (CYP51). In *Advances in Parasitology*; Elsevier, 2011; Vol. 75, pp 65–87. https://doi.org/10.1016/B978-0-12-385863-4.00004-6.

(9) Soeiro, M. N. C.; de Castro, S. L. *Trypanosoma Cruzi* Targets for New Chemotherapeutic Approaches. *Expert Opinion on Therapeutic Targets* **2009**, *13* (1), 105–121. https://doi.org/10.1517/14728220802623881.

(10) Lepesheva, G. I.; Zaitseva, N. G.; Nes, W. D.; Zhou, W.; Arase, M.; Liu, J.; Hill, G. C.; Waterman, M. R. CYP51 from Trypanosoma Cruzi. *Journal of Biological Chemistry* **2006**, *281* (6), 3577–3585. https://doi.org/10.1074/jbc.M510317200.

(11) Lepesheva, G. I.; Friggeri, L.; Waterman, M. R. CYP51 as Drug Targets for Fungi and Protozoan Parasites: Past, Present and Future. *Parasitology* **2018**, *145* (14), 1820–1836. https://doi.org/10.1017/S0031182018000562.

(12) Lazardi, K.; Urbina, J. A.; De Souza, W. Ultrastructural Alterations Induced by Two Ergosterol Biosynthesis Inhibitors, Ketoconazole and Terbinafine, on Epimastigotes and Amastigotes of Trypanosoma (Schizotrypanum) Cruzi. *Antimicrob Agents Chemother* **1990**, *34* (11), 2097–2105. https://doi.org/10.1128/AAC.34.11.2097.

(13) Sánchez-Delgado, R. A.; Navarro, M.; Lazardi, K.; Atencio, R.; Capparelli, M.; Vargas, F.; Urbina, J. A.; Bouillez, A.; Noels, A. F.; Masi, D. Toward a Novel Metal Based Chemotherapy against Tropical Diseases 4. Synthesis

and Characterization of New Metal-Clotrimazole Complexes and Evaluation of Their Activity against Trypanosoma Cruzi. *Inorganica Chimica Acta* **1998**, *275–276*, 528–540. https://doi.org/10.1016/S0020-1693(98)00114-5.

(14) Urbina, J. A.; Payares, G.; Molina, J.; Sanoja, C.; Liendo, A.; Lazardi, K.; Piras, M. M.; Piras, R.; Perez, N.; Wincker, P.; Ryley, J. F. Cure of Short- and Long-Term Experimental Chagas' Disease Using D0870. *Science* **1996**, *273* (5277), 969–971. https://doi.org/10.1126/science.273.5277.969.

(15) PubChem. *Fluconazole*. https://pubchem.ncbi.nlm.nih.gov/compound/3365 (accessed 2022-01-09).

(16) Graninger, W.; Diab-Elschahawi, M.; Presterl, E. Antifungal Agents. In *Clinically Relevant Mycoses*; Presterl, E., Ed.; Springer International Publishing: Cham, 2019; pp 31–42. https://doi.org/10.1007/978-3-319-92300-0_3.

(17) Kathiravan, M. K.; Salake, A. B.; Chothe, A. S.; Dudhe, P. B.; Watode, R. P.; Mukta, M. S.; Gadhwe, S. The Biology and Chemistry of Antifungal Agents: A Review. *Bioorganic & Medicinal Chemistry* **2012**, *20* (19), 5678–5698. https://doi.org/10.1016/j.bmc.2012.04.045.

(18) Arendrup, M. C.; Patterson, T. F. Multidrug-Resistant Candida: Epidemiology, Molecular Mechanisms, and Treatment. *The Journal of Infectious Diseases* **2017**, *216* (suppl_3), S445–S451. https://doi.org/10.1093/infdis/jix131.

(19) Lin, Y.; Jung, H.; Bulman, C. A.; Ng, J.; Vinck, R.; O'Beirne, C.; Moser, M. S.; Tricoche, N.; Peguero, R.; Li, R. W.; Urban, J. F.; Pape, P. L.; Pagniez, F.; Moretto, M.; Weil, T.; Lustigman, S.; Cariou, K.; Mitreva, M.; Sakanari, J. A.; Gasser, G. Discovery of New Broad-Spectrum Anti-Infectives for Eukaryotic Pathogens Using Bioorganometallic Chemistry. *bioRxiv* **2023**. https://doi.org/10.1101/2023.06.28.546819.

(20) Cationic RuII Cyclopentadienyl Complexes with Antifungal Activity against Several Candida Species. **2020**.

(21) Lin, Y.; Betts, H.; Keller, S.; Cariou, K.; Gasser, G. Recent Developments of Metal-Based Compounds against Fungal Pathogens. *Chem. Soc. Rev.* **2021**, *50* (18), 10346–10402. https://doi.org/10.1039/D0CS00945H.

(22) Gasser, G.; Ott, I.; Metzler-Nolte, N. Organometallic Anticancer Compounds. *J. Med. Chem.* **2011**, *54* (1), 3–25. https://doi.org/10.1021/jm100020w.

(23) Gasser, G. Metal Complexes and Medicine: A Successful Combination. *chimia (aarau)* **2015**, *69* (7), 442–446. https://doi.org/10.2533/chimia.2015.442.

(24) Patra, M.; Gasser, G. Organometallic Compounds: An Opportunity for Chemical Biology? *ChemBioChem* **2012**, *13* (9), 1232–1252. https://doi.org/10.1002/cbic.201200159.

(25) Gasser, G.; Metzler-Nolte, N. The Potential of Organometallic Complexes in Medicinal Chemistry. *Current Opinion in Chemical Biology* **2012**, *16* (1–2), 84–91. https://doi.org/10.1016/j.cbpa.2012.01.013.

(26) Karges, J.; Giardini, M. A.; Blacque, O.; Woodworth, B.; Siqueira-Neto, J. L.; Cohen, S. M. Enantioselective Inhibition of the SARS-CoV-2 Main Protease with Rhenium(ı) Picolinic Acid Complexes. *Chem. Sci.* **2023**, *14* (3), 711–720. https://doi.org/10.1039/D2SC05473F.

(27) Chellan, P.; Sadler, P. J. Enhancing the Activity of Drugs by Conjugation to Organometallic Fragments. *Chemistry A European J* **2020**, *26* (40), 8676–8688. https://doi.org/10.1002/chem.201904699.

(28) Hillard, E. A.; Jaouen, G. Bioorganometallics: Future Trends in Drug Discovery, Analytical Chemistry, and Catalysis ᵛ. *Organometallics* **2011**, *30* (1), 20–27. https://doi.org/10.1021/om100964h.

(29) Frei, A.; Elliott, A. G.; Kan, A.; Dinh, H.; Bräse, S.; Bruce, A. E.; Bruce, M. R.; Chen, F.; Humaidy, D.; Jung, N.; King, A. P.; Lye, P. G.; Maliszewska, H. K.; Mansour, A. M.; Matiadis, D.; Muñoz, M. P.; Pai, T.-Y.; Pokhrel, S.; Sadler, P. J.; Sagnou, M.; Taylor, M.; Wilson, J. J.; Woods, D.; Zuegg, J.; Meyer, W.; Cain, A. K.; Cooper, M. A.; Blaskovich, M. A. T. Metal Complexes as Antifungals? From a Crowd-Sourced Compound Library to the First *In Vivo* Experiments. *JACS Au* **2022**, *2* (10), 2277–2294. https://doi.org/10.1021/jacsau.2c00308.

(30) Gil-Moles, M.; Türck, S.; Basu, U.; Pettenuzzo, A.; Bhattacharya, S.; Rajan, A.; Ma, X.; Büssing, R.; Wölker, J.; Burmeister, H.; Hoffmeister, H.; Schneeberg, P.; Prause, A.; Lippmann, P.; Kusi-Nimarko, J.; Hassell-Hart, S.; McGown, A.; Guest, D.; Lin, Y.; Notaro, A.; Vinck, R.; Karges, J.; Cariou, K.; Peng, K.; Qin, X.; Wang, X.; Skiba, J.; Szczupak, Ł.; Kowalski, K.; Schatzschneider, U.; Hemmert, C.; Gornitzka, H.; Milaeva, E. R.; Nazarov, A. A.; Gasser, G.; Spencer, J.; Ronconi, L.; Kortz, U.; Cinatl, J.; Bojkova, D.; Ott, I. Metallodrug Profiling against SARS-CoV-2 Target Proteins Identifies Highly Potent Inhibitors of the S/ACE2 Interaction and the Papain-like Protease PL ^{pro}. *Chemistry A European J* **2021**, *27* (71), 17928–17940. https://doi.org/10.1002/chem.202103258.

(31) Hartinger, C. G.; Dyson, P. J. Bioorganometallic Chemistry—from Teaching Paradigms to Medicinal Applications. *Chem. Soc. Rev.* **2009**, *38* (2), 391–401. https://doi.org/10.1039/B707077M.

(32) Top, S.; Dauer, B.; Vaissermann, J.; Jaouen, G. Facile Route to Ferrocifen, 1-[4-(2-Dimethylaminoethoxy)]-1-(Phenyl-2-Ferrocenyl-but-1-Ene), First Organometallic Analogue of Tamoxifen, by the McMurry Reaction. *Journal of Organometallic Chemistry* **1997**, *541* (1–2), 355–361. https://doi.org/10.1016/S0022-328X(97)00086-7.

(33) Biot, C.; Glorian, G.; Maciejewski, L. A.; Brocard, J. S.; Domarle, O.; Blampain, G.; Millet, P.; Georges, A. J.; Abessolo, H.; Dive, D.; Lebibi, J. Synthesis and Antimalarial Activity in Vitro and in Vivo of a New Ferrocene−Chloroquine Analogue. *J. Med. Chem.* **1997**, *40* (23), 3715–3718. https://doi.org/10.1021/jm970401y.

(34) Dubar, F.; Egan, T. J.; Pradines, B.; Kuter, D.; Ncokazi, K. K.; Forge, D.; Paul, J.-F.; Pierrot, C.; Kalamou, H.; Khalife, J.; Buisine, E.; Rogier, C.; Vezin, H.; Forfar, I.; Slomianny, C.; Trivelli, X.; Kapishnikov, S.; Leiserowitz,

L.; Dive, D.; Biot, C. The Antimalarial Ferroquine: Role of the Metal and Intramolecular Hydrogen Bond in Activity and Resistance. *ACS Chem. Biol.* **2011**, *6* (3), 275–287. https://doi.org/10.1021/cb100322v.

(35) Chantson, J. T.; Falzacappa, M. V. V.; Crovella, S.; Metzler-Nolte, N. Antibacterial Activities of Ferrocenoyl- and Cobaltocenium-Peptide Bioconjugates. *Journal of Organometallic Chemistry* **2005**, *690* (21–22), 4564–4572. https://doi.org/10.1016/j.jorganchem.2005.07.007.

(36) Geiger, W. E. Electroreduction of Cobaltocene. Evidence for a Metallocene Anion. *J. Am. Chem. Soc.* **1974**, *96* (8), 2632–2634. https://doi.org/10.1021/ja00815a062.

(37) Rogers, E. I.; Silvester, D. S.; Poole, D. L.; Aldous, L.; Hardacre, C.; Compton, R. G. Voltammetric Characterization of the Ferrocene|Ferrocenium and Cobaltocenium|Cobaltocene Redox Couples in RTILs. *J. Phys. Chem. C* **2008**, *112* (7), 2729–2735. https://doi.org/10.1021/jp710134e.

(38) Blau, S.; Jubeh, T. T.; Haupt, S. M.; Rubinstein, A. Drug Targeting by Surface Cationization. *Critical Reviews™ in Therapeutic Drug Carrier Systems* **2000**, *17* (5), 425–465.

(39) Swarts, J. C.; Nafady, A.; Roudebush, J. H.; Trupia, S.; Geiger, W. E. One-Electron Oxidation of Ruthenocene: Reactions of the Ruthenocenium Ion in Gentle Electrolyte Media. *Inorg. Chem.* **2009**, *48* (5), 2156–2165. https://doi.org/10.1021/ic802105b.

(40) Sansook, S.; Tuo, W.; Bollier, M.; Barczyk, A.; Dezitter, X.; Klupsch, F.; Leleu-Chavain, N.; Farce, A.; Tizzard, G. J.; Coles, S. J.; Spencer, J.; Millet, R. Synthesis and Biological Evaluation of Ferrocene-Based Cannabinoid Receptor 2 Ligands. *Future Medicinal Chemistry* **2018**, *10* (6), 631–638. https://doi.org/10.4155/fmc-2017-0200.

(41) Tron, G. C.; Pirali, T.; Billington, R. A.; Canonico, P. L.; Sorba, G.; Genazzani, A. A. Click Chemistry Reactions in Medicinal Chemistry: Applications of the 1,3-Dipolar Cycloaddition between Azides and Alkynes. *Med. Res. Rev.* **2008**, *28* (2), 278–308. https://doi.org/10.1002/med.20107.

(42) Bonandi, E.; Christodoulou, M. S.; Fumagalli, G.; Perdicchia, D.; Rastelli, G.; Passarella, D. The 1,2,3-Triazole Ring as a Bioisostere in Medicinal Chemistry. *Drug Discovery Today* **2017**, *22* (10), 1572–1581. https://doi.org/10.1016/j.drudis.2017.05.014.

(43) Tasaka, A.; Tamura, N.; Matsushita, Y.; Teranishi, K.; Hayashi, R.; Okonogi, K.; Itoh, K.Optically Active Antifungal Azoles. I. Synthesis and Antifungal Activity of (2R, 3R)-2-(2, 4-Difluorophenyl)-3-Mercapto-1-(1H-1, 2, 4-Triazol-1-Yl)-2-Butanol and Its Stereoisomers. *CHEMICAL & PHARMACEUTICAL BULLETIN* **1993**, *41* (6), 1035–1042. https://doi.org/10.1248/cpb.41.1035.

(44) Rostovtsev, V. V.; Green, L. G.; Fokin, V. V.; Sharpless, K. B. A Stepwise Huisgen Cycloaddition Process: Copper(I)-Catalyzed Regioselective "Ligation" of Azides and Terminal Alkynes. *Angew. Chem. Int. Ed.* **2002**, *114* (14), 2596–2599. https://doi.org/10.1002/1521-3757(20020715)114:14<2708::AID-ANGE2708>3.0.CO;2-0.

(45) Zhang, J.; Yan, J.; Pageni, P.; Yan, Y.; Wirth, A.; Chen, Y.-P.; Qiao, Y.; Wang, Q.; Decho, A. W.; Tang, C. Anion-Responsive Metallopolymer Hydrogels for Healthcare Applications. *Sci Rep* **2015**, *5* (1), 11914. https://doi.org/10.1038/srep11914.

(46) Alcalde, E.; Dinarès, I.; Ibáñez, A.; Mesquida, N. A Simple Halide-to-Anion Exchange Method for Heteroaromatic Salts and Ionic Liquids. *Molecules* **2012**, *17* (4), 4007–4027. https://doi.org/10.3390/molecules17044007.

(47) Balakin, K. V.; Ivanenkov, Y. A.; Skorenko, A. V.; Nikolsky, Y. V.; Savchuk, N. P.; Ivashchenko, A. A. In Silico Estimation of DMSO Solubility of Organic Compounds for Bioscreening. *J Biomol Screen* **2004**, *9* (1), 22–31. https://doi.org/10.1177/1087057103260006.

(48) Carretero, M.; Solis, M. G.; Petrascheck, M. C. Elegans as Model for Drug Discovery. *Current Topics in Medicinal Chemistry* **2017**, *17* (18), 2067–2076. https://doi.org/10.2174/1568026617666170131114401.

(49) Marcellino, C.; Gut, J.; Lim, K. C.; Singh, R.; McKerrow, J.; Sakanari, J. WormAssay: A Novel Computer Application for Whole-Plate Motion-Based Screening of Macroscopic Parasites. *PLoS Negl Trop Dis* **2012**, *6* (1), e1494. https://doi.org/10.1371/journal.pntd.0001494.

(50) Bulman, C. A.; Bidlow, C. M.; Lustigman, S.; Cho-Ngwa, F.; Williams, D.; Rascón, Jr, A. A.; Tricoche, N.; Samje, M.; Bell, A.; Suzuki, B.; Lim, K. C.; Supakorndej, N.; Supakorndej, P.; Wolfe, A. R.; Knudsen, G. M.; Chen, S.; Wilson, C.; Ang, K.-H.; Arkin, M.; Gut, J.; Franklin, C.; Marcellino, C.; McKerrow, J. H.; Debnath, A.; Sakanari, J. A. Repurposing Auranofin as a Lead Candidate for Treatment of Lymphatic Filariasis and Onchocerciasis. *PLoS Negl Trop Dis* **2015**, *9* (2), e0003534. https://doi.org/10.1371/journal.pntd.0003534.

(51) Tyagi, R.; Elfawal, M. A.; Wildman, S. A.; Helander, J.; Bulman, C. A.; Sakanari, J.; Rosa, B. A.; Brindley, P. J.; Janetka, J. W.; Aroian, R. V.; Mitreva, M. Identification of Small Molecule Enzyme Inhibitors as Broad-Spectrum Anthelmintics. *Sci Rep* **2019**, *9* (1), 9085. https://doi.org/10.1038/s41598-019-45548-7.

(52) Gu, J.; Bourne, P. E. *Structural Bioinformatics, 2nd Edition*; Wiley-Blackwell, 2009.

(53) Chen, C.-K.; Leung, S. S. F.; Guilbert, C.; Jacobson, M. P.; McKerrow, J. H.; Podust, L. M. Structural Characterization of CYP51 from Trypanosoma Cruzi and Trypanosoma Brucei Bound to the Antifungal Drugs Posaconazole and Fluconazole. *PLoS Negl Trop Dis* **2010**, *4* (4), e651. https://doi.org/10.1371/journal.pntd.0000651.

Table of Contents Graphic

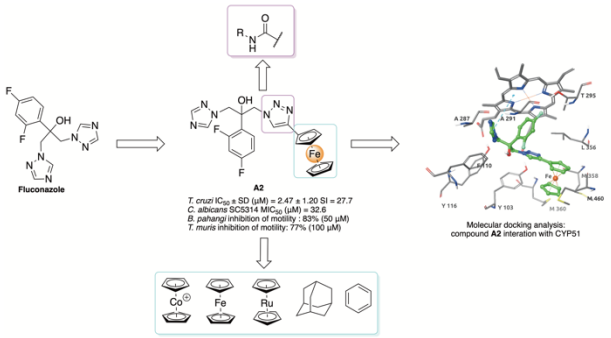

Antifungal and Antiparasitic Activity of Novel Metallocene-containing Fluconazole Derivatives

Yan Lin,[a] Gonzalo Scalese,[b] Christina A Bulman,[c] Robin Vinck,[a] Olivier Blacque,[d] Margot Paulino,[e] Andrés Ballesteros-Casallas, [e] Leticia Pérez Díaz,[f] Gustavo Salinas,[g,h] Makedonka Mitreva,[i,*] Tobias Weil,[j,*] Kevin Cariou,[a,*] Judy A. Sakanari,[c,*] Dinorah Gambino,[b,*] and Gilles Gasser[a,*]

a) Chimie ParisTech, PSL University, CNRS, Institute of Chemistry for Life and Health Sciences, Laboratory for Inorganic Chemical Biology, 75005 Paris, France. WWW: www.gassergroup.com.
b) Área Química Inorgánica, Facultad de Química, Universidad de la República, 11800 Montevideo, Uruguay.
c) University of California, San Francisco, Department of Pharmaceutical Chemistry, San Francisco, CA 94158, USA.
d) Department of Chemistry, University of Zurich, Winterthurerstrasse 190, 8057 Zurich, Switzerland.
e) Área Bioinformática, Departamento DETEMA, Facultad de Química, Universidad de la República, 11600 Montevideo, Uruguay.
f) Sección Genómica Funcional, Facultad de Ciencias, Universidad de la República, 11400 Montevideo, Uruguay
g) Worm Biology Lab, Institut Pasteur de Montevideo, 11400 Montevideo, Uruguay.
h) Departamento de Biociencias, Facultad de Química, Universidad de la República, 11800 Montevideo, Uruguay.
i) Department of Medicine, Washington University School of Medicine, St. Louis, MO 63108, USA.
j) Research and Innovation Centre, Fondazione Edmund Mach Via E. Mach 1, 38010 San Michele all'Adige, Italy.

Contents

Experimental section in chemistry part

Materials and methods

All manipulations of the complexes were performed using standard Schlenk techniques under a nitrogen atmosphere. Commercially available regents were used without further purification. Solvents were dried over molecular sieves if necessary. Evaporation of solvents *in vacuo* was done with a rotary evaporator at 40°C. Thin layer chromatography (TLC) was performed using silica gel 60 F-254 (Merck) plates with detection of spots being achieved by exposure to UV light. NMR spectra were recorded in deuterated solvents on Bruker AV-400 (^{1}H, 400 MHz; ^{13}C, 101 MHz; ^{19}F, 376.5 MHz) and AV-500 (^{1}H, 500 MHz; ^{13}C, 126 MHz; ^{19}F, 470.6 MHz) spectrometers at room temperature. The chemical shifts, δ, are reported in ppm (parts per million). The residual solvent peaks have been used as an internal reference. The abbreviations for the peak multiplicities are as follows: s (singlet), d (doublet), t (triplet), dd (doublet of doublet), p (pentet), sept (septet), brs (broad singlet), and m (multiplet).

Synthesis and compound characterization

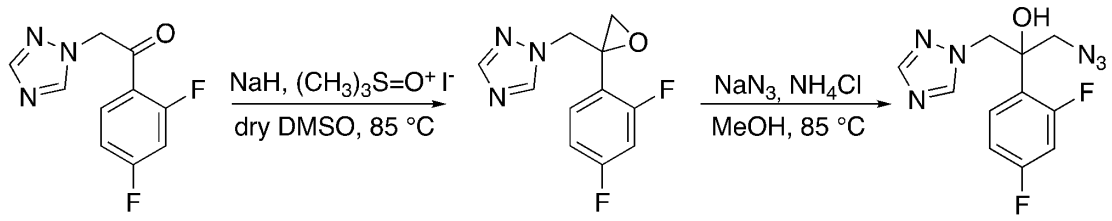

SS0 **SS1**

Scheme S1 Synthetic pathways for **SS1**.

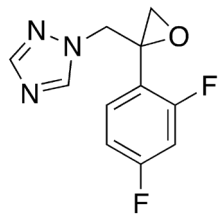

SS0

Compound **SS0** was synthesized following an adapted literature procedure.[1] A suspension of NaH (96 mg, 2.4 mmol, 1.2 equiv.) in dry DMSO (16 mL) and trimethylsulfoxonium iodide (528 mg, 2.4 mmol, 1.2 equiv.) was stirred for 30 min at room temperature until the mixture became clear. 1-(2,4-difluorophenyl)-2-(1H-1,2,4-triazol-1-yl)ethan-1-one (446 mg, 2.0 mmol, 1 equiv.) in dry DMSO (32 mL) was added to the previous solution and the reaction mixture was heated to 85°C for 5 h. After cooling the solution to room temperature, the reaction mixture was poured into cold H_2O (50 mL, 4°C). The

product was extracted with EtOAc (2 × 50 mL) and the combined organic phases were washed with H_2O (50 mL), brine (50 mL), dried over $MgSO_4$, filtered and evaporated. The residue was purified by flash chromatography on silica with EtOAc : cyclohexane (3 : 2) as the eluent system (Rf = 0.26, EtOAc : cyclohexane (3 : 2)) to obtain compound 17 as an orange oil (313 mg, 1.32 mmol, 66%). **^{1}H NMR** (400 MHz, Chloroform-d): δ 8.02 (s, 1H), 7.80 (s, 1H), 7.15 – 7.08 (m, 1H), 6.80 – 6.71 (m, 2H), 4.78 (d, *J* = 14.9 Hz, 1H), 4.45 (d, *J* = 14.9 Hz, 1H), 2.95 (d, *J* = 4.7 Hz, 1H), 2.89 (d, *J* = 4.7 Hz, 1H). The spectral data corresponds to previously reported data.[1]

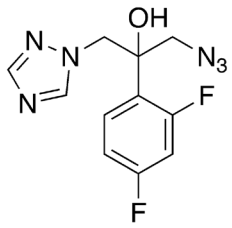

SS1

Compound **SS1** was prepared following an adapted literature procedure. The spectral data corresponds to previously reported data.[2] **^{1}H NMR** (400 MHz, Chloroform-d) δ 7.88 (s, 1H), 7.76 (s, 1H), 7.49 – 7.43 (m, 1H), 6.79 – 6.68 (m, 2H), 4.69 (d, *J* = 14.3 Hz, 1H), 4.61 (d, *J* = 14.2 Hz, 1H), 3.62 (d, *J* = 12.9 Hz, 1H), 3.46 (dd, *J* = 12.9, 1.0 Hz, 1H).

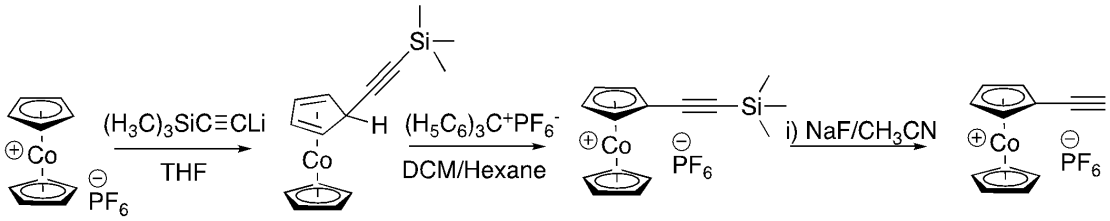

S-SA1 **SA1**

Scheme S2 Synthetic pathways for **SA1**.

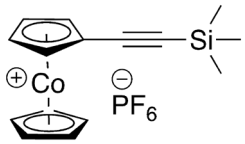

S-SA1

Compound **S-SA1** was prepared following an adapted literature procedure with minor modification. A Schlenk flask was charged under an atmosphere of N_2 with 50 mL dry THF and 0.79 mL of (trimethylsilyl)acetylene (1.14 equiv). The mixture was cooled to -78 °C and 2.2 mL 2.5 M *n*BuLi (1.1 equiv) was added. Stirring was continued for 1h and then the mixture was warmed to -15 °C, 1.67g Bis(cyclopentadienyl)cobalt(III) hexafluorophosphate (1 equiv) was added. The reaction mixture was

slowly warmed to room temperature for 30 min with vigorous stirring, further treated by ultrasonic instrument for an additional 15 min, resulting in a dark red homogeneous solution. The solvent was removed *in vacuo*, and the residues was isolated by solid-phase extraction over 50 mL dry hexane which was dried by Na_2SO_4. A round-bottom flask was charged with 2.5 g triphenylcarbenium salts and 50 mL freshly opened dichloromethane, the mixture protected from the light was stirred for 10 min at room temperature. The previously collected solution in hexane was added to this yellow-brown mixture and the product was allowed to participate during 30 min of further stirring. The tan precipitate was filtered off and thoroughly washed with diethyl ether and cold water.[3] The spectral data corresponds to previously reported data.[1]**H NMR** (400 MHz, Acetonitrile-d3) δ 5.85 (t, *J* = 2.1 Hz, 2H), 5.68 – 5.66 (m, 7H), 0.27 (s, 9H).

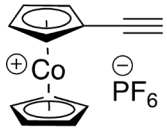

SA1

Compound **SA1** was prepared following an adapted literature procedure. The spectral data corresponds to previously reported data.[3] **^{1}H NMR** (400 MHz, Acetonitrile-d3) δ 5.94 – 5.93 (m, 2H), 5.73 (s, 5H), 5.72 – 5.71 (m, 2H), 3.74 (s, 1H).

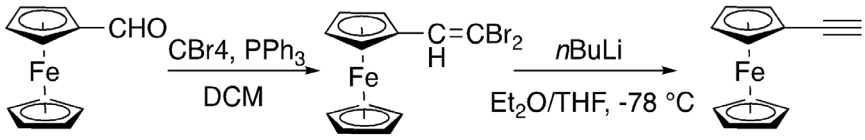

S-SA2 **SA2**

Scheme S3 Synthetic pathways for **SA2**.

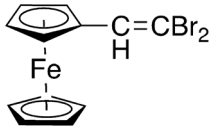

S-SA2

Compound **S-SA2** was prepared following an adapted literature procedure. The spectral data corresponds to previously reported data.[4] **^{1}H NMR** (400 MHz, Chloroform-d) δ 7.14 (s, 1H), 4.67 (s, 2H), 4.31 (s, 2H), 4.21 (s, 5H).

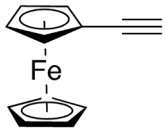

SA2

Compound **SA2** was prepared following an adapted literature procedure. The spectral data corresponds to previously reported data.[4] **^{1}H NMR** (400 MHz, Chloroform-d) δ 4.39 (t, *J* = 1.9 Hz, 2H), 4.15 (s, 5H), 4.13 (t, *J* = 1.9 Hz, 2H), 2.65 (s, 1H).

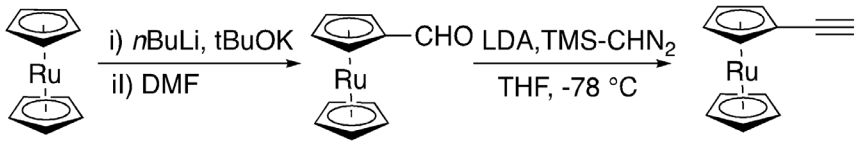

S-SA3 **SA3**

Scheme S4 Synthetic pathways for **SA3**.

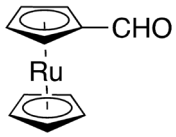

S-SA3

Compound **S-SA3** was prepared following several adapted literature procedures.[5,6,7] A solution of ruthenium trichloride hydrate ($RuCl_3 \times H_2O$, 31.4 g, 0.12 mol, 1 equiv.) in 200 mL of absolute ethanol was placed in an ice bath cooled to 0 °C. Subsequently, cyclopentadiene (100 mL, 79.5 g, 1.20 mol, 10 equiv.) was added to the solution. Zinc dust (78 g, 1.20 mol, 10 equiv.) was added to the reaction mixture over 1 h in 10 portions, while the temperature was kept between 0 – 10 °C during the addition. The reaction mixture was stirred at 0 °C for 30 min, and then warmed to room temperature (23 °C) with continued stirring for 3 h. The suspension was filtered, and the grey metallic residue was washed with hot toluene (90 °C). The filtrate was concentrated in vacuo, the residue was dissolved in toluene at room temperature. The solution was passed through a plug of silica gel with toluene as eluent. The toluene was removed in vacuo to obtain ruthenocene as an off-white solid (9.02 g, 0.039 mol, 33%).

Ruthenocene (1.00 g, 4.3 mmol, 1 equiv), and KO*t*Bu (56 mg, 0.5 mmol, 0.12 equiv) were dissolved in dry THF (100 mL) and cooled to -78 °C. At -78 °C, *t*BuLi in pentane (4.6 mL, 8.6 mmol, 1.9 M, 2 equiv.) was added dropwise to the solution over a period of 30 min. After the addition of *t*BuLi, dry dimethylformamide (0.8 mL, 0.8 g, 10.9 mmol, 2.5 equiv.) was added dropwise into the reaction mixture, and stirred for another 10 min. The reaction mixture was then warmed to -40 °C, and stirred for a further 10 min, before deionized water (50 mL) was added. The THF was removed in vacuo and the

aqueous solution was extracted with dichloromethane (DCM) (50 mL × 3). The DCM layers were combined, washed with water (50 mL × 2), dried with $MgSO_4$, filtered, and the DCM removed in vacuo. The residue was purified by flash chromatography using DCM as eluent (Rf = 0.61), to obtain **1** as a bright yellow solid (0.90 g, 3.49 mmol, 82%). **^{1}H NMR** (400 MHz, Chloroform-d) δ 9.72 (s, 1H), 5.10 – 5.05 (m, 2H), 4.87 – 4.83 (m, 2H), 4.64 (s, 5H). The spectral data corresponds to previously reported data.

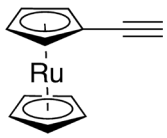

SA3

Compound **SA3** was prepared following an adapted literature procedure. The spectral data corresponds to previously reported data.[8] **^{1}H NMR** (400 MHz, Methylene Chloride-d2) δ 4.72 – 4.70 (m, 2H), 4.46 (s, 5H), 4.43 – 4.41 (m, 2H), 2.55 (s, 1H).

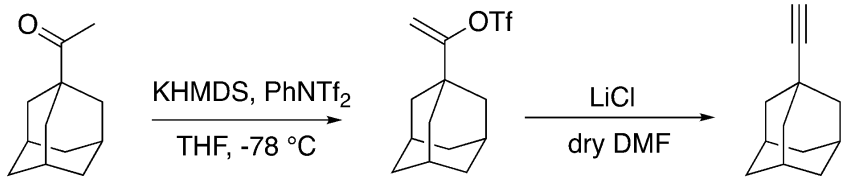

S-SA4 **SA4**

Scheme S5 Synthetic pathways for **SA4**.

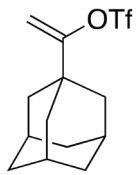

S-SA4

Compound **S**-S**A4** was prepared following an adapted literature procedure. The spectral data corresponds to previously reported data.[9] **^{1}H NMR** (400 MHz, Chloroform-d) δ 4.98 (d, *J* = 4.2 Hz, 1H), 4.80 (d, *J* = 4.1 Hz, 1H), 2.00 – 1.98 (m, 3H), 1.70 – 1.65 (m, 9H), 1.63 – 1.58 (m, 3H).

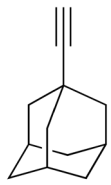

SA4

Compound **SA4** was prepared following an adapted literature procedure. The spectral data corresponds to previously reported data.[9] **^{1}H NMR** (400 MHz, Chloroform-d) δ 1.97 (s, 1H), 1.85 – 1.82 (m, 3H), 1.76 (d, *J* = 3.0 Hz, 6H), 1.56 (t, *J* = 3.2 Hz, 6H).

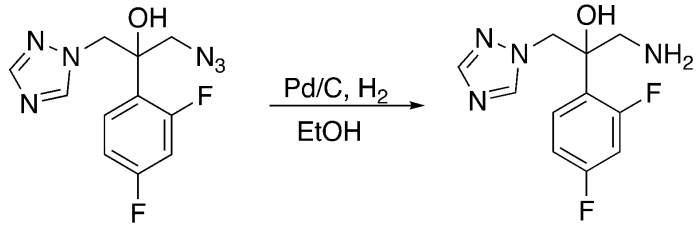

SS1 **SS2**

Scheme S6 Synthetic pathways for **SS2**.

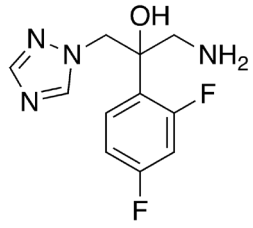

SS2

Compound **SS2** was prepared following an adapted literature procedure. The spectral data corresponds to previously reported data.[2] **^{1}H NMR** (400 MHz, Chloroform-d) δ 8.01 (s, 1H), 7.76 (s, 1H), 7.49 (td, *J* = 8.9, 6.5 Hz, 1H), 6.80 – 6.65 (m, 2H), 4.56– 4.48 (m, 2H), 3.13 (dd, *J* = 12.9, 1.3 Hz, 1H), 2.91 (dd, *J* = 13.0, 1.5 Hz, 1H).

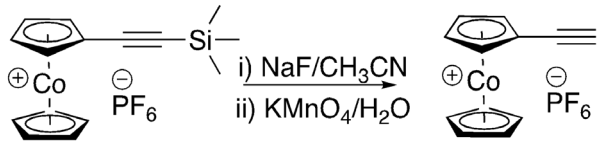

S-SA1 **SB1**

Scheme S7 Synthetic pathways for **SB1**.

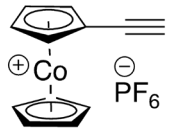

SB1

Compound **SB1** was prepared following an adapted literature procedure. The spectral data corresponds to previously reported data.[3] **^{1}H NMR** (400 MHz, Acetonitrile-d3) δ 6.09 (t, *J* = 2.2 Hz, 2H), 5.79 (t, *J* = 2.2 Hz, 2H), 5.75 (s, 5H).

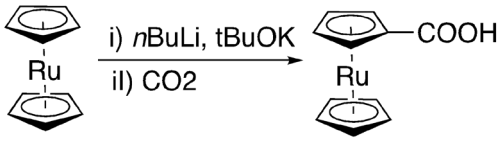

SB3

Scheme S8 Synthetic pathways for **SB3**.

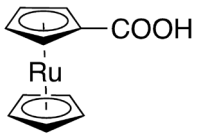

SB3

Compound **SB3** was prepared following an adapted literature procedure. The spectral data corresponds to previously reported data.[10] **^{1}H NMR** (400 MHz, Chloroform-*d*) δ 5.11 – 5.08 (m, 2H, C_5H_4), 4.70 – 4.66 (m, 2H, C_5H_4), 4.56 (s, 5H, C_5H_5).

General Procedure A

To a mixture of azide (1 equiv) and alkyne (1 equiv) in degassed THF: H_2O (3: 2, 0.013M) being cooled to 0 °C. Then, an aqueous solution of $CuSO_4$ (1.1 equiv, 1M) was added dropwise, followed by the dropwise addition of freshly prepared aqueous solution of sodium ascorbate (2.2 equiv, 1M). The reaction mixture was allowed to stir for 18h at room temperature under N_2 atmosphere. An aqueous solution of ammonia (5 mL per mmol) was added, after stir for 10 min, the mixture was extracted with DCM, and washed with water, dried by Na_2SO_4, the organic solvent was evaporated to afford the crude product.

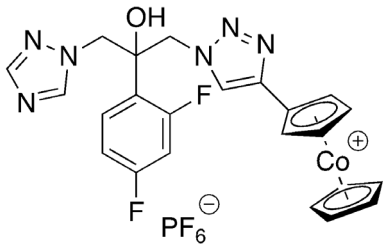

A1-PF_6

Compound **A1**-**PF_6** was prepared according to the general procedure A using azide **SS1** (1.65 mmol) and alkyne **SA1** (1.65 mmol), the crude product was purified by recrystallization from MeCN/Et_2O at 4 °C. Yield: 71%. **IR** (cm^{-1}): 1498, 1137, 837, 818, 677. **^{1}H NMR** (500 MHz, DMSO-d_6) δ 8.46 (s, 1H), 8.40 (s, 1H), 7.90 (s, 1H), 7.30 – 7.25 (m, 1H), 7.23 – 7.18 (m, 1H), 6.92 – 6.89 (m, 1H), 6.61 (s, 1H), 6.36 (pseudo-t, *J* = 5 Hz, 2H), 5.91 (pseudo-t, *J* = 5 Hz, 2H), 5.55 (s, 5H), 5.11 (d, *J* = 14.4 Hz, 1H), 4.77 (d, *J* = 14.5 Hz, 1H), 4.72 (d, *J* = 14.6 Hz, 1H), 4.66 (d, *J* = 14.3 Hz, 1H). **^{13}C NMR** (126 MHz, DMSO-d_6) δ 162.2 (dd, *J* =

246.7, 12.5 Hz), 159.0 (dd, *J* = 247.2, 12.8 Hz), 151.1, 145.4, 137.3, 129.7 (d, *J* = 10.1 Hz), 125.7, 122.9 (d, *J* = 12.2 Hz), 111.1 (d, *J* = 20.7 Hz), 104.2 (t, *J* = 27.0 Hz), 94.8, 85.5, 84.3, 80.5 (d, *J* = 11.1 Hz), 73.9 (d, *J* = 4.8 Hz), 55.9, 54.8. **^{19}F NMR** (471 MHz, DMSO-d6) δ -70.11 (d, *J* = 711.3 Hz), -106.99 (d, *J* = 8.5 Hz), -110.76 (d, *J* = 8.3 Hz). **^{31}P NMR** (162 MHz, DMSO-d6) δ -144.18 (hept, *J* = 711.3 Hz). **HRMS (ESI)** m/z: $[M+]^+$ Calcd. for $C_{23}H_{20}CoF_2N_6O^+$ 493.0993, found 493.0990. **Elemental Analysis**: calcd. for $C_{23}H_{20}CoF_8N_6OP$ = C, 43.28; H, 3.16; N, 13.17. Found = C, 43.63; H, 3.02; N, 12.87.

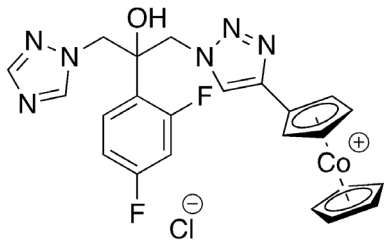

A1-Cl

Ion exchange: To a mixture slurry of compound **A1**-**PF_6** (1.44 mmol) in 20 mL methanol was added Amberlite IRA-402 (Cl) (7.35 g), after 20 min vigorously stirred, the reaction mixture became clear, and was left stirring overnight. The mixture was filtered through Buchner funnel and the filtrate was concentrated under reduced pressure. The residue was further recrystallized from EtOH/hexane to give the pure compound **A1**-**Cl** as yellow solid. **IR** (cm^{-1}): 1417, 1271, 1140, 826, 672. **^{1}H NMR** (500 MHz, DMSO-d6) δ 8.61 – 8.50 (m, 2H), 7.86 (s, 1H), 7.32 – 7.16 (m, 2H), 7.09 (s, 1H), 6.90 – 6.86 (m, 1H), 6.37 (q, *J* = 1.7 Hz, 2H), 5.92 (t, *J* = 2.1 Hz, 2H), 5.57 (s, 5H), 5.12 (d, *J* = 14.3 Hz, 1H), 4.82 (d, *J* = 1.8 Hz, 2H), 4.70 (d, *J* = 14.3 Hz, 1H). **^{13}C NMR** (126 MHz, DMSO-d6) δ 162.1 (dd, *J* = 246.8, 12.5 Hz), 159.0 (dd, *J* = 247.3, 12.6 Hz), 150.9, 145.5, 137.2, 129.9 (d, *J* = 9.7 Hz), 125.8, 123.0 (d, *J* = 12.0 Hz), 111.0 (d, *J* = 20.7 Hz), 104.1 (t, *J* = 26.7 Hz), 94.9, 85.5, 84.3, 80.6 (d, *J* = 6.4 Hz), 73.9 (d, *J* = 4.6 Hz), 55.86 (d, *J* = 2.5 Hz) , 54.5 (d, *J* = 5.1 Hz). **^{19}F NMR** (471 MHz, DMSO-d6) δ -107.13 (d, *J* = 8.4 Hz), -110.99 (d, *J* = 8.3 Hz). **HRMS (ESI)** m/z: $[M+]^+$ Calcd. for $C_{23}H_{20}CoF_2N_6O^+$ 493.0993, found 493.0990. **Elemental Analysis**: calcd. for $C_{23}H_{20}ClCoF_2N_6O \cdot 0.5H_2O$ = C, 51.36; H, 3.94; N, 15.63. Found = C, 51.64; H, 3.76; N, 15.28.

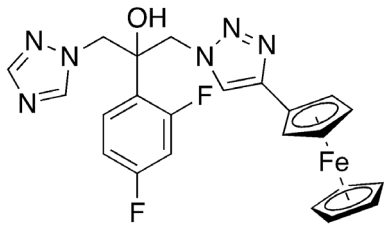

A2

Compound **A2** was prepared according to the general procedure A using azide **SS1** (0.5 mmol) and alkyne **SA2** (0.5 mmol), the crude product was chromatographed on silica (Ethyl acetate) to give compound **A2** as yellow solid. Yield: 94%. **IR** (cm^{-1}): 1497, 1272, 1139, 818, 675. **^{1}H NMR** (500 MHz, DMSO-d6) δ 8.37 (s, 1H), 7.86 (s, 1H), 7.85 (s, 1H), 7.29 – 7.19 (m, 2H), 6.91 – 6.81 (m, 1H), 6.50 (s, 1H), 5.01 (d, *J* = 14.4 Hz, 1H), 4.76 (d, *J* = 14.5 Hz, 1H), 4.68 – 4.60 (m, 4H), 4.25 (pseudo-t, *J* = 1.85 Hz 2H), 3.93 (s, 5H). **^{13}C NMR** (126 MHz, DMSO-d6) δ 162.1 (dd, *J* = 246.3, 12.7 Hz), 159.0 (dd, *J* = 247.2, 12.5 Hz), 151.0, 145.3, 144.8, 129.8 (d, *J* = 9.3 Hz), 123.1 (d, *J* = 12.9 Hz), 121.3, 111.0 (d, *J* = 20.0 Hz), 104.0 (t, *J* = 27.0 Hz), 75.7, 74.0 (d, *J* = 4.8 Hz), 69.2, 68.2, 66.2, 55.5 (d, *J* = 4.6 Hz), 55.0 (d, *J* = 5.1 Hz). **^{19}F NMR** (376 MHz, DMSO-d6) δ -107.12 (d, *J* = 8.2 Hz), -111.16 (d, *J* = 8.1 Hz). **HRMS (ESI)** m/z: $[M+H]^+$ Calcd. for $C_{23}H_{21}F_2FeN_6O$ 491.1089, found 491.1093. **Elemental Analysis**: calcd. for $C_{23}H_{20}F_2FeN_6O$ = C, 56.34; H, 4.11; N, 17.14. Found = C, 56.03; H, 3.96; N, 16.94.

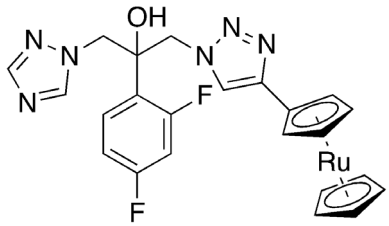

A3

Compound **A3** was prepared according to the general procedure A using azide **SS1** (0.6 mmol) and alkyne **SA3** (0.6 mmol), the crude product was chromatographed on silica (EA: hexane = 4: 1□ EA) to give compound **A3** as pale yellow solid. Yield: 50%. **IR** (cm^{-1}): 1501, 1271, 1136, 964, 808, 679. **^{1}H NMR** (500 MHz, DMSO-d6) δ 8.35 (s, 1H), 7.83 (s, 1H), 7.73 (s, 1H), 7.30 – 7.14 (m, 2H), 6.90 – 6.86 (m, 1H), 6.44 (s, 1H), 5.06 – 5.04 (m, 2H), 4.94 (d, *J* = 14.4 Hz, 1H), 4.74 (d, *J* = 14.5 Hz, 1H), 4.64 – 4.56 (m, 4H), 4.38 (s, 5H). **^{13}C NMR** (126 MHz, DMSO-d6) δ 162.6 (dd, *J* = 246.6, 12.6 Hz), 159.4 (dd, *J* = 247.5, 12.2 Hz), 151.4, 145.7, 144.5, 130.3, 123.6 (d, *J* = 13.0 Hz), 122.1, 111.5 (d, *J* = 21.1 Hz), 104.5 (t, *J* = 26.9 Hz), 79.9, 74.4 (d, *J* = 4.7 Hz), 71.6, 70.9, 69.5, 55.9, 55.5. **^{19}F NMR** (471 MHz, DMSO-d6) δ -107.15 (d, *J* = 8.4 Hz), -111.14 (d, *J* = 8.3 Hz). **HRMS (ESI)** m/z: $[M+H]^+$ Calcd. for $C_{23}H_{21}F_2N_6ORu$ 537.0789, found 537.0775. **Elemental Analysis**: calcd. for $C_{23}H_{20}F_2N_6ORu \cdot 1/3H_2O$ = C, 51.01; H, 3.85; N, 15.52. Found = C, 51.46; H, 3.52; N, 15.01.

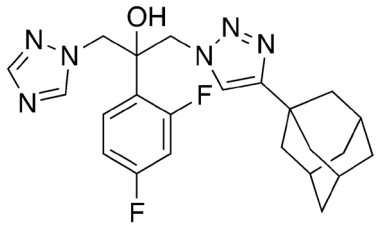

A4

Compound **A4** was prepared according to the general procedure A using azide **SS1** (0.5 mmol) and alkyne **SA4** (0.5 mmol), the crude product was chromatographed on silica (EA: hexane = 4: 1□ EA) to give compound **A4** as white solid. Yield: 68%. **IR** (cm^{-1}): 2903, 1744, 1501, 1271, 1139, 1089, 868, 675. **^{1}H NMR** (500 MHz, DMSO-d6) δ 8.32 (s, 1H), 7.81 (s, 1H), 7.49 (s, 1H), 7.25 – 7.11 (m, 2H), 7.00 – 6.79 (m, 1H), 6.38 (s, 1H), 4.87 (d, *J* = 14.4 Hz, 1H), 4.75 (d, *J* = 14.4 Hz, 1H), 4.62 (d, *J* = 14.3 Hz, 1H), 4.55 (d, *J* = 14.5 Hz, 1H), 1.99 – 1.97 (m, 3H), 1.78 (d, *J* = 2.9 Hz, 6H), 1.74 – 1.62 (m, 6H). **^{13}C NMR** (126 MHz, DMSO-d6) δ 162.1 (dd, *J* = 246.6, 12.4 Hz), 159.0 (dd, *J* = 247.2, 12.4 Hz), 155.9, 150.9, 145.2, 129.9 (d, *J* = 7.0 Hz), 123.2 (d, *J* = 11.5 Hz), 120.5, 110.8 (d, *J* = 20.4 Hz), 103.9 (t, *J* = 26.9 Hz), 73.9 (d, *J* = 4.7 Hz), 55.5 – 55.3 (m), 54.9 (d, *J* = 5.4 Hz), 42.1, 36.2, 32.0, 27.8. **^{19}F NMR** (471 MHz, DMSO-d6) δ -107.18 (d, *J* = 8.4 Hz), -111.33 (d, *J* = 8.2 Hz). **HRMS (ESI)** m/z: $[M+H]^+$ Calcd. for $C_{23}H_{27}F_2N_6O$ 441.2209, found 441.2204. **Elemental Analysis**: calcd. for $C_{23}H_{26}F_2N_6O\cdot$ ½EA = C, 61.97; H, 6.24; N, 17.34. Found = C, 62.40; H, 6.14; N, 17.81. Compound cocrystallization with ethyl acetate in a ration 1/2 was verified by crystal structure.

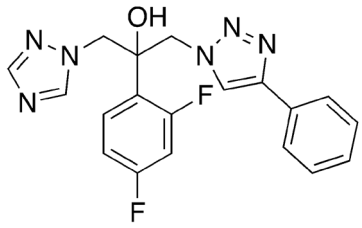

A5

Compound **A5** was prepared according to the general procedure A using azide **SS1** (1 mmol) and phenylacetylene (1 mmol), the crude product was chromatographed on silica (Ethyl acetate) to give compound **A5** as white solid. Yield: 90%. **IR** (cm^{-1}): 1619, 1497, 1275, 1149, 967, 766, 697. **^{1}H NMR** (500 MHz, DMSO-d6) δ 8.36 (s, 1H), 8.32 (s, 1H), 7.84 (s, 1H), 7.80 – 7.75 (m, 2H), 7.43 – 7.40 (m, 2H), 7.34 – 7.15 (m, 3H), 6.89 – 6.85 (m, 1H), 6.50 (s, 1H), 5.01 (d, *J* = 14.4 Hz, 1H), 4.78 (d, *J* = 14.5 Hz, 1H), 4.72 (d, *J* = 14.4 Hz, 1H), 4.64 (d, *J* = 14.5 Hz, 1H). **^{13}C NMR** (126 MHz, DMSO-d6) δ 162.1 (dd, *J* = 246.6, 12.8 Hz), 159.1 (dd, *J* = 247.0, 12.5 Hz), 151.0, 145.7, 145.3, 130.6, 129.8 (t, *J* = 7.8 Hz), 128.9, 127.8, 125.1, 123.2 (d, *J* = 13.6 Hz), 122.6, 111.0 (d, *J* = 20.8 Hz), 104.1 (t, *J* = 27.1 Hz), 73.9 (d, *J* = 5.0 Hz), 55.6 (d, *J* = 4.8 Hz),

54.9 (d, *J* = 5.3 Hz). **^{19}F NMR** (471 MHz, DMSO-d6) δ -107.11 (d, *J* = 8.2 Hz), -111.11 (d, *J* = 8.3 Hz). **HRMS (ESI)** m/z: $[M+H]^+$ Calcd. for $C_{19}H_{17}F_2N_6O$ 383.1426, found 383.1427. **Elemental Analysis**: calcd. for $C_{19}H_{16}F_2N_6O$ = C, 59.68; H, 4.22; N, 21.98. Found = C, 59.51; H, 4.07; N, 21.76.

General Procedure B

Treat appropriate substituted carboxylic acid (1 eqiv) in thionyl chloride (0.1 M) under reflux for 18 h. The solution was concentrated to yield yellow solid which was used for next step without further purification.

To a stirred mixture of amide **SS2** (1 eqiv) and triethylamine (2 eqiv) in dry THF (0.1 M), a solution of corresponding acyl chlorides (1 eqiv) in dry THF (0.1 M) were added dropwise. The resulting mixture was stirred at room temperature under nitrogen atmosphere overnight. After completion of the reaction, the solvent was removed to afford the crude product.

General Procedure C

To a solution of appropriate substituted carboxylic acid (1 eqiv) in dry dichloromethane (0.2 M), oxalyl chloride (2 eqiv) and a catalytic amount of DMF was added. The reaction mixture was stirred at 30 °C for 3h under N_2 atmosphere, the solvent was then evaporated under vacuum to obtain corresponding acyl chlorides which was further used for the next step without purification.

To a stirred mixture of amide **SS2** (1 eqiv) and triethylamine (2 eqiv) in dry dichloromethane (0.1 M), a solution of corresponding acyl chlorides (1 eqiv) in dry DCM (0.1 M) were added dropwise. The resulting mixture was stirred at room temperature under nitrogen atmosphere overnight. After completion of the reaction, the reaction was quenched with water and extracted with DCM/H_2O, the organic layer was dried and concentrated to afford the crude product.

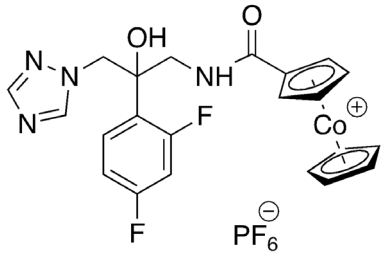

B1-PF_6

Compound **B1**-**PF_6** was prepared according to the general procedure B using carboxylic acid **SB1** (1.5 mmol) and amine **SS2** (1.5 mmol), the crude product was dissolved in saturated NH_4PF_6 methanol and stirred for 30min. After removing the methanol in vacuo, the residue was chromatographed on neutral aluminium oxide (MeCN: H_2O = 20: 1) to give the yellow solid. The yellow solid was washed by cold

water and further recrystallized from EtOH/hexane to give compound **B1**-$\mathbf{PF_6}$ as yellow solid. Yield: 50%. **^{1}H NMR** (500 MHz, DMSO-d6) δ 8.67 (t, *J* = 6.2 Hz, 1H), 8.36 (s, 1H), 7.81 (s, 1H), 7.50 – 7.45 (m, 1H), 7.28 – 7.23 (m, 1H), 7.04 – 7.00 (m, 1H), 6.22 – 6.18 (m, 2H), 5.89 (t, *J* = 2.1 Hz, 2H), 5.69 (s, 5H), 4.69 (d, *J* = 14.5 Hz, 1H), 4.62 (d, *J* = 14.5 Hz, 1H), 3.95 (dd, *J* = 14.0, 6.9 Hz, 1H), 3.63 (dd, *J* = 13.9, 5.6 Hz, 1H). **^{13}C NMR** (126 MHz, DMSO-d6) δ 162.2, 162.0 (dd, *J* = 246.1, 12.5 Hz), 159.3 (dd, *J* = 247.6, 12.4 Hz), 150.7, 145.1, 130.2 (t, *J* = 8.0 Hz), 124.7 (d, *J* = 12.5 Hz), 110.8 (d, *J* = 20.5 Hz), 104.2 (t, *J* = 27.0 Hz), 93.5, 85.9, 85.7 (d, *J* = 5.1 Hz), 84.0 (d, *J* = 34.0 Hz), 74.7 (d, *J* = 5.0 Hz), 55.0 (d, *J* = 5.5 Hz), 46.0 (d, *J* = 4.2 Hz). **^{19}F NMR** (376 MHz, DMSO-d6) δ -70.11 (d, *J* = 711.3 Hz), -106.48 – -106.54 (m), -111.68 – -111.74 (m). **^{31}P NMR** (162 MHz, DMSO-d6) δ -144.19 (hept, *J* = 711.3 Hz). **HRMS (ESI)** m/z: $[M+]^+$ Calcd. for $C_{22}H_{20}CoF_2N_4O_2$ 469.0881, found 469.0880.

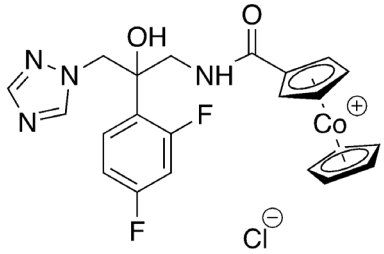

B1-Cl

Ion exchange: To a mixture slurry of compound **B1**-$\mathbf{PF_6}$ (0.46 mmol) in 10 mL methanol was added Ambelite IRA-402 (Cl) (2.32 g), after 20 min vigorously stirred, the reaction mixture became clear, and was left stirring overnight. The mixture was filtered through Buchner funnel and the filtrate was concentrated under reduced pressure. The residue was further recrystallized from EtOH/hexane to give compound **B1**-**Cl** as yellow solid. **IR** (cm^{-1}): 1660, 1563, 1497, 1417, 1120, 1095, 862,677. **^{1}H NMR** (500 MHz, DMSO-d6) δ 9.18 – 9.15 (m, 1H), 8.44 (s, 1H), 7.77 (s, 1H), 7.53 – 7.48 (m, 1H), 7.25 – 7.21 (m, 1H), 7.03 – 6.99 (m, 1H), 6.67 (s, 1H), 6.43 – 6.30 (m, 2H), 5.90 (td, *J* = 2.6, 1.5 Hz, 2H), 5.69 (s, 5H), 4.67 (s, 2H), 4.09 (dd, *J* = 13.9, 7.6 Hz, 1H), 3.57 (dd, *J* = 13.9, 4.8 Hz, 1H). **^{13}C NMR** (126 MHz, DMSO-d6) δ 161.9 (dd, *J* = 246.1, 12.4 Hz), 161.9, 159.2 (dd, *J* = 248.0, 12.2 Hz), 150.5, 145.2, 130.5 – 130.4 (m), 124.9 – 124.8 (m), 110.8 (d, *J* = 20.4 Hz), 104.0 (t, *J* = 27.0 Hz), 93.3, 85.9, 85.7 (d, *J* = 6.4 Hz), 84.3 (d, *J* = 35.9 Hz), 74.6 (d, *J* = 4.8 Hz), 55.0 (d, *J* = 5.3 Hz), 46.2 (d, *J* = 4.5 Hz). **^{19}F NMR** (376 MHz, DMSO-d6) δ -106.52 – -106.60 (m), -111.81 – -111.88 (m). **HRMS (ESI)** m/z: $[M+]^+$ Calcd. for $C_{22}H_{20}CoF_2N_4O_2$ 469.0881, found 469.0880. **Elemental Analysis**: calcd. for $C_{22}H_{20}ClCoF_2N_4O_2$ = C, 52.35; H, 3.99; N, 11.10. Found = C, 51.80; H, 3.45; N, 10.83.

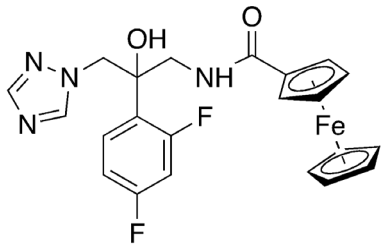

B2

Compound **B2** was prepared according to the general procedure C using ferrocenecarboxylic acid (1 mmol) and amine **SS2** (1 mmol), the crude product was chromatographed on silica gel (DCM: MeOH = 95: 5) to give compound **B2** as yellow solid. Yield: 53%. **IR** (cm^{-1}): 1612, 1545, 1271, 1129, 965, 887, 678. **^{1}H NMR** (500 MHz, DMSO-d6) δ 8.35 (s, 1H), 7.95 (t, *J* = 5.9 Hz, 1H), 7.78 (s, 1H), 7.52 – 7.47 (m, 1H), 7.26 – 7.21 (m, 1H), 7.01 – 6.97 (m, 1H), 6.69 (s, 1H), 4.73 – 4.68 (m, 2H), 4.60 (d, *J* = 14.3 Hz, 1H), 4.54 (d, *J* = 14.3 Hz, 1H), 4.33 (t, *J* = 2.0 Hz, 2H), 3.98 (s, 5H), 3.87 – 3.83 (m, 1H), 3.59 – 3.55 (m, 1H). **^{13}C NMR** (126 MHz, DMSO-d6) δ 171.8, 161.9 (dd, *J* = 245.6, 12.7 Hz), 159.0 (dd, *J* = 247.2, 12.4 Hz), 150.6, 145.1, 130.4, 125.0 (d, *J* = 13.8 Hz), 110.9 (d, *J* = 20.2 Hz), 104.0 (t, *J* = 26.9 Hz), 75.2 – 75.1 (m, two carbons were overlapped which identified in the HMBC spectrum), 70.3 (d, *J* = 6.1 Hz), 69.4, 68.3 (d, *J* = 12.0 Hz), 55.6 (d, *J* = 4.6 Hz), 46.9 (d, *J* = 4.6 Hz). **^{19}F NMR** (471 MHz, DMSO-d6) δ -107.16 (d, *J* = 7.9 Hz), -112.07 (d, *J* = 7.9 Hz). **HRMS (ESI)** m/z: $[M+H]^+$ Calcd. for $C_{22}H_{21}F_2FeN_4O_2$ 467.0977, found 467.0976. **Elemental Analysis**: calcd. for $C_{22}H_{20}F_2FeN_4O_2$ = C, 56.67; H, 4.32; N, 12.02. Found = C, 56.45; H, 4.03; N, 11.67.

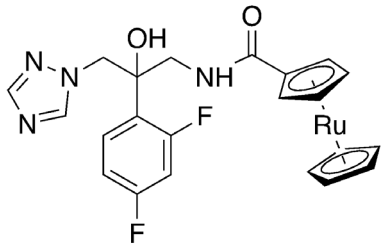

B3

Compound **B3** was prepared according to the general procedure C using carboxylic acid **SB3** (2 mmol) and amine **SS2** (2 mmol), the crude product was chromatographed on silica gel (EA: Hexane = 2: 1□ EA) to give compound **B3** as pale yellow solid. Yield: 65%. **IR** (cm^{-1}): 1614, 1544, 1270, 1140, 965, 816, 678. **^{1}H NMR** (500 MHz, DMSO-d6) δ 8.32 (s, 1H), 7.83 (t, *J* = 5.9 Hz, 1H), 7.77 (s, 1H), 7.46 – 7.41 (m, 1H), 7.24 – 7.20 (m, 1H), 7.02 – 6.98 (m, 1H), 6.57 (s, 1H), 5.08 – 5.03 (m, 2H), 4.67 – 4.65 (m, 2H), 4.57 (d, *J* = 14.3 Hz, 1H), 4.48 (d, *J* = 14.2 Hz, 1H), 4.41 (s, 5H), 3.74 – 3.70 (m, 1H), 3.56 – 3.52 (m, 1H). **^{13}C NMR** (126 MHz, DMSO-d6) δ 170.3, 161.9 (dd, *J* = 245.7, 12.7 Hz), 159.0 (dd, *J* = 247.4, 12.3 Hz), 150.6, 145.0,

130.4 – 130.2 (m), 125.0 (d, *J* = 13.6 Hz), 110.8 (d, *J* = 20.6 Hz), 104.0 (t, *J* = 26.8 Hz), 79.5, 75.2 (d, *J* = 4.8 Hz), 72.1, 71.5, 70.2, 55.4 (d, *J* = 4.8 Hz), 46.7 (d, *J* = 4.5 Hz). **^{19}F NMR** (471 MHz, DMSO-d6) δ -107.14 (d, *J* = 7.9 Hz), -112.07 (d, *J* = 8.0 Hz). **HRMS (ESI)** m/z: $[M+H]^+$ Calcd. for $C_{22}H_{21}F_2N_4O_2Ru$ 513.0677, found 513.0662. **Elemental Analysis**: calcd. for $C_{22}H_{20}F_2N_4O_2Ru$ = C, 51.66; H, 3.94; N, 10.95. Found = C, 51.71; H, 3.55; N, 10.68.

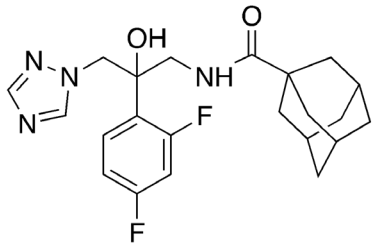

B4

Compound **B4** was prepared according to the general procedure C using1-adamantanecarboxylic acid (2 mmol) and amine **SS2** (2 mmol), the crude product was chromatographed on silica gel (DCM: MeOH = 100:3) to give compound **B4** as white solid. Yield: 93%.**IR** (cm^{-1}): 1613, 1495, 1265, 1122, 965, 850, 678. **^{1}H NMR** (500 MHz, DMSO-d6) δ 8.32 (s, 1H), 7.76 (s, 1H), 7.44 – 7.41 (m, 1H), 7.39 – 7.36 (m, 1H), 7.18 – 7.13 (m, 1H), 6.97 – 6.93 (m, 1H), 6.42 (s, 1H), 4.58 (d, *J* = 14.3 Hz, 1H), 4.48 (d, *J* = 14.2 Hz, 1H), 3.70 – 3.66 (m, 1H), 3.42 (dd, *J* = 14.0, 5.0 Hz, 1H), 1.90 – 1.89 (m, 3H), 1.65 – 1.54 (m, 12H). **^{13}C NMR** (126 MHz, DMSO-d6) δ 178.8, 161.8 (dd, *J* = 245.7, 12.4 Hz), 159.0 (dd, *J* = 247.4, 12.3 Hz), 150.5, 145.0, 130.3 – 130.1 (m), 124.8 (d, *J* = 14.1 Hz), 110.5 (d, *J* = 20.7 Hz), 103.8 (t, *J* = 26.8 Hz), 75.2 (d, *J* = 5.0 Hz), 55.2 (d, *J* = 5.5 Hz), 46.2, 39.7 (overlapping within solvent peak which identified in the HMBC spectrum), 38.4, 36.0, 27.5. **^{19}F NMR** (471 MHz, DMSO-d6) δ -106.77 (d, *J* = 8.1 Hz), -112.26 (d, *J* = 8.1 Hz). **HRMS (ESI)** m/z: $[M+H]^+$ Calcd. for $C_{22}H_{27}F_2N_4O_2$ 417.2097, found 417.2087. **Elemental Analysis**: calcd. for $C_{22}H_{26}F_2N_4O_2$ = C, 63.45; H, 6.29; N, 13.45. Found = C, 62.70; H, 6.34; N, 13.26.

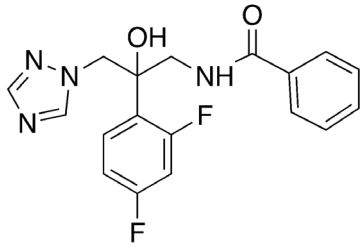

B5

Compound **B5** was prepared according to the general procedure C using benzoic acid (2 mmol) and amine **SS2** (2 mmol), the crude product was chromatographed on silica gel (EA: Hexane = 2: 1) to give compound **B5** as white solid. Yield: 89%. **IR** (cm^{-1}): 1631, 1499, 1322, 1138, 965, 853, 678. **^{1}H NMR** (500

MHz, DMSO-d6) δ 8.51 (t, *J* = 6.1 Hz, 1H), 8.34 (s, 1H), 7.76 – 7.74 (m, 3H), 7.53 – 7.50 (m, 1H), 7.46 – 7.38 (m, 3H), 7.20 – 7.15 (m, 1H), 6.94 – 6.90 (m, 1H), 6.28 (s, 1H), 4.71 (d, *J* = 14.3 Hz, 1H), 4.58 (d, *J* = 14.4 Hz, 1H), 3.83 – 3.74 (m, 2H). **^{13}C NMR** (126 MHz, DMSO-d6) δ 167.7, 161.8 (dd, *J* = 245.7, 12.7 Hz), 159.1 (dd, *J* = 247.2, 12.5 Hz), 150.5, 145.0, 133.9, 131.4, 130.1 – 129.9 (m), 128.3, 127.3, 124.8 (d, *J* = 13.8 Hz), 110.7 (d, *J* = 20.6 Hz), 103.9 (t, *J* = 27.0 Hz), 75.2 (d, *J* = 4.6 Hz), 55.1 (d, *J* = 5.6 Hz), 46.6 (d, *J* = 4.3 Hz). **^{19}F NMR** (471 MHz, DMSO-d6) δ -106.81 (d, *J* = 8.1 Hz), -112.11 (d, *J* = 8.0 Hz). **HRMS (ESI)** m/z: $[M+H]^+$ Calcd. for $C_{18}H_{17}F_2N_4O_2$ 359.1314, found 359.1314. **Elemental Analysis**: calcd. for $C_{18}H_{16}F_2N_4O_2$ = C, 60.33; H, 4.50; N, 15.64. Found = C, 60.44; H, 4.99; N, 15.31.

Experimental Section in Biological part

***In vitro* activity against *Trypanosoma cruzi* and cytotoxicity on a mammalian cell model (VERO cells)**

Parasite and culture

T. cruzi. Parasites experiments were carried out using *T. cruzi* CL Brener strain.

Epimastigotes were grown until a high proportion of metacyclic trypomastigote parasites were observed (~21 days). Trypomastigote-rich cultures were incubated overnight with a monolayer of VERO cells in a 10:1 parasite:cell ratio in RPMI medium at 37°C in a humidified 5 % CO_2 incubator. Extracellular parasites were removed the following day by aspirating cell culture media, washing the VERO cell monolayer three times with PBS, followed by addition of fresh supplemented RPMI. Trypomastigotes emerged from VERO cells (6-7 days) were used to set new VERO cell infections up.[11]

Cell-derived trypomastigotes were obtained from the supernant of infected VERO cells collected 72 h post established infection with cell-emerged trypomastigotes.

VERO cells. VERO cells (ATCC CCL81) were used as mammalian cell model for testing unspecific cytotoxicity. This cell lineage has been used as eukaryotic model in *Trypanosoma cruzi* infections.[12]

Cells were cultured in RPMI medium (Gibco) supplemented with 10 % heat inactivated fetal bovine serum, penicillin (100 units/mL) and streptomycin (100 µg/mL) at 37°C in a humidified 5 % CO_2 incubator. For maintenance, confluent cells were washed with PBS, incubated for 3 min with trypsin-EDTA (Gibco), diluted and re-plated.[13–15]

Compounds´ treatment

The compounds were initially dissolved in DMSO (stock concentration). Freshly solutions were diluted in the culture medium to obtain the different concentrations tested. Throughout the experimental procedures, the concentration of DMSO never exceeded 1%, which is non-toxic for the protozoa.[13–15]

In vitro activity against trypomastigotes of *Trypanosoma cruzi*

$5x10^6$ parasites per well were seeded in black 96 well plates in RPMI medium with increasing concentration of compounds for 24 h. Viability was tested using alamar Blue™ (Thermo Fisher), where resazurin is reduced to resofurin, a compound that is red in color and highly fluorescent. 10 µL of alamar Blue were added to each well. Black plates were incubated for 3 h at 28°C. Fluorescence (excitation 530 nm / emission 590 nm) was measured in a Thermo Scientific Varioskan® Flash Multimode instrument. Dose-response curves were recorded and the IC_{50} values were determined using GraphPad Prism version 6.00 for Windows (GraphPad Software, La Jolla California USA). The results are presented as averages ± SD (standard deviation) of three independent biological replicates.

Cytotoxicity on VERO cells

For the cytotoxicity assay, 10000 cells per well were seeded in a 96 well plate in RPMI medium and were incubated at 37 °C in a 5 % CO_2 atmosphere. Once adhered to the plate, cells were incubated with the indicated compound concentrations for 24 h. Cell viability was assessed using MTT (3-(4, 5-dimethylthiazolyl-2)-2, 5-diphenyltetrazolium bromide) assay, where MTT is reduced by metabolically active cells to generate reducing equivalents such as NADH and NADPH, resulting in the formation of an intracellular purple formazan which can be solubilized by the addition of DMSO. Briefly, 20 µL of MTT 5 mg/mL were added to each well. Plates were incubated for 4 h at 37°C in a 5 % CO_2 atmosphere. After incubation, the medium was removed and the cells were disrupted with 100 µL of DMSO. Plates were kept for 15 min with agitation and absorbance was measured at 570 nm in a Thermo Scientific Varioskan® Flash Multimode instrument. Each assay was performed three times.[13–16]

In vitro motility assays with adult female *Brugia pahangi* and adult *Trichuris muris*

The efficacy of the derivatives was tested on adult female *B. pahangi* (11 derivatives) and *T. muris* (6 derivatives) in *in vitro* inhibition of motility assays.[17-19] Briefly, a single *B. pahangi* female worm was placed into a single well of a 24-well plate (4 replicates per compound) with 500 µL of media (RPMI-1640 with 25 mM HEPES, 2.0 g/L $NaHCO_3$, 5% heat inactivated FBS, and 1X antibiotic/antimycotic solution). Worms were treated with 50 uM of compound in DMSO and incubated for 6 days at 37°C with 5% CO_2. The motility of the worms was measured using the Worminator instrument on days 0, 1, 2, 3, and 6. Each plate was recorded for 60 s to determine the number of pixels displaced by the worms per second. The percentage of inhibition of motility was calculated by dividing the mean movement units (MMUs) of treated worms by the average MMUs of the control worms (treated with 1% DMSO), then subtracting

that value from 1. The values were floored to zero and multiplied by 100%. Adult *T. muris* were assayed in the same manner as *B. pahangi* except each well contained 2 worms in culture media (4 replicates wells per compound) and the worms were treated with 100 uM of compound for 3 days.

***In vitro* activity against *Candida* strains**

The *C. albicans* reference strain SC5134 and a series of clinical isolates of *Candida* strains were tested for their susceptibility to fluconazole and the derivates. *Candida* strains were grown on Sabouraud agar medium (Sigma Aldrich, St. Louis, MO, USA) for 48 h at 30°C and resuspended in distilled water at a concentration of 1-5 x 105 CFU/ml before testing. Minimal inhibitory concentration (MIC) values for FCZ and derivates were determined following the European Committee for Antimicrobial Susceptibility Testing protocol (EUCAST Definitive Document EDef 7.3.2 Revision, 2020). Briefly, cells were grown in RPMI-1640 medium supplied with 2.0% glucose, counted and inoculated at a concentration of 1-5 x 105 CFU/ml. MIC_{50} values were detected using a spectrophotometer (at 530 nm) after 48 h of incubation, as the lowest concentration of the drug that resulted in a ≥ 50% inhibition of growth, relative to the control.

Assessment of compound toxicity using C. elegans

The wild-type Caenorhabditis elegans (*C. elegans*) Bristol strain N2 and Escherichia coli (E. coli) OP50 strain were obtained from the Caenorhabditis Genomics Center (Minneapolis, MN, USA). Worms were maintained under standard conditions at 20 °C on Nematode Growth Media (NGM) agar plates seeded with E. coli OP50 as a source of food as previously described.[20]

The method used to assess toxicity is based on worm motility according to (Simonetta and Golombek, 2007, and Risi et al 2019).[21,22] Briefly, the locomotor activity recording system, WMicrotrackerTM ONE (PhylumTech), detects infrared microbeam interruptions. Synchronized *C. elegans* worms were removed from culture plates and washed three times with M9 buffer (3 g KH2PO4; 6 g Na2HPO4; 5 g NaCl; 1 mL 1 M MgSO4 per liter) by centrifugation at 1000 g. Worms in M9 1% DMSO were then plated in 96-well flat microtiter plates (Deltalab). Approximately 70 worms per well were seeded in 60 µL M9 buffer containing 1% DMSO and their basal movement was measured for 30 minutes to normalize the movement activity for each well at the beginning of the assay. Then, compounds A1-Cl and A2 in M9 buffer 1% DMSO were added at 25 and 100 µM final concentrations in a total volume of 100 µL per well. Vehicle alone (1% DMSO) with no compound and the anthelmintic ivermectin at 2 µM were used as used as controls. The motility using WMicrotrackerTM ONE was measured at 20 °C for 18 hours. Motility

of worms with vehicle only after 18 h was considered for reference as 100% motility. Four replicas were performed for each concentration in 96-microwell plates. Three biological replicas (worms from three plates) were performed. In addition to motility, development from L1 larval worms to adult worms was assessed after 5 hours treatment of synchronized L1 with 100 µM A1-Cl, A2 or vehicle. After treatment 100 L1 were placed on NGM plates and food, and development followed for 4 days.

X-ray Crystallograyphy

Single crystal X-ray diffraction data were collected at 160(1) K on a Rigaku Oxford Diffraction Synergy-Pilatus diffractometer for **A1-Cl**, **A3**, **A4**, **A5**, **B1-PF_6** and **B4** and on a Rigaku Oxford Diffraction Supernova-Atlas diffractometer for **A1-PF_6**, **A2**, **B1-Cl**, **B3** and **B5** using the copper X-ray radiation (l = 1.54184 Å) from a dual wavelength X-ray source and an Oxford Instruments Cryo*j*et XL cooler. The provided single crystals were covered with a polybutene oil, selected and mounted on a flexible loop fixed on a goniometer head and transferred to the diffractometer. Pre-experiments, data collections, data reductions and analytical absorption corrections[23] were performed with the program suite *CrysAlisPro*.[24] Using *Olex2*,[25] the structures were solved with the *SHELXT*[26] small molecule structure solution program and refined with the *SHELXL* program package[27] by full-matrix least-squares minimization on F^2. *PLATON*[28] was used to check the result of the X-ray analyses. The crystal data collections and structure refinement parameters are shown in Tables S1 – S6 . CCDC 2118250 (for **A1-PF_6**), CCDC 2118251 (for **A1-Cl**), CCDC 2118252 (for **A2**), CCDC 2118253 (for **A3**), CCDC 2118254 (for **A4**), CCDC 2118255 (for **A5**), CCDC 2118256 (for **B1-PF_6**), CCDC 2118257 (for **B3**), CCDC 2118258 (for **B4**), CCDC 2118259 (for **B5**), and CCDC 2118260 (for **B1-Cl**) contain the supplementary crystallographic data for these compounds, and can be obtained free of charge from the Cambridge Crystallographic Data Centre via www.ccdc.cam.ac.uk/data_request/cif. In the crystal structure of **A3**, solvent molecules of isopropanol cocrystallized with the main species in a ratio 1:1. The terminal triazole ring is disordered over two sets of positions with site-occupancy factors of 0.11(4) and 0.89(4). In the crystal structure of **A4**, solvent molecules of ethyl acetate cocrystallized with the main species in a ratio 1:2. In the asymmetric unit, the solvent molecule lies around a two-fold axis and is disordered over two sets of positions with a site occupancy factor of 0.5. In the crystal structure of **B1-PF_6**, four fluorido atoms of the PF_6^- anions are disordered over two sets of positions with site-occupancy factors of 0.343(8) and 0.657(8).

Table S1. Selected crystal data and structure refinement parameters for **A1-PF_6** and **A1-Cl**.

	A1-PF_6	A1-Cl
CCDC number	2118250	2118251
Empirical formula	$C_{23}H_{21}CoF_6N_3OP$	$C_{23}H_{21}ClCoF_2N_3O$
Formula weight	638.35	528.83
Temperature/K	160(1)	160(1)
Crystal system	monoclinic	monoclinic
Space group	C2/c	P2$_1$/n
a/Å	21.8677(4)	11.94434(18)
b/Å	9.4687(1)	8.46728(13)
c/Å	25.9372(6)	22.8388(3)
α/°	90	90
β/°	111.706(2)	104.8028(14)
γ/°	90	90
Volume/Å^3	4989.72(17)	2233.17(6)
Z	8	4
ρ_{calc}g/cm^3	1.700	1.573
μ/mm^{-1}	6.844	7.533
F(000)	2576.0	1080.0
Crystal size/mm^3	0.31 × 0.21 × 0.03	0.22 × 0.17 × 0.03
Radiation	Cu Kα (λ = 1.54184)	Cu Kα (λ = 1.54184)
2Θ range for data collection/°	7.3 to 152.8	7.7 to 149.0
Index ranges	-20 ≤ h ≤ 27, -11 ≤ k ≤ 11, -32 ≤ l ≤ 32	-14 ≤ h ≤ 14, -10 ≤ k ≤ 10, ≤ l ≤ 28
Reflections collected	26318	25039
Independent reflections	5188 [R_{int} = 0.0291, R_{sigma} = 0.0205]	4576 [R_{int} = 0.0387, R_{sigma} = 0.02
Data/restraints/parameters	5188/0/362	4576/0/311
Goodness-of-fit on F^2	1.075	1.050
Final R indexes [I>=2σ (I)]	R_1 = 0.0374, wR_2 = 0.0954	R_1 = 0.0296, wR_2 = 0.0750
Final R indexes [all data]	R_1 = 0.0390, wR_2 = 0.0966	R_1 = 0.0346, wR_2 = 0.0777
Largest diff. peak/hole / e Å^{-3}	0.40/-0.36	0.24/-0.30

Table S2. Selected crystal data and structure refinement parameters for **A2** and **A3**.

	A2	A3
CCDC number	2118252	2118253
Empirical formula	$C_{25}H_{20}F_2FeN_4O$	$C_{23}H_{22}F_6N_6ORu$, C_3H_6O
Formula weight	490.30	595.61
Temperature/K	160(1)	160(1)
Crystal system	monoclinic	orthorhombic
Space group	$P2_1/c$	$Pca2_1$
a/Å	10.7742(1)	14.5104(3)
b/Å	13.9956(2)	15.7747(3)
c/Å	13.9629(2)	10.8718(3)
α/°	90	90
β/°	94.692(1)	90
γ/°	90	90
Volume/Å^3	2098.43(5)	2488.52(10)
Z	4	4
ρ_{calc}g/cm^3	1.552	1.590
μ/mm^{-1}	6.180	5.545
F(000)	1008.0	1216.0
Crystal size/mm^3	0.11 × 0.10 × 0.05	0.10 × 0.05 × 0.02
Radiation	Cu Kα (λ = 1.54184)	Cu Kα (λ = 1.54184)
2Θ range for data collection/°	8.2 to 149.0	5.6 to 149.0
Index ranges	-13 ≤ h ≤ 13, -17 ≤ k ≤ 17, -15 ≤ l ≤ 17	-17 ≤ h ≤ 18, -11 ≤ k ≤ 19, ≤ l ≤ 13
Reflections collected	21908	25691
Independent reflections	4292 [R_{int} = 0.0243, R_{sigma} = 0.0156]	4944 [R_{int} = 0.0338, R_{sigma} = 0.02
Data/restraints/parameters	4292/0/302	4944/367/376
Goodness-of-fit on F^2	1.046	1.114
Final R indexes [I>=2σ (I)]	R_1 = 0.0257, wR_2 = 0.0681	R_1 = 0.0709, wR_2 = 0.1824
Final R indexes [all data]	R_1 = 0.0275, wR_2 = 0.0695	R_1 = 0.0722, wR_2 = 0.1836
Largest diff. peak/hole / e Å^{-3}	0.32/-0.35	2.40/-2.11
Flack parameter	-	0.05(3)

Table S3. Selected crystal data and structure refinement parameters for **A4** and **A5**.

	A4	A5
CCDC number	2118254	2118255
Empirical formula	$C_{28}H_{25}F_2N_5O$, $0.5(C_4H_8O_2)$	$C_{18}H_{16}F_3N_6O$
Formula weight	484.55	382.38
Temperature/K	160(1)	160(1)
Crystal system	monoclinic	tetragonal
Space group	I2/a	$P4_2$
a/Å	12.5942(2)	10.50361(5)
b/Å	15.9761(2)	10.50361(5)
c/Å	23.8181(3)	16.99755(12)
α/°	90	90
β/°	93.723(1)	90
γ/°	90	90
Volume/Å^3	4782.23(11)	1875.27(2)
Z	8	4
ρ_{calc}g/cm^3	1.346	1.354
μ/mm^{-1}	0.821	0.865
F(000)	2048.0	792.0
Crystal size/mm^3	0.13 × 0.03 × 0.02	0.18 × 0.07 × 0.07
Radiation	Cu Kα (λ = 1.54184)	Cu Kα (λ = 1.54184)
2Θ range for data collection/°	6.7 to 149.0	8.418 to 148.536
Index ranges	-14 ≤ h ≤ 15, -17 ≤ k ≤ 19, -29 ≤ l ≤ 29	-13 ≤ h ≤ 11, -9 ≤ k ≤ 13, -l ≤ 21
Reflections collected	25916	19895
Independent reflections	4877 [R_{int} = 0.0312, R_{sigma} = 0.0241]	3832 [R_{int} = 0.0192, R_{sigma} = 0.01
Data/restraints/parameters	4877/68/349	3832/1/257
Goodness-of-fit on F^2	1.049	1.061
Final R indexes [I>=2σ (I)]	R_1 = 0.0403, wR_2 = 0.1054	R_1 = 0.0249, wR_2 = 0.0619
Final R indexes [all data]	R_1 = 0.0456, wR_2 = 0.1088	R_1 = 0.0253, wR_2 = 0.0625
Largest diff. peak/hole / e Å^{-3}	0.32/-0.33	0.08/-0.18
Flack parameter	-	0.01(3)

Table S4. Selected crystal data and structure refinement parameters for **B1-PF_6** and **B1-Cl**.

	B1-PF_6	**B1-Cl**
CCDC number	2118256	2118260
Empirical formula	$C_{29}H_{28}CoF_6N_4O_2P$	$C_{29}H_{28}ClCoF_2N_4O_2$
Formula weight	614.32	504.80
Temperature/K	160(1)	160(1)
Crystal system	monoclinic	triclinic
Space group	P2$_1$/n	P-1
a/Å	10.0854(1)	8.5421(3)
b/Å	10.0322(1)	9.4418(2)
c/Å	23.9807(2)	13.4518(3)
α/°	90	95.807(2)
β/°	98.085(1)	102.451(2)
γ/°	90	97.882(2)
Volume/Å^3	2402.22(4)	1039.77(5)
Z	4	2
ρ_{calc}g/cm^3	1.699	1.612
μ/mm^{-1}	7.086	8.065
F(000)	1240.0	516.0
Crystal size/mm^3	0.31 × 0.1 × 0.07	0.11 × 0.09 × 0.04
Radiation	Cu Kα (λ = 1.54184)	Cu Kα (λ = 1.54184)
2Θ range for data collection/°	7.4 to 149.0	6.8 to 149.0
Index ranges	-12 ≤ h ≤ 12, -6 ≤ k ≤ 12, -29 ≤ l ≤ 29	-10 ≤ h ≤ 10, -11 ≤ k ≤ 11, ≤ l ≤ 16
Reflections collected	25912	21055
Independent reflections	4914 [R_{int} = 0.0334, R_{sigma} = 0.0234]	4242 [R_{int} = 0.0356, R_{sigma} = 0.02
Data/restraints/parameters	4914/148/386	4242/0/297
Goodness-of-fit on F^2	1.035	1.042
Final R indexes [I>=2σ (I)]	R_1 = 0.0447, wR_2 = 0.1205	R_1 = 0.0378, wR_2 = 0.0994
Final R indexes [all data]	R_1 = 0.0479, wR_2 = 0.1232	R_1 = 0.0409, wR_2 = 0.1017
Largest diff. peak/hole / e Å^{-3}	0.70/-0.60	0.50/-0.47

Table S5. Selected crystal data and structure refinement parameters for **B3** and **B4**.

	B3	**B4**
CCDC number	2118257	2118258
Empirical formula	$C_{22}H_{20}F_2N_4O_2Ru$	$C_{22}H_{26}F_2N_2O_2$
Formula weight	511.49	416.47
Temperature/K	160(1)	160(1)
Crystal system	tetragonal	monoclinic
Space group	$P4_2bc$	$P2_1/n$
a/Å	22.53915(12)	8.2885(1)
b/Å	22.53915(12)	20.4119(3)
c/Å	8.04515(8)	12.2818(2)
α/°	90	90
β/°	90	100.368(1)
γ/°	90	90
Volume/Å^3	4087.04(6)	2043.96(5)
Z	8	4
ρ_{calc}g/cm^3	1.663	1.353
μ/mm^{-1}	6.613	0.840
F(000)	2064.0	880.0
Crystal size/mm^3	0.15 × 0.06 × 0.06	0.4 × 0.25 × 0.06
Radiation	Cu Kα (λ = 1.54184)	Cu Kα (λ = 1.54184)
2Θ range for data collection/°	5.5 to 149.0	8.5 to 149.0
Index ranges	-19 ≤ h ≤ 28, -28 ≤ k ≤ 28, -9 ≤ l ≤ 9	-10 ≤ h ≤ 10, -25 ≤ k ≤ 25, ≤ l ≤ 15
Reflections collected	36905	22013
Independent reflections	4143 [R_{int} = 0.0349, R_{sigma} = 0.0168]	4179 [R_{int} = 0.0223, R_{sigma} = 0.01
Data/restraints/parameters	4143/3/288	4179/0/280
Goodness-of-fit on F^2	1.081	1.023
Final R indexes [I>=2σ (I)]	R_1 = 0.0209, wR_2 = 0.0534	R_1 = 0.0339, wR_2 = 0.0892
Final R indexes [all data]	R_1 = 0.0220, wR_2 = 0.0541	R_1 = 0.0360, wR_2 = 0.0906
Largest diff. peak/hole / e Å^{-3}	0.67/-0.53	0.27/-0.15
Flack parameter	-0.019(3)	-

Table S6. Selected crystal data and structure refinement parameters for **B5**.

	B5
CCDC number	2118259
Empirical formula	$C_{18}H_{16}F_2N_2O_2$
Formula weight	358.35
Temperature/K	160(1)
Crystal system	monoclinic
Space group	I2/a
a/Å	20.9428(3)
b/Å	8.63250(10)
c/Å	19.8001(3)
α/°	90
β/°	107.323(2)
γ/°	90
Volume/Å^3	3417.27(9)
Z	8
ρ_{calc}g/cm^3	1.393
μ/mm^{-1}	0.919
F(000)	1488.0
Crystal size/mm^3	0.26 × 0.15 × 0.05
Radiation	Cu Kα (λ = 1.54184)
2Θ range for data collection/°	8.8 to 149.0
Index ranges	-26 ≤ h ≤ 25, -7 ≤ k ≤ 10, -24 ≤ l ≤ 24
Reflections collected	16473
Independent reflections	3483 [R_{int} = 0.0161, R_{sigma} = 0.0105]
Data/restraints/parameters	3483/0/243
Goodness-of-fit on F^2	1.140
Final R indexes [I>=2σ (I)]	R_1 = 0.0394, wR_2 = 0.1008
Final R indexes [all data]	R_1 = 0.0411, wR_2 = 0.1021
Largest diff. peak/hole / e Å^3	0.20/-0.18

NMR spectra of compounds

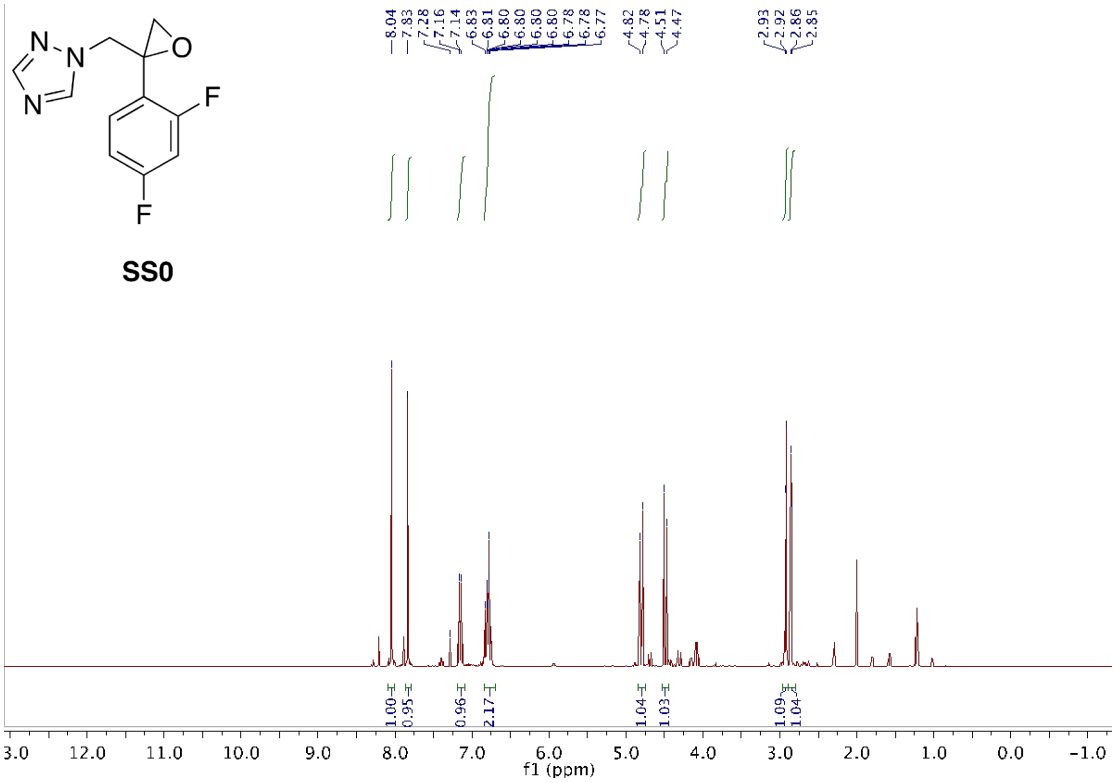

Figure S1 ^{1}H NMR spectrum of **SS0**

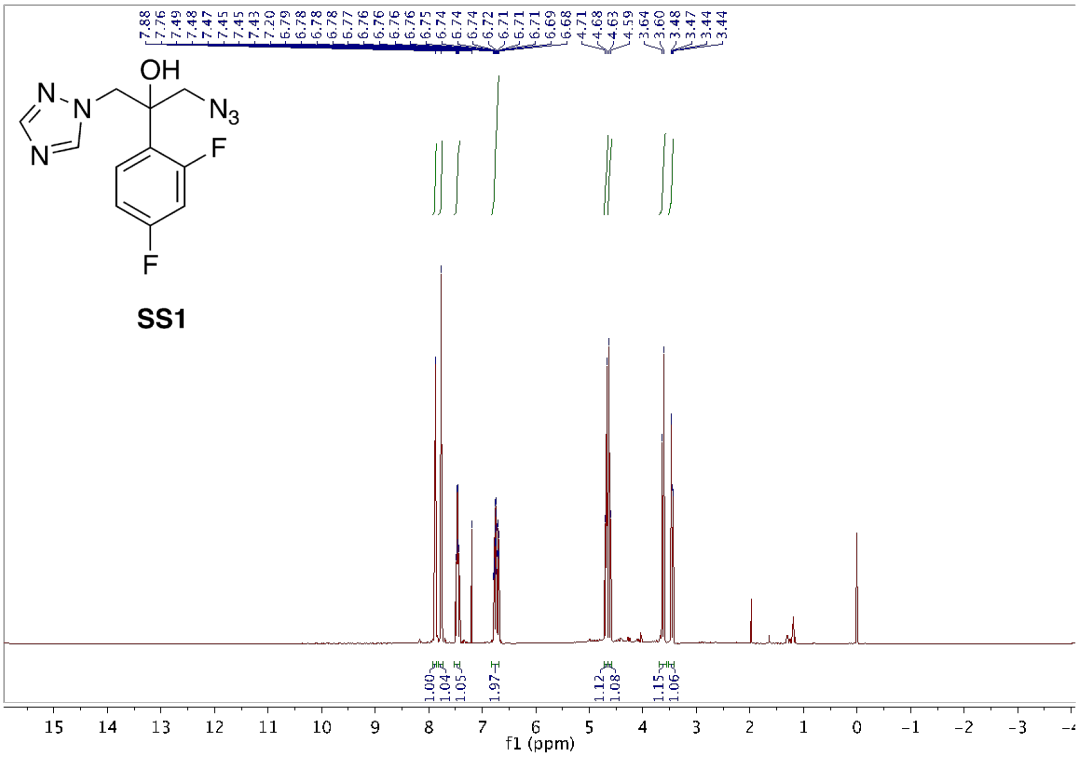

Figure S2 ^{1}H NMR spectrum of **SS1**

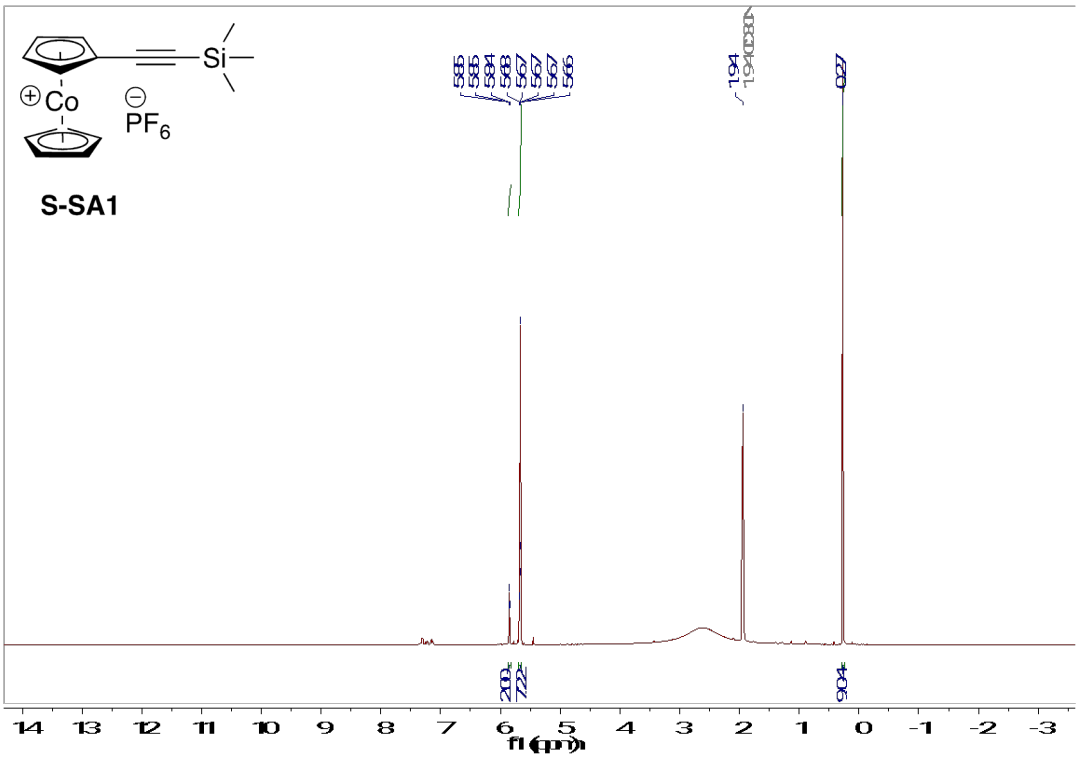

Figure S3 ^{1}H NMR spectrum of **S-SA1**

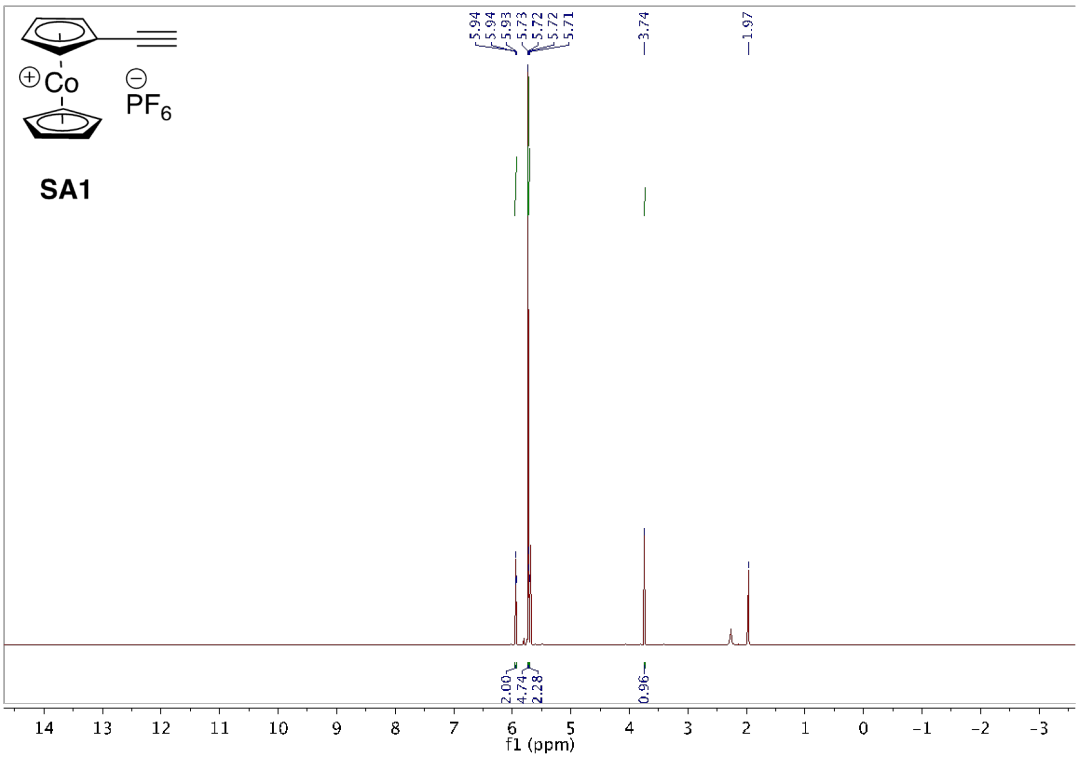

Figure S4 ^{1}H NMR spectrum of **SA1**

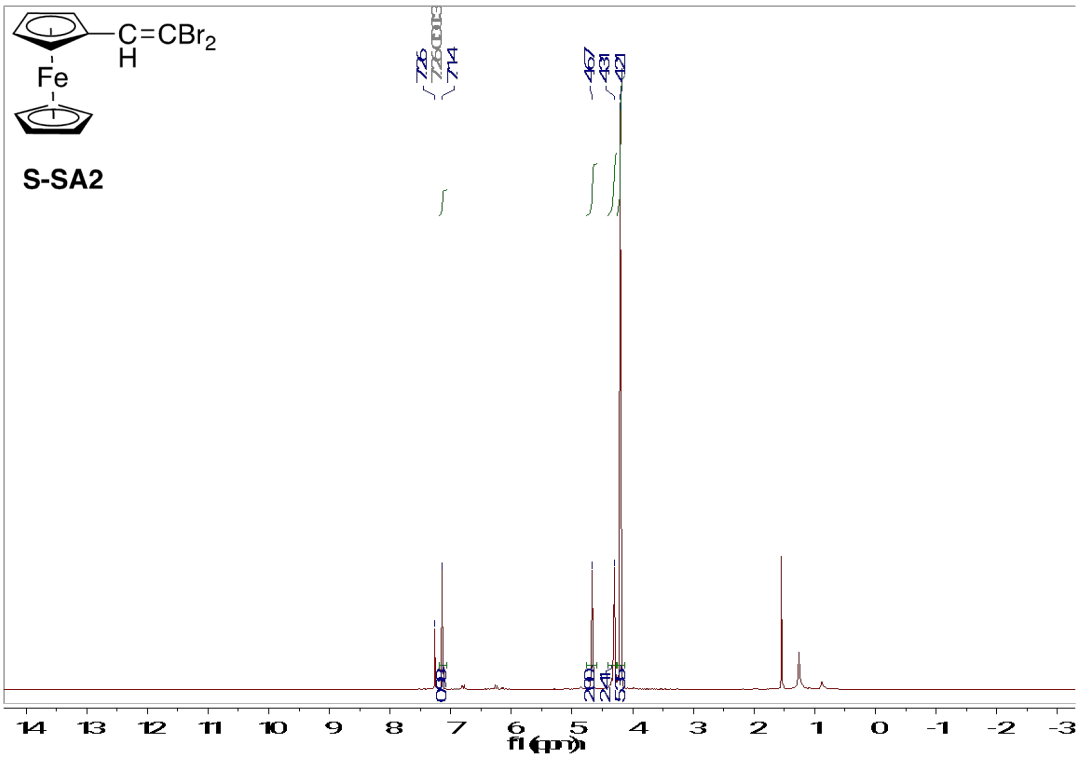

Figure S5 ^{1}H NMR spectrum of **S-SA2**

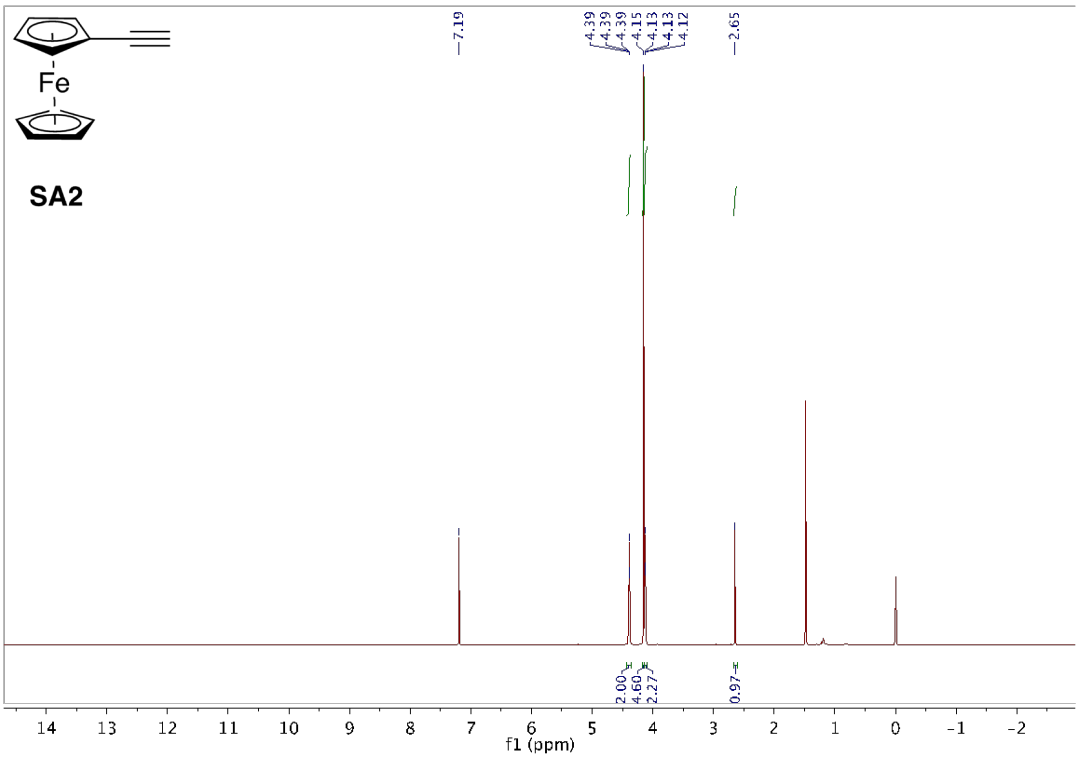

Figure S6 ^{1}H NMR spectrum of **SA2**

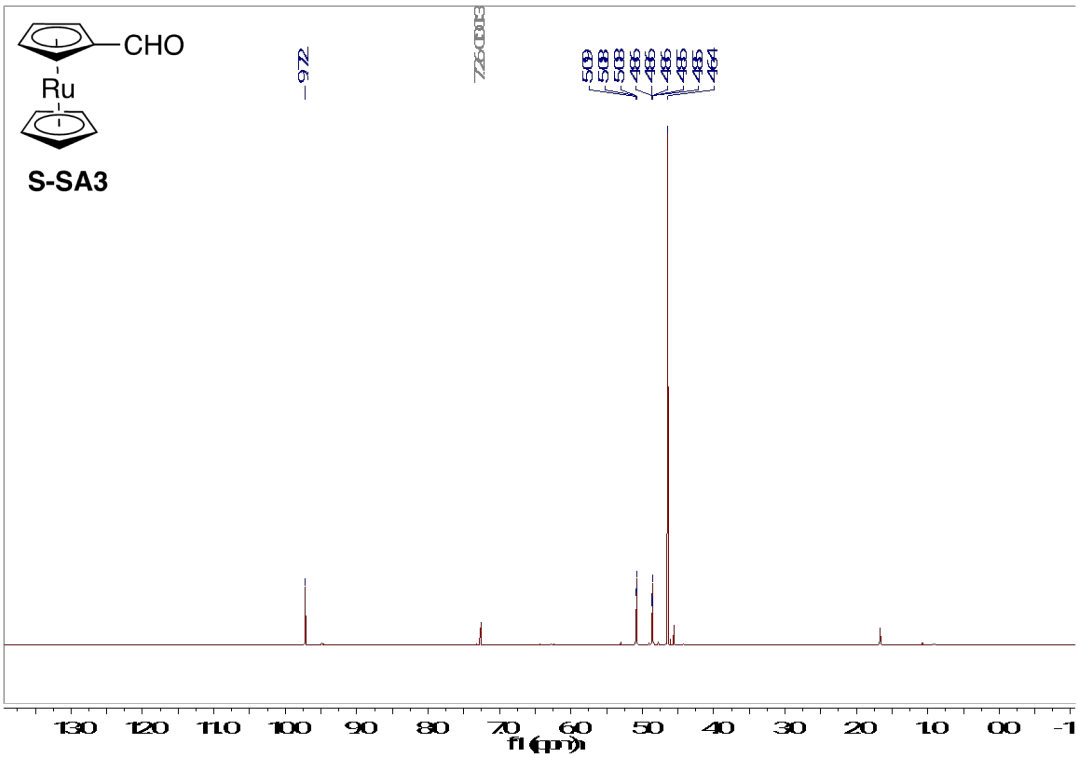

Figure S7 ^{1}H NMR spectrum of **S-SA3**

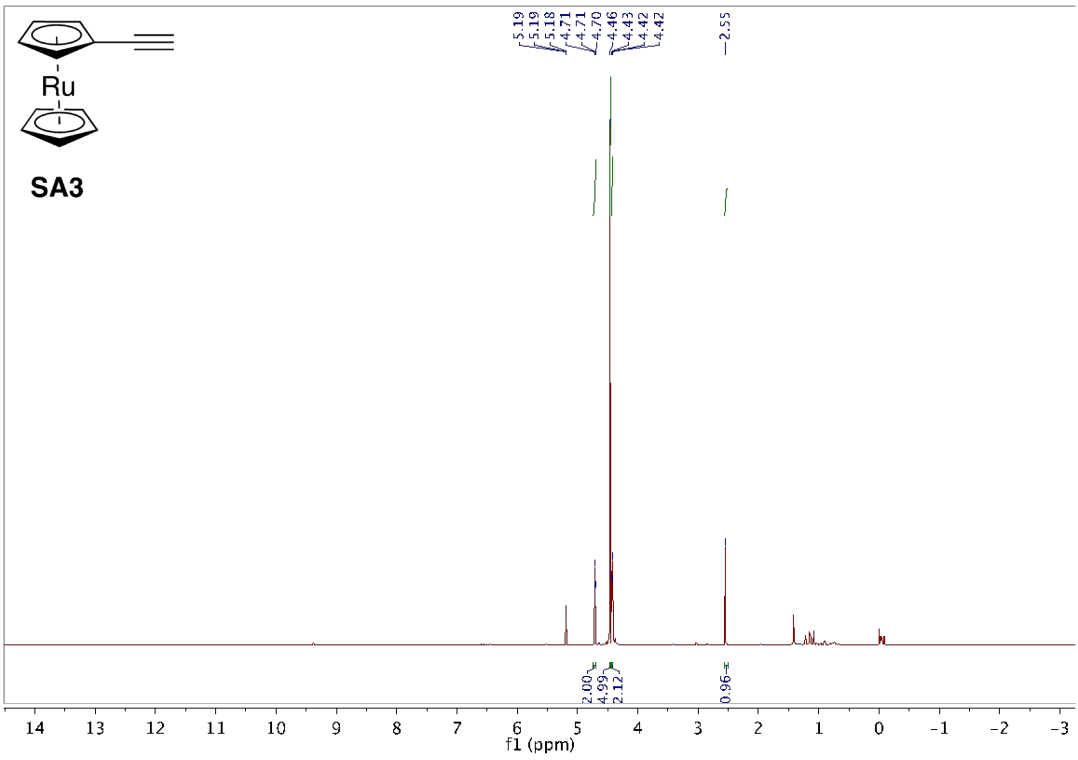

Figure S8 ^{1}H NMR spectrum of **SA3**

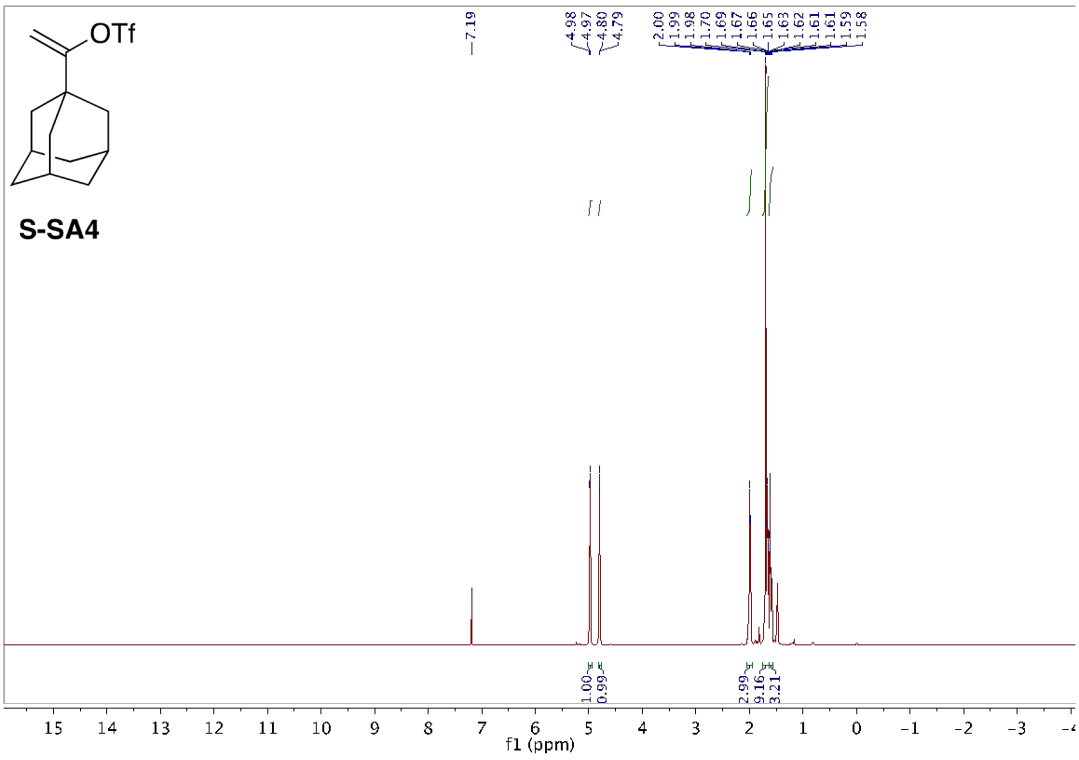

Figure S9 ^{1}H NMR spectrum of **S-SA4**

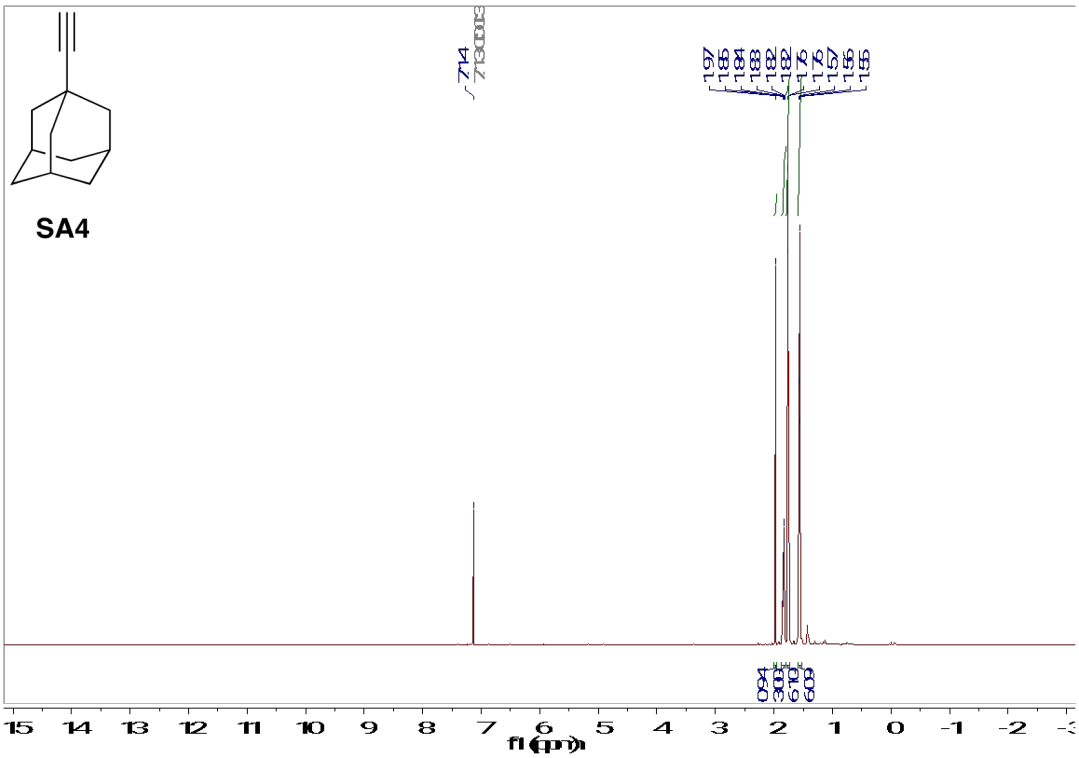

Figure S10 ^{1}H NMR spectrum of **SA4**

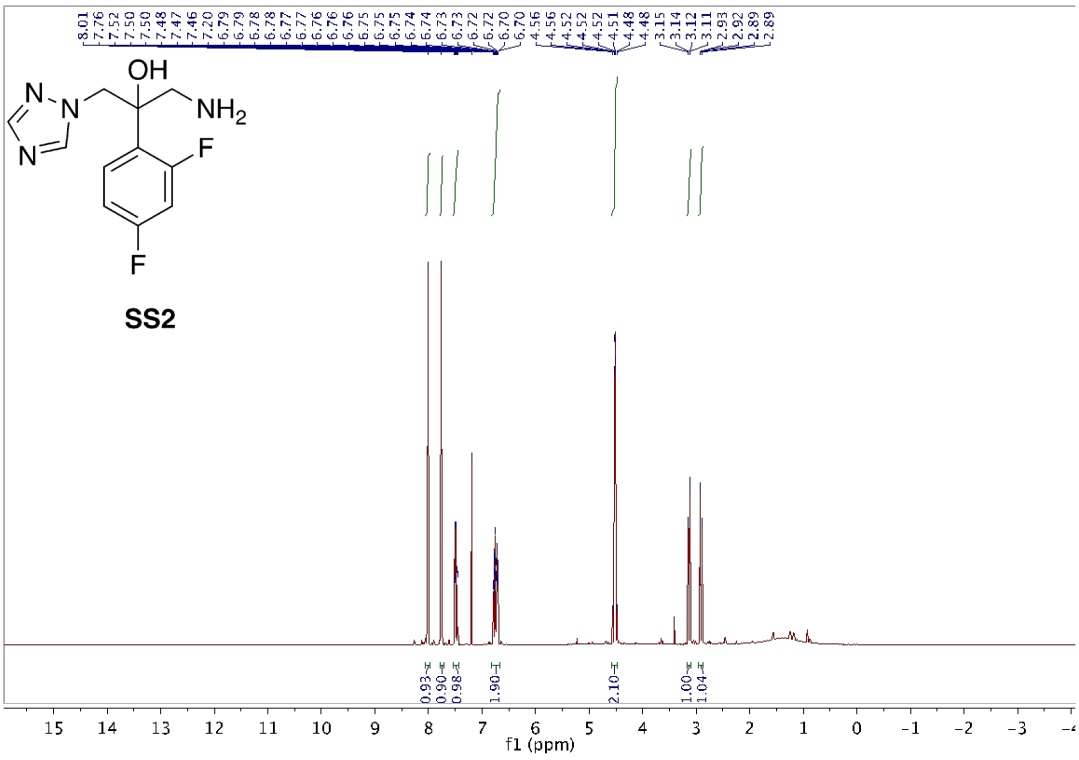

Figure S11 ^{1}H NMR spectrum of **SS2**

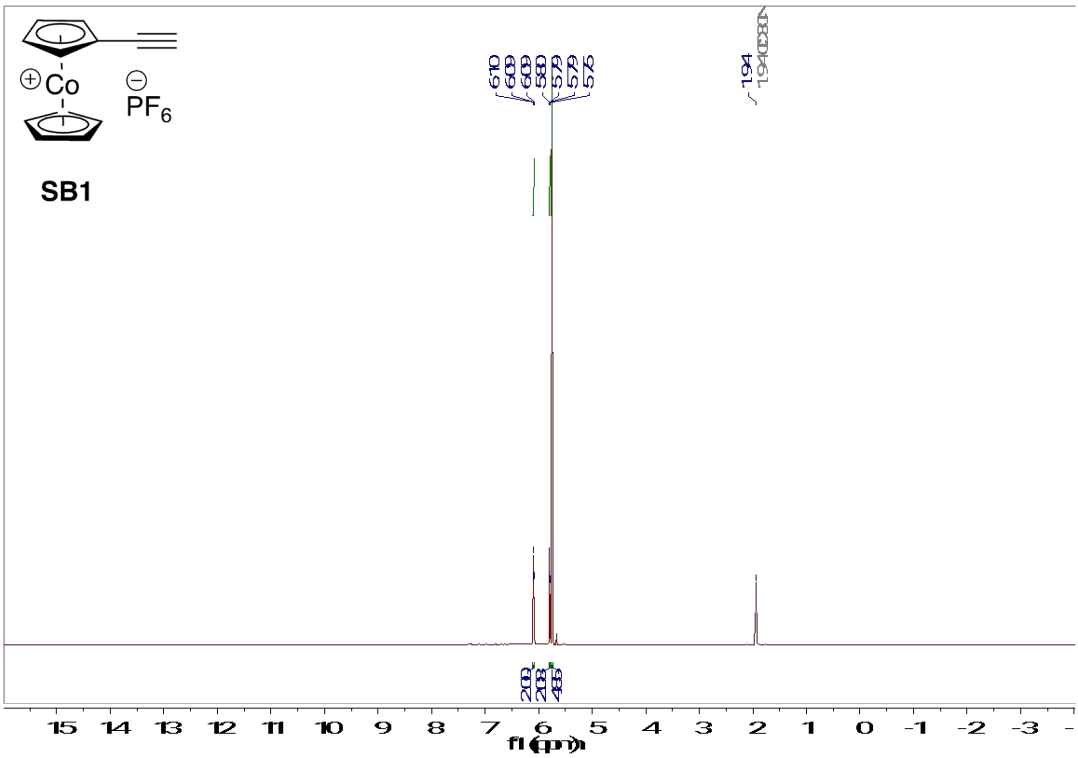

Figure S12 ^{1}H NMR spectrum of **SB1**

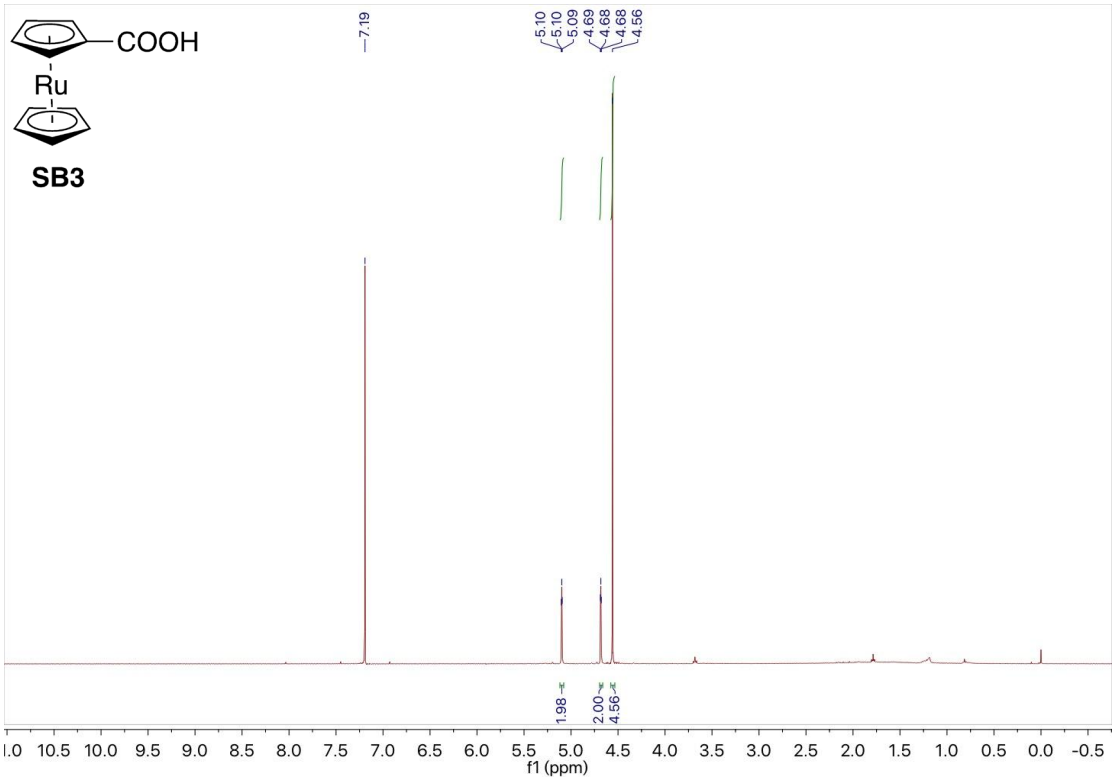

Figure S13 ^{1}H NMR spectrum of **SB3**

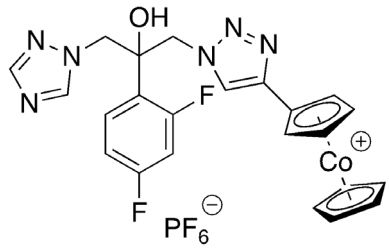

A1-PF$_6$

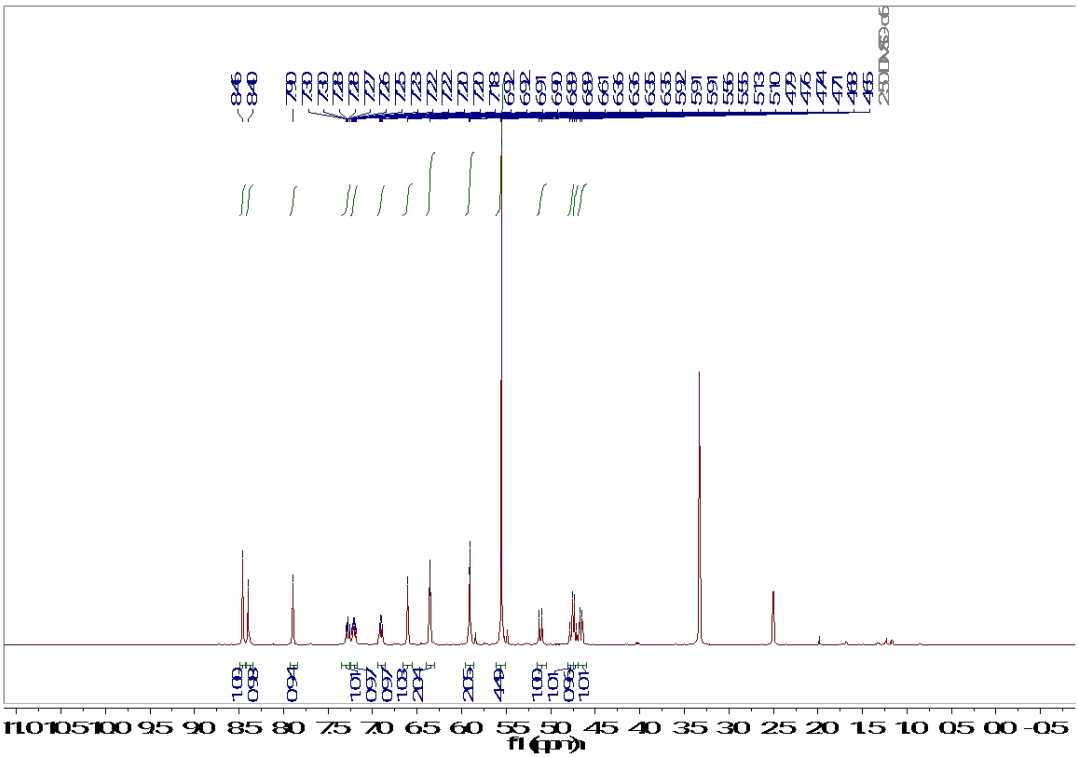

Figure S14 ^{1}H NMR spectrum of **A1-PF$_6$**

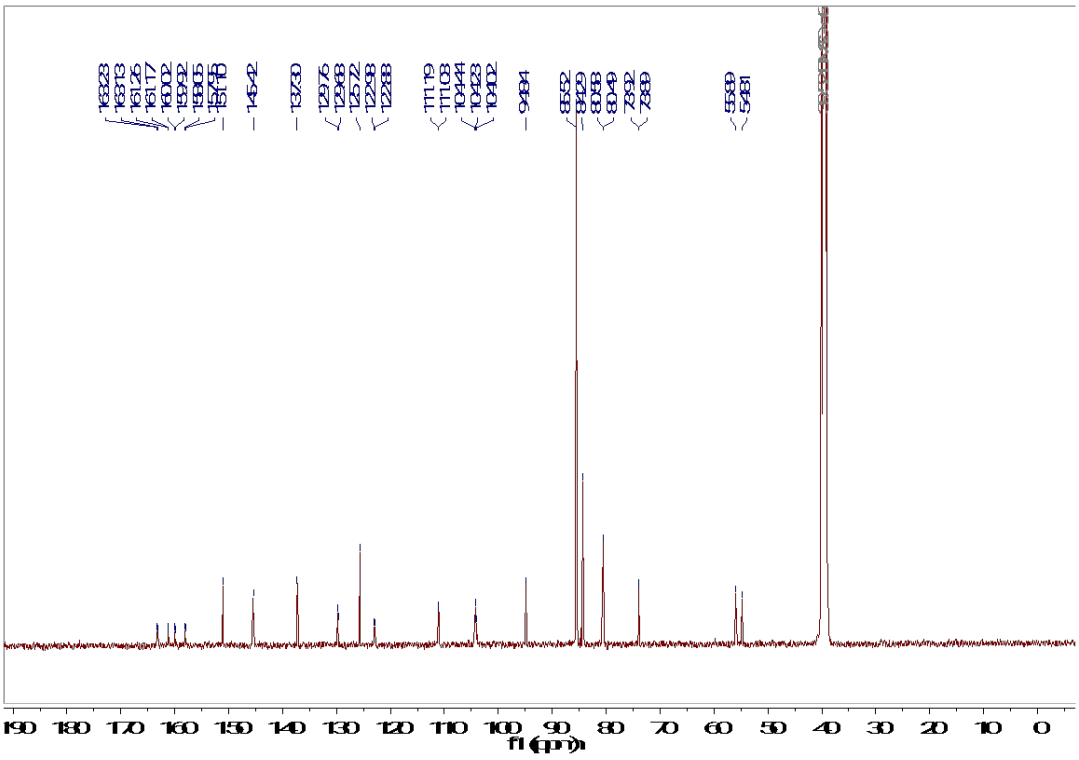

Figure S15 ^{13}C NMR spectrum of **A1-PF$_6$**

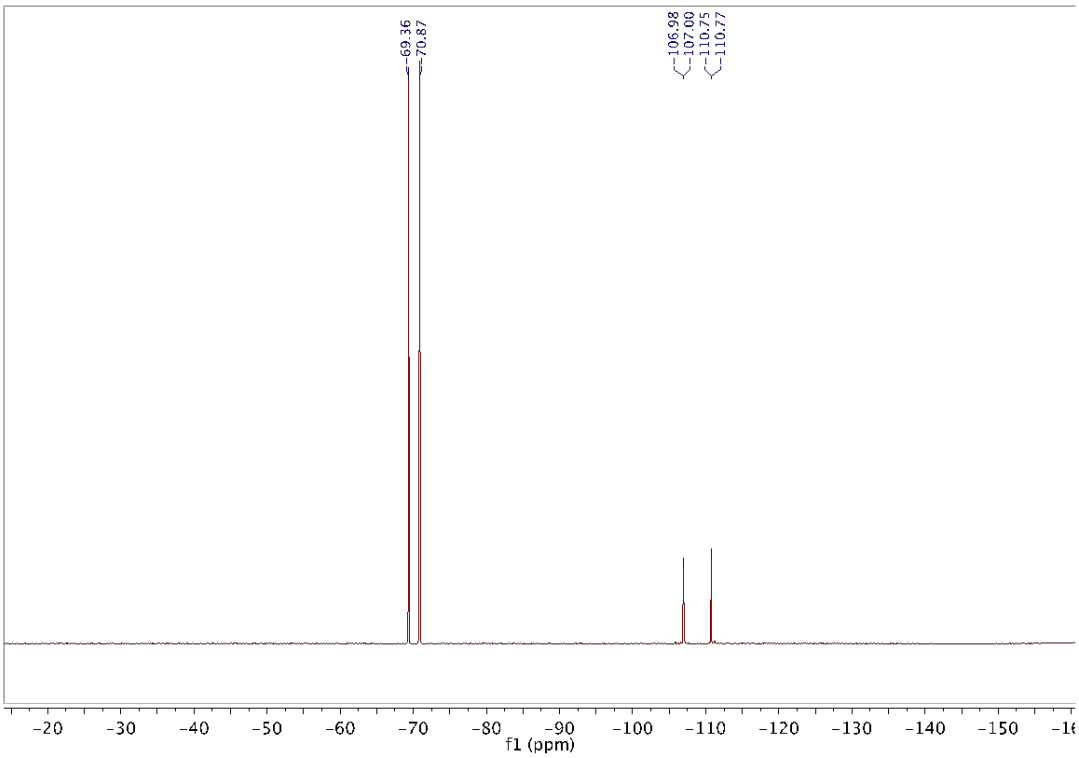

Figure S16 ^{19}F NMR spectrum of **A1-PF$_6$**

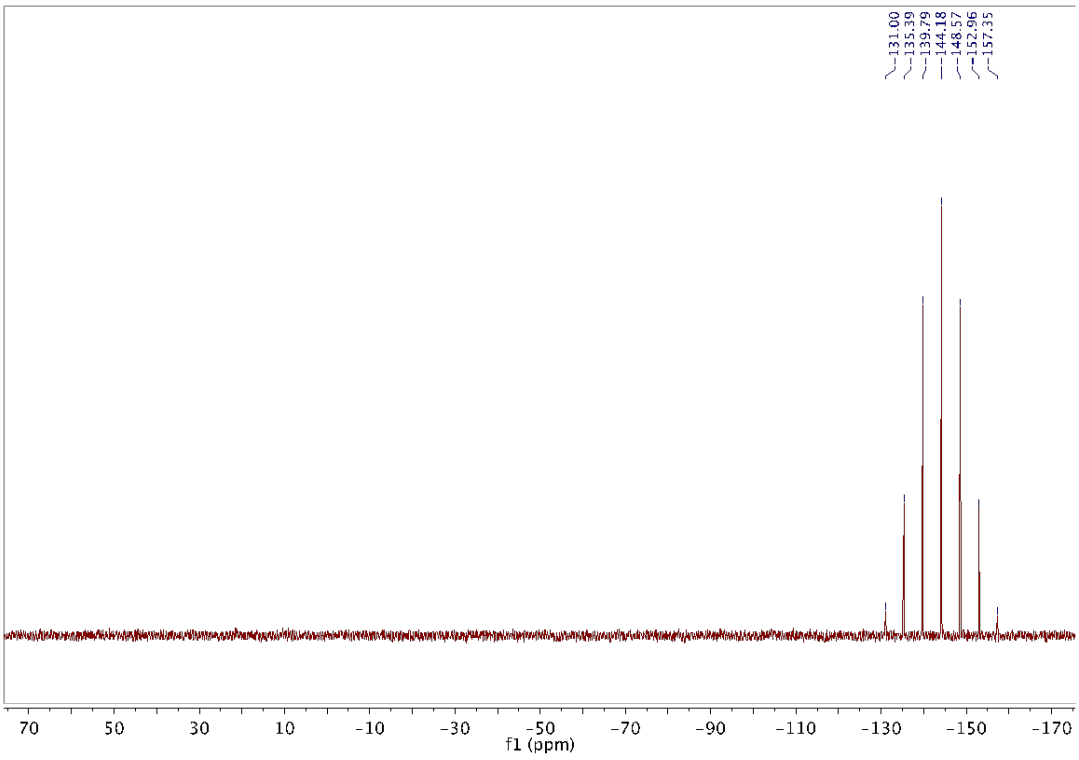

Figure S17 ^{31}P NMR spectrum of **A1-PF$_6$**

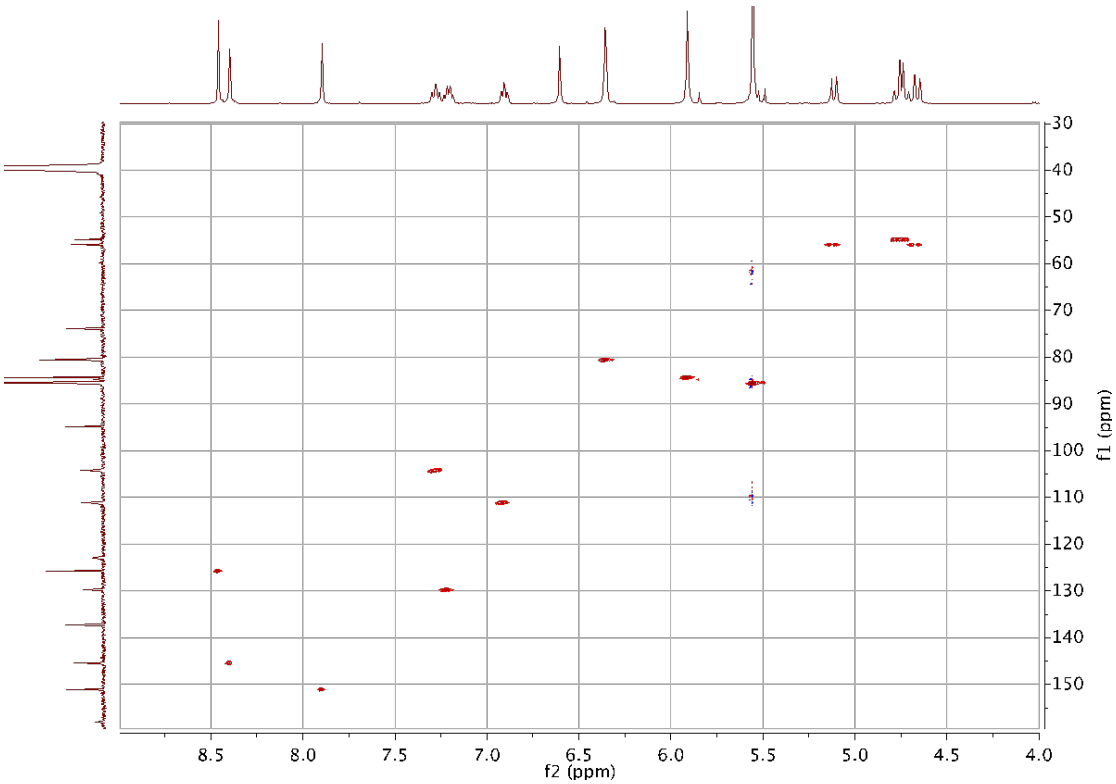

Figure S18 HSQC spectrum of **A1-PF_6** in DMSO-D6

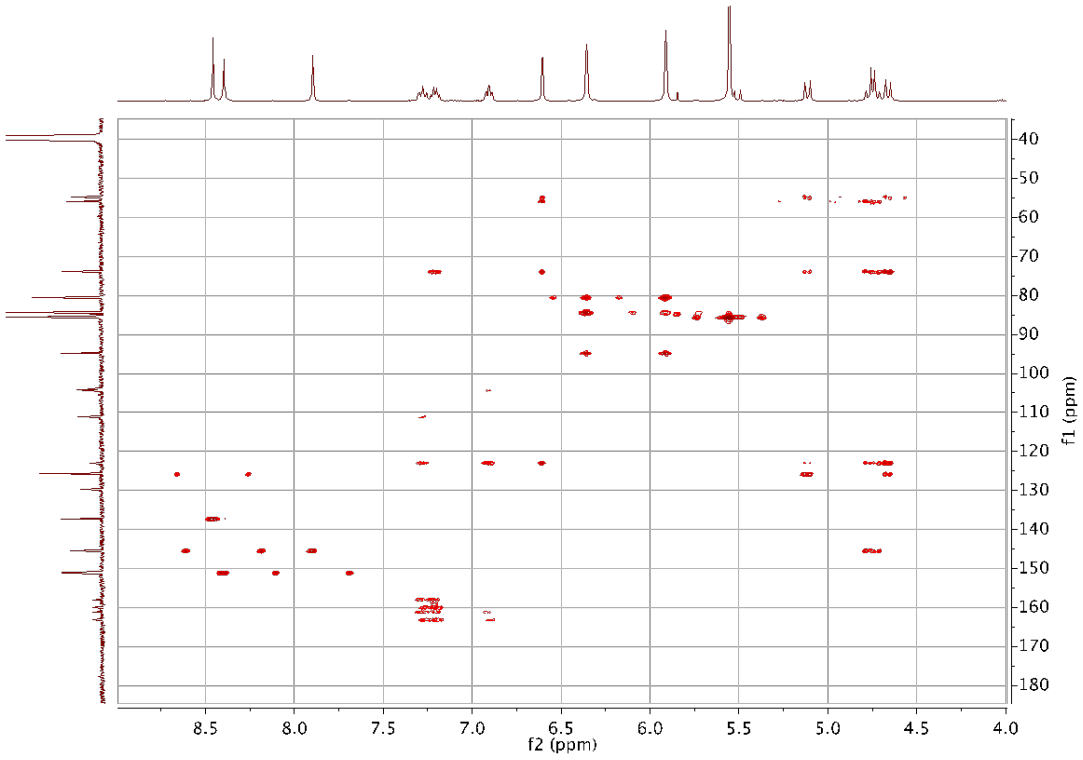

Figure S19 HMBC spectrum of **A1-PF_6** in DMSO-D6

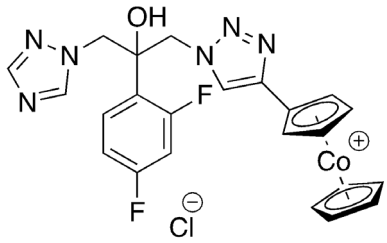

A1-Cl

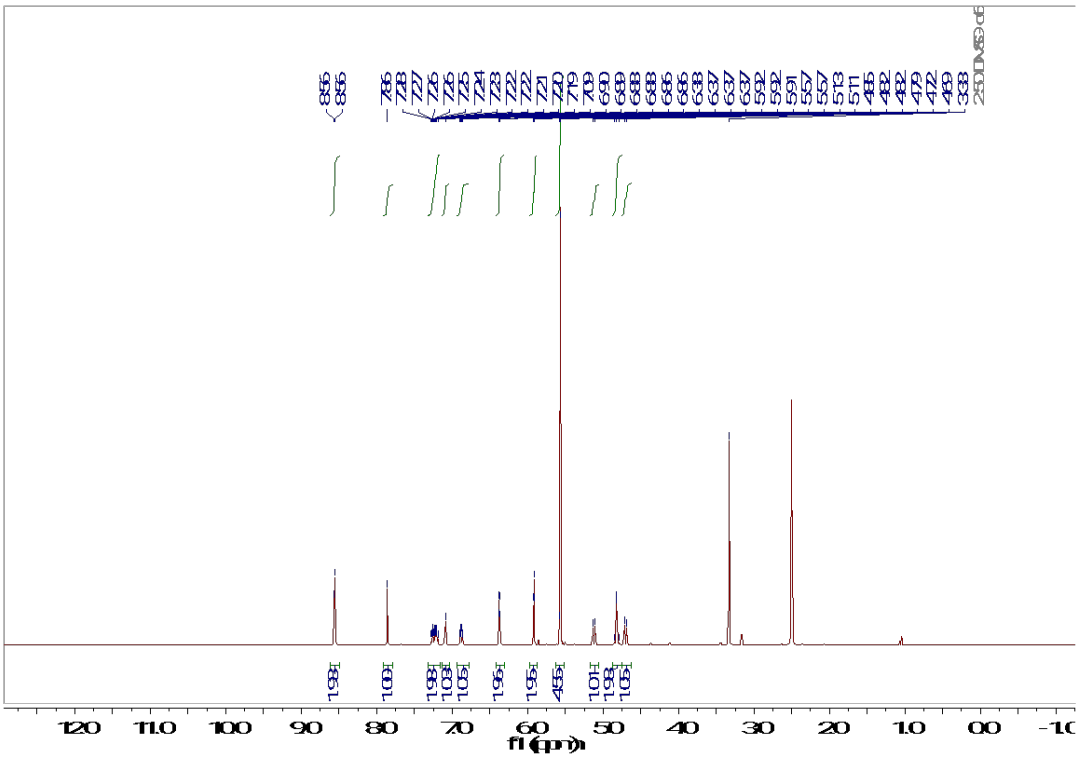

Figure S20 ^{1}H NMR spectrum of **A1-Cl**

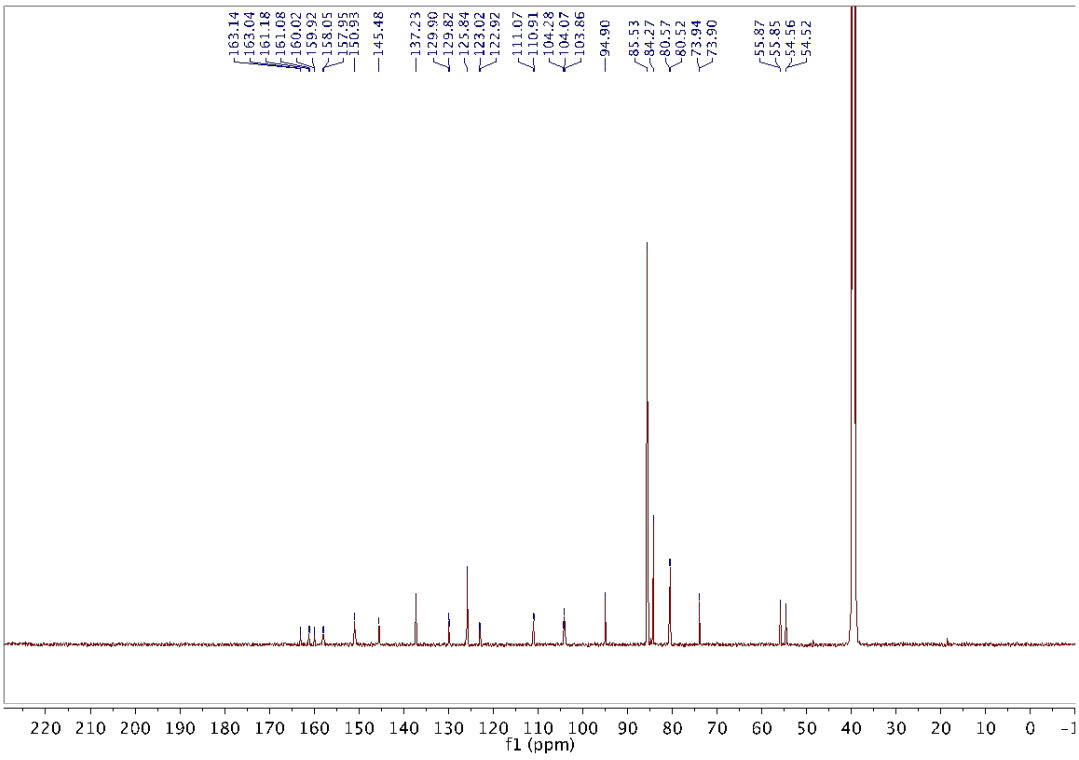

Figure S21 ^{13}C NMR spectrum of **A1-Cl**

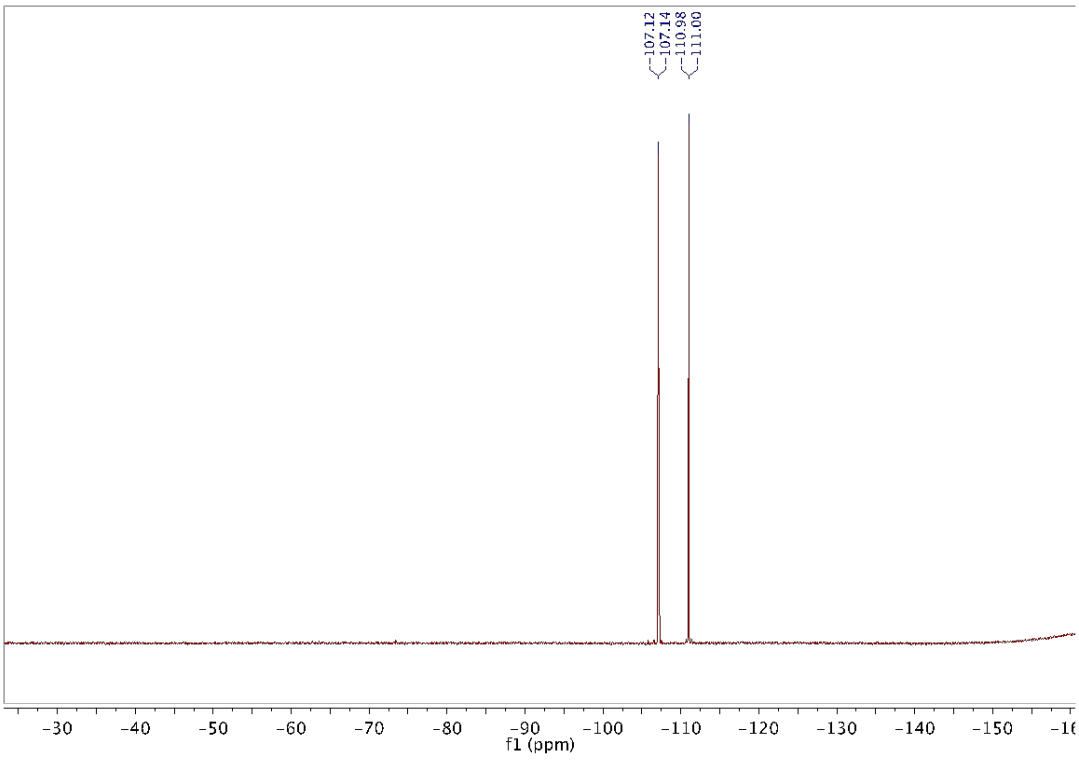

Figure S22 ^{19}F NMR spectrum of **A1-Cl**

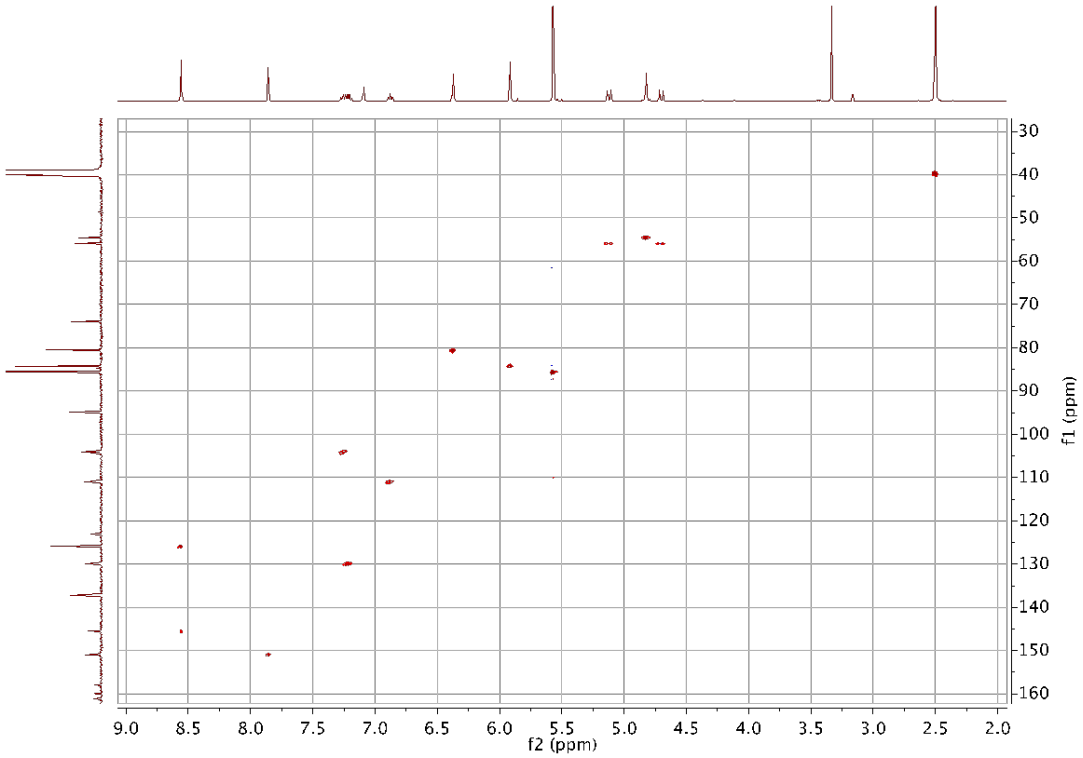

Figure S23 HSQC spectrum of **A1-Cl** in DMSO-D6

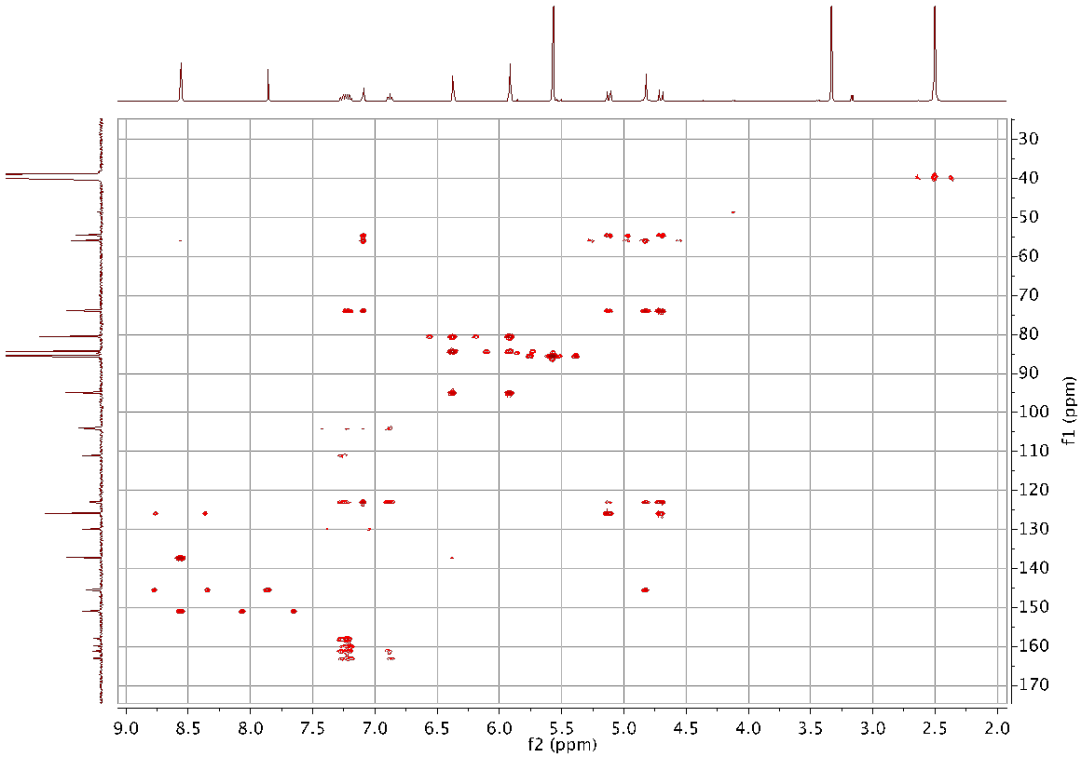

Figure S24 HMBC spectrum of **A1-Cl** in DMSO-D6

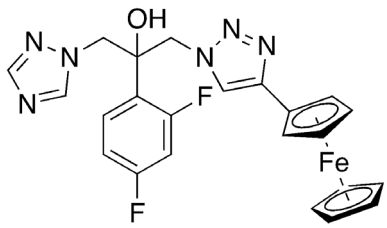

A2

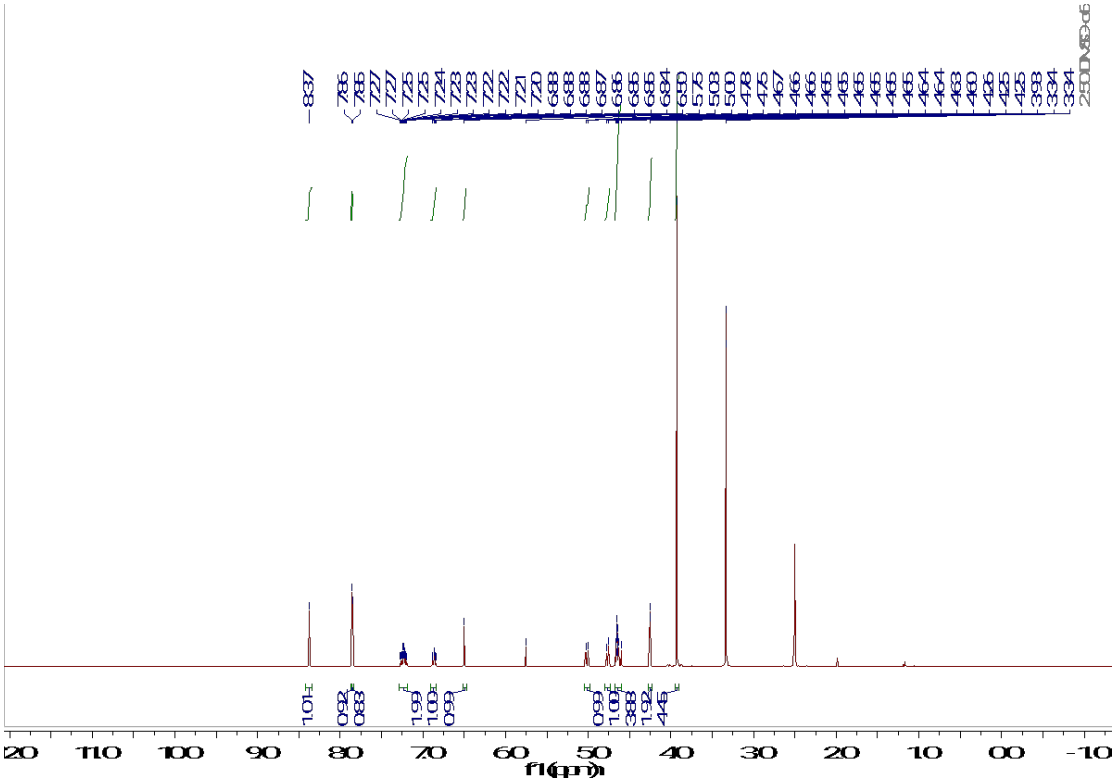

Figure S25 ^{1}H NMR spectrum of **A2**

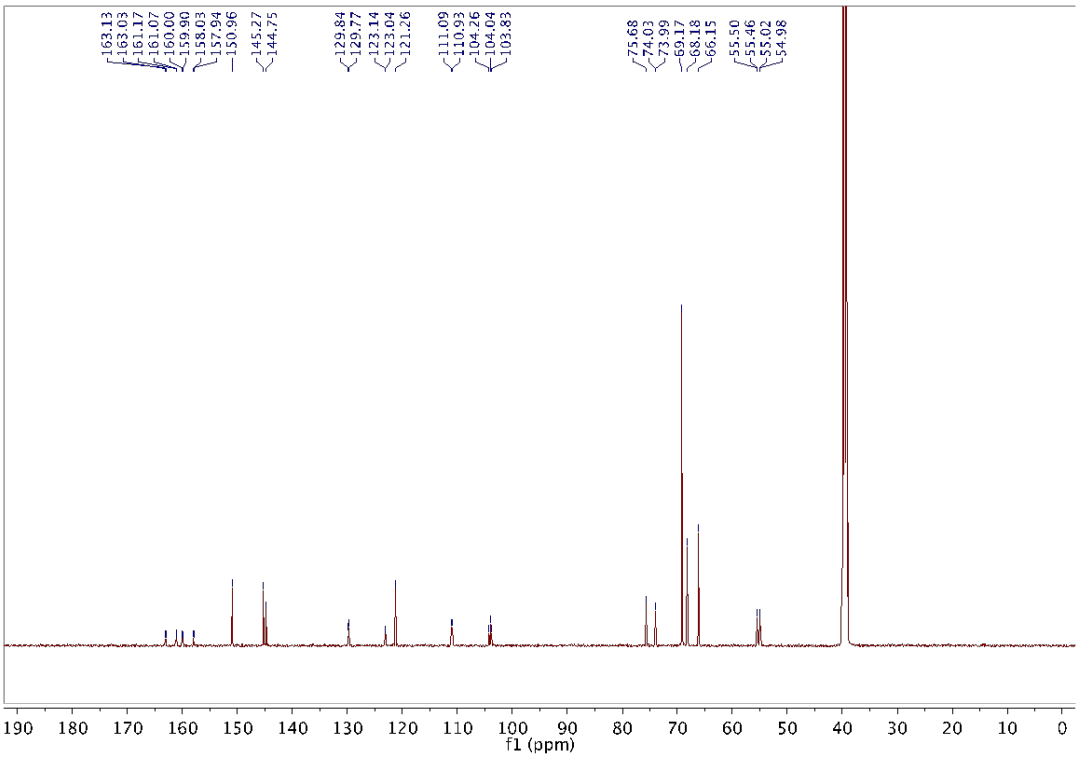

Figure S26 ^{13}C NMR spectrum of **A2**

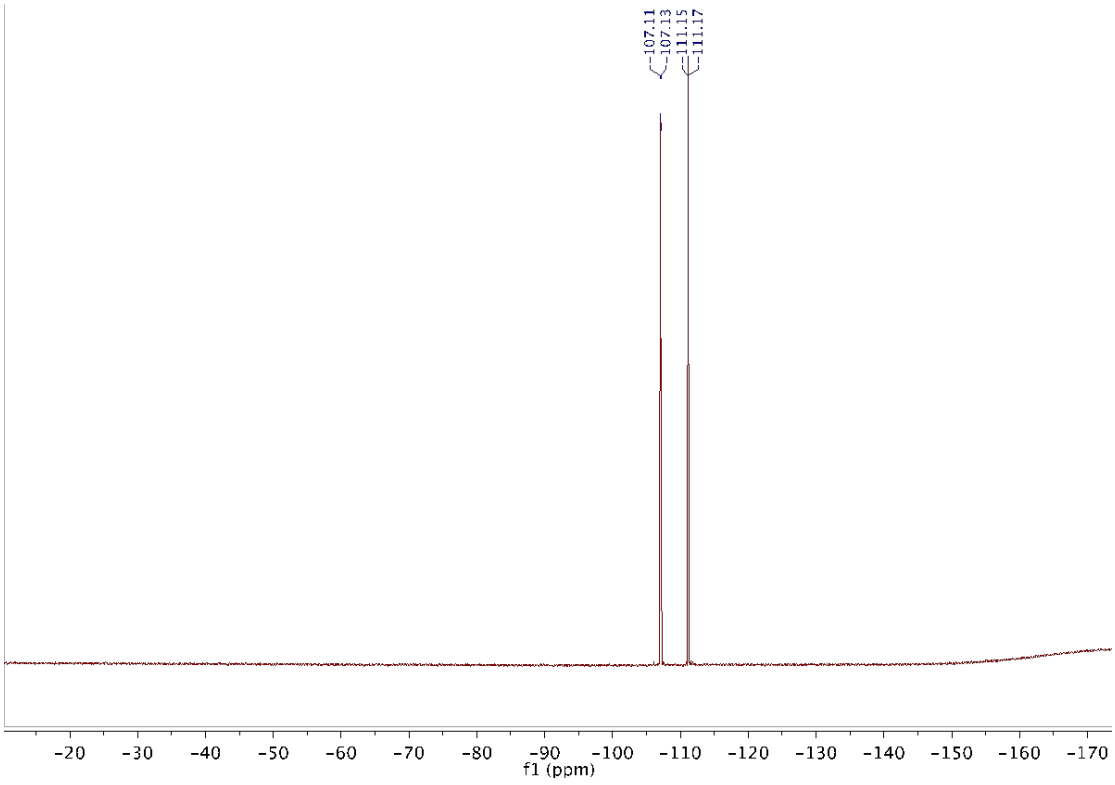

Figure S27 ^{19}F NMR spectrum of **A2**

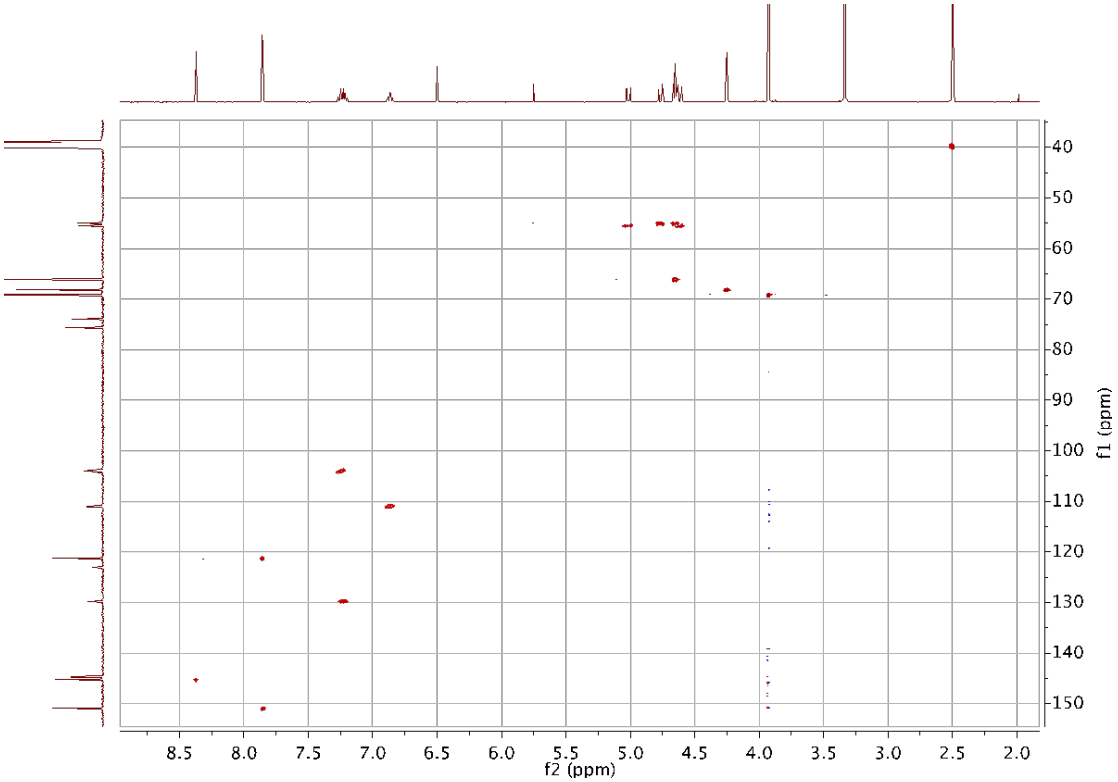

Figure S28 HSQC spectrum of **A2** in DMSO-D6

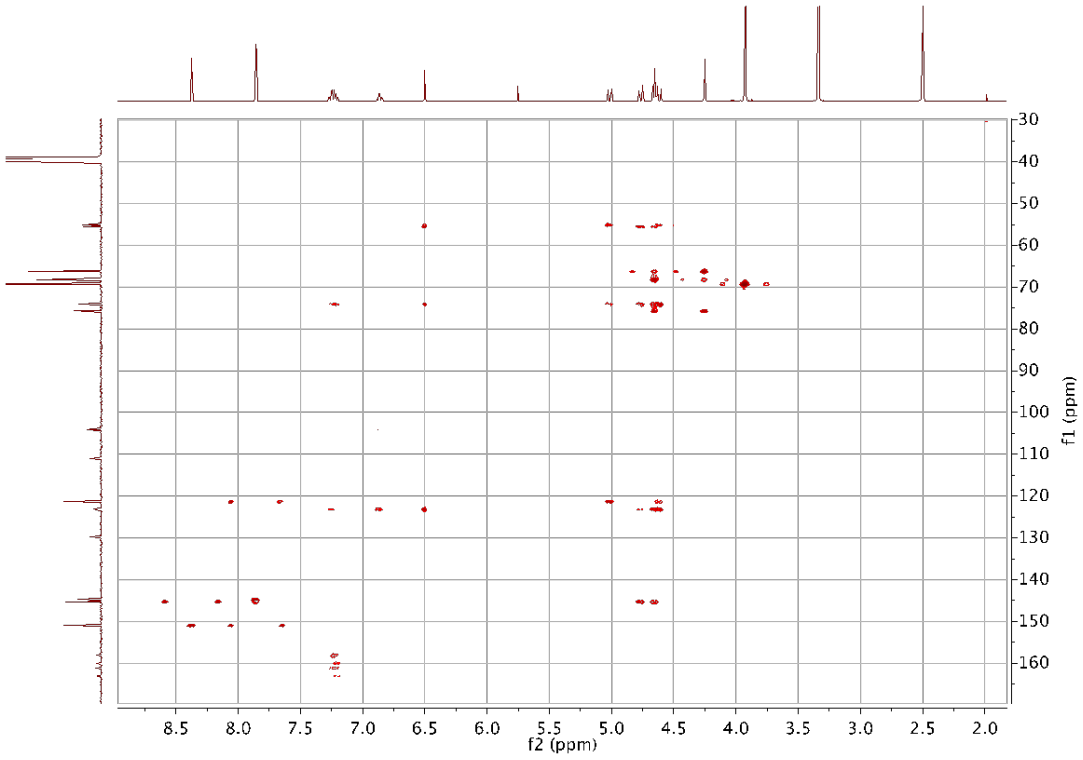

Figure S28 HMBC spectrum of **A2** in DMSO-D6

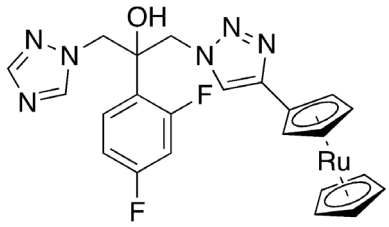

A3

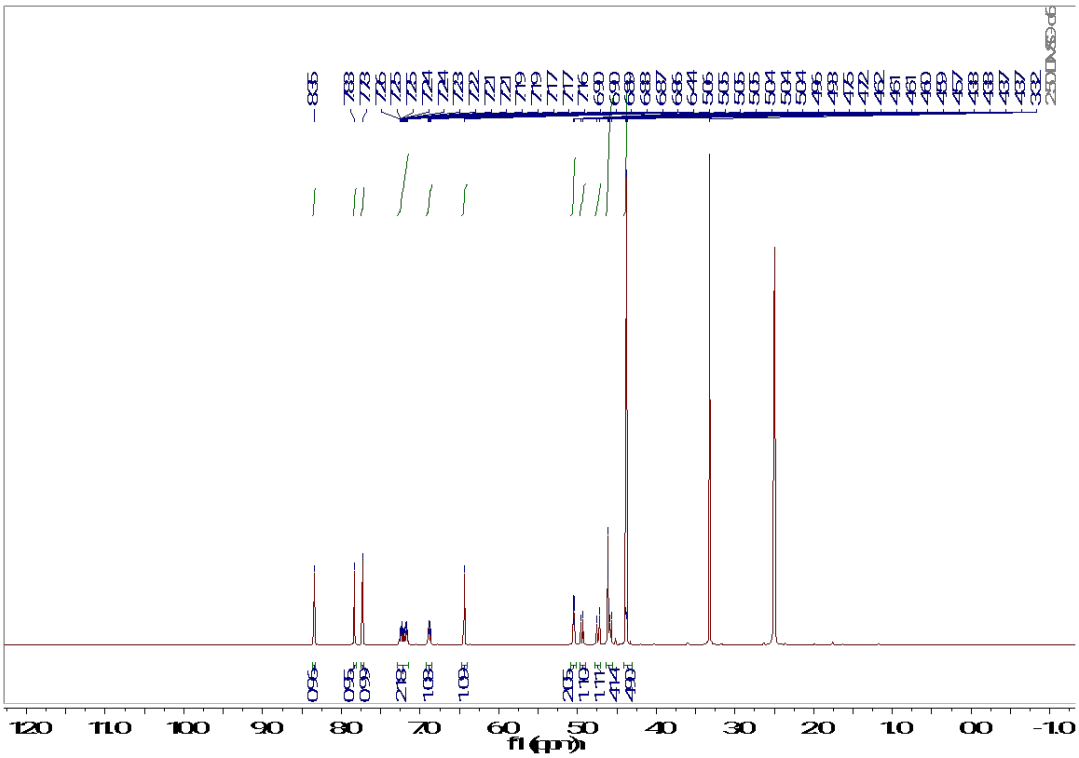

Figure S29 ^{1}H NMR spectrum of **A3**

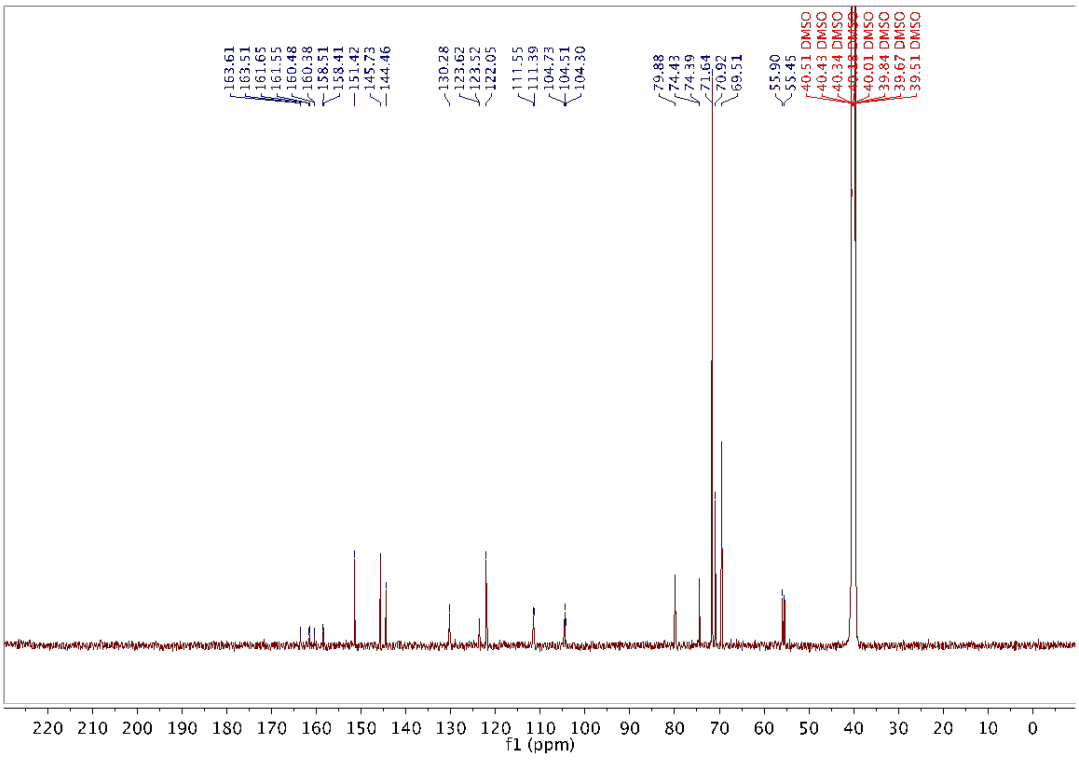

Figure S30 ^{13}C NMR spectrum of **A3**

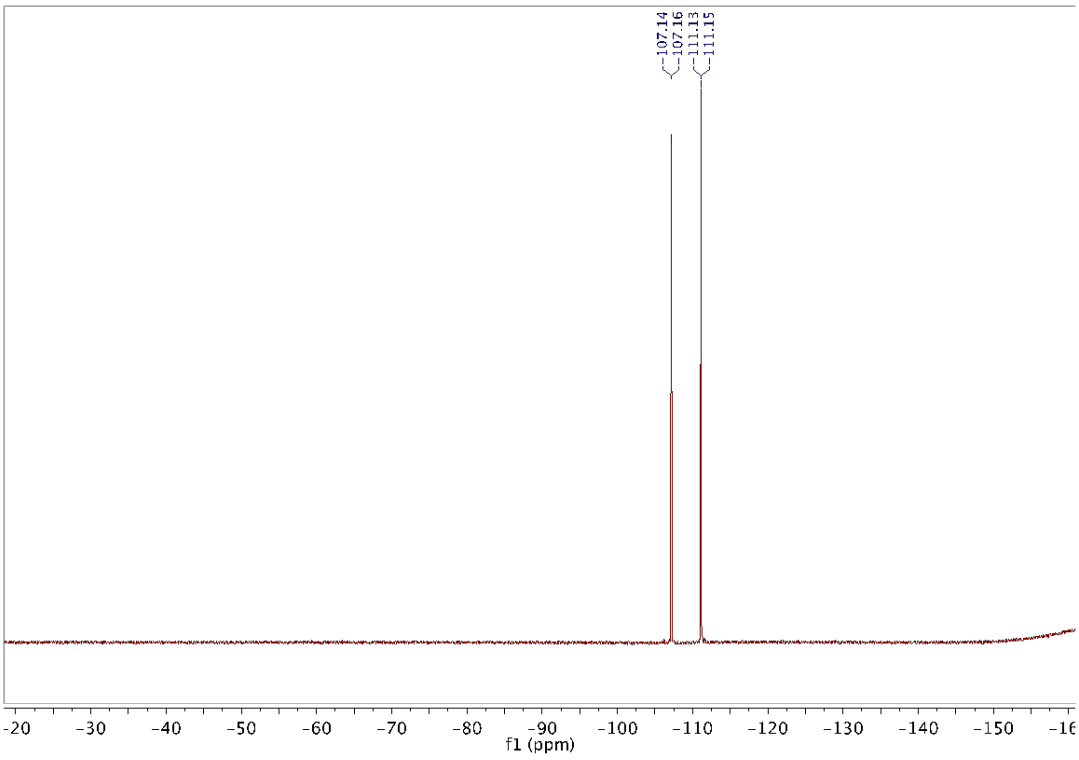

Figure S31 ^{19}F NMR spectrum of **A3**

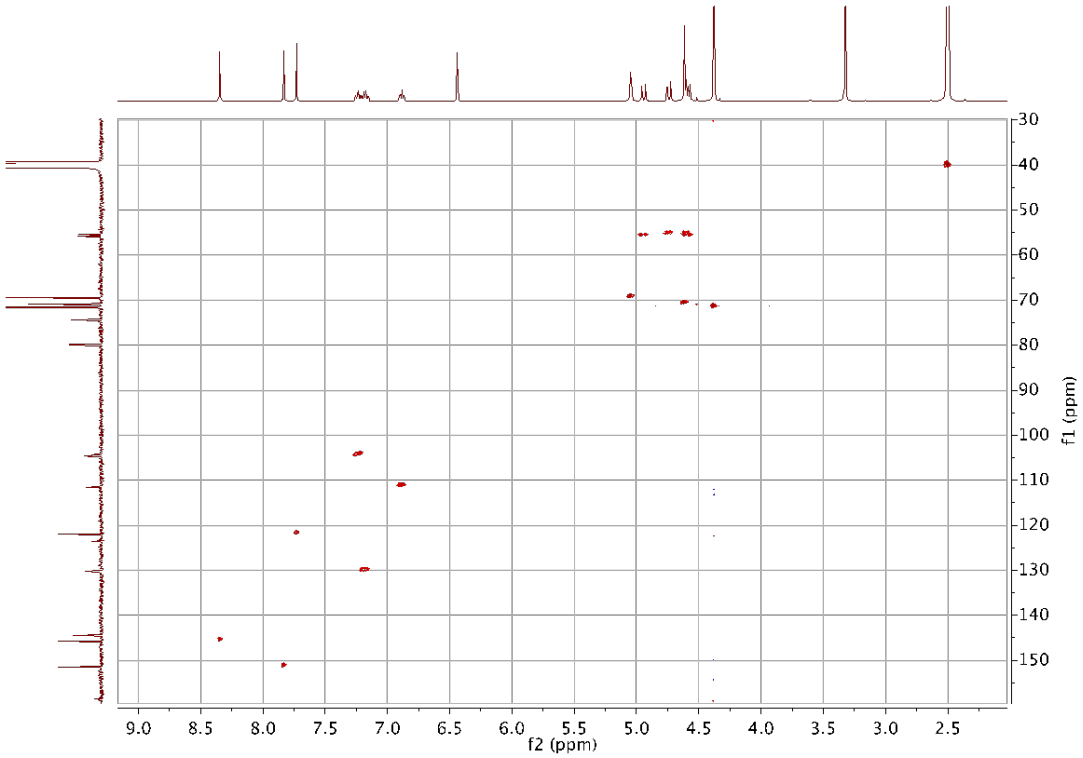

Figure S32 HSQC spectrum of **A3** in DMSO-D6

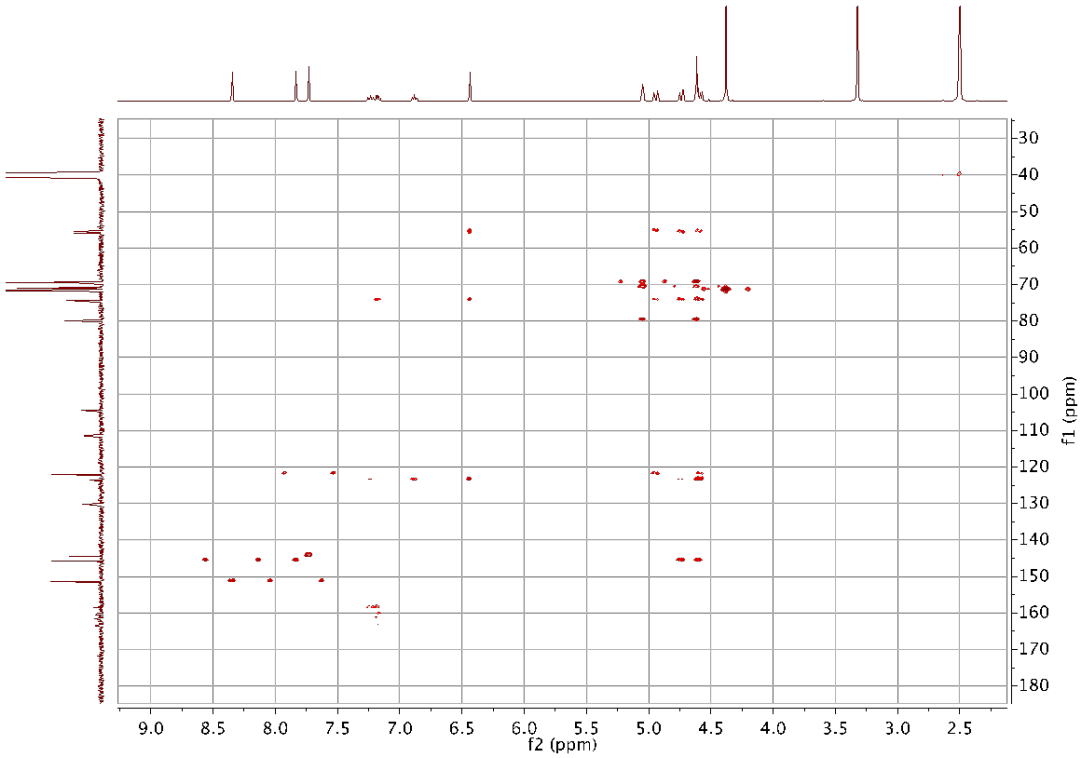

Figure S32 HMBC spectrum of **A3** in DMSO-D6

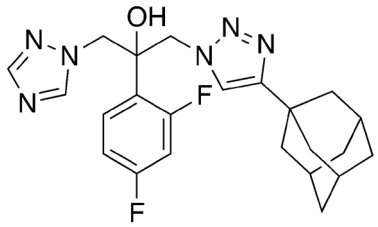

A4

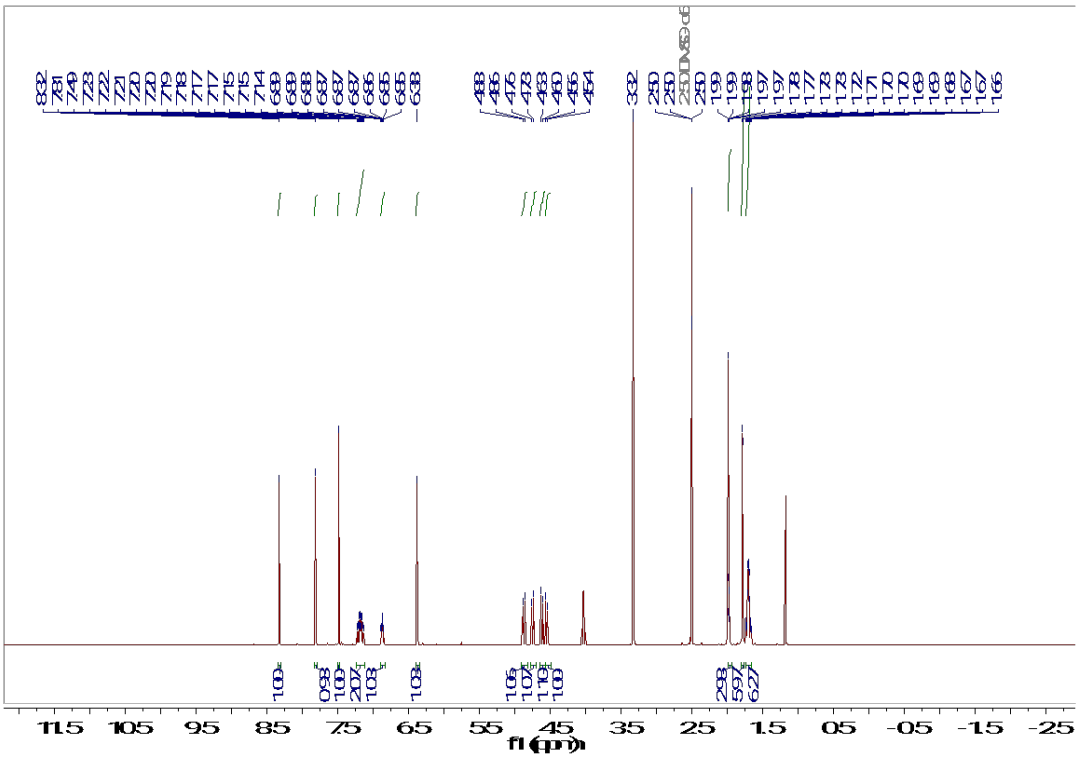

Figure S33 ^{1}H NMR spectrum of **A4**

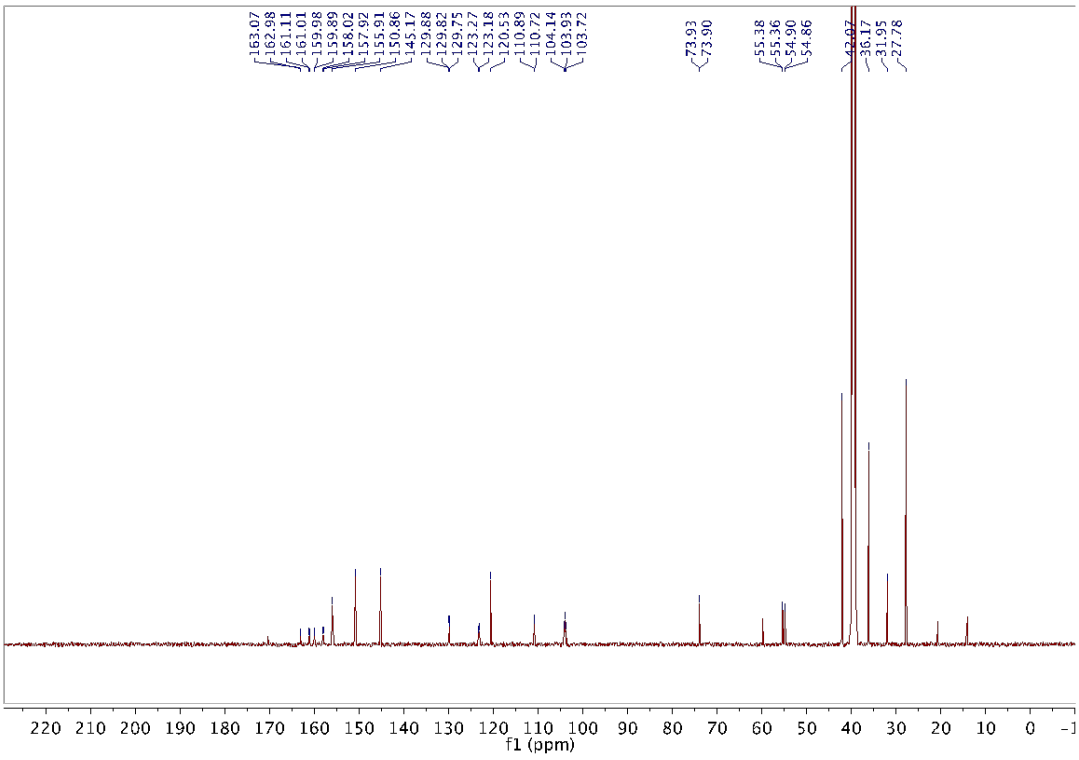

Figure S34 ^{13}C NMR spectrum of **A4**

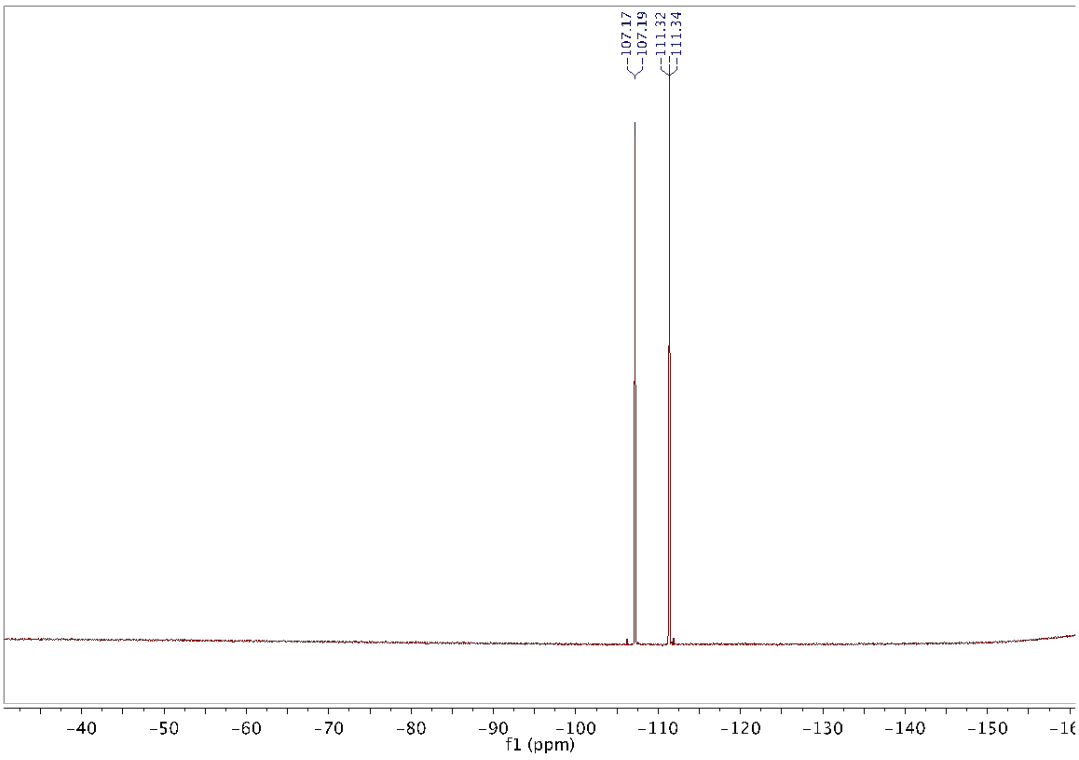

Figure S35 ^{19}F NMR spectrum of **A4**

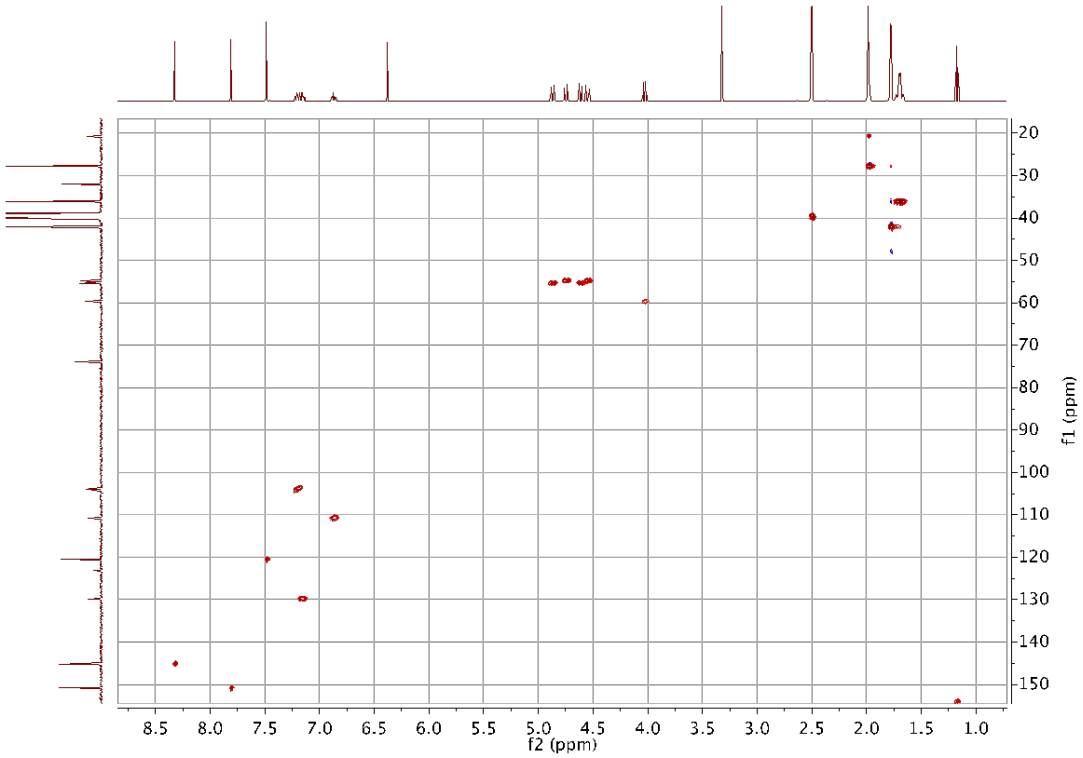

Figure S36 HSQC spectrum of **A4** in DMSO-D6

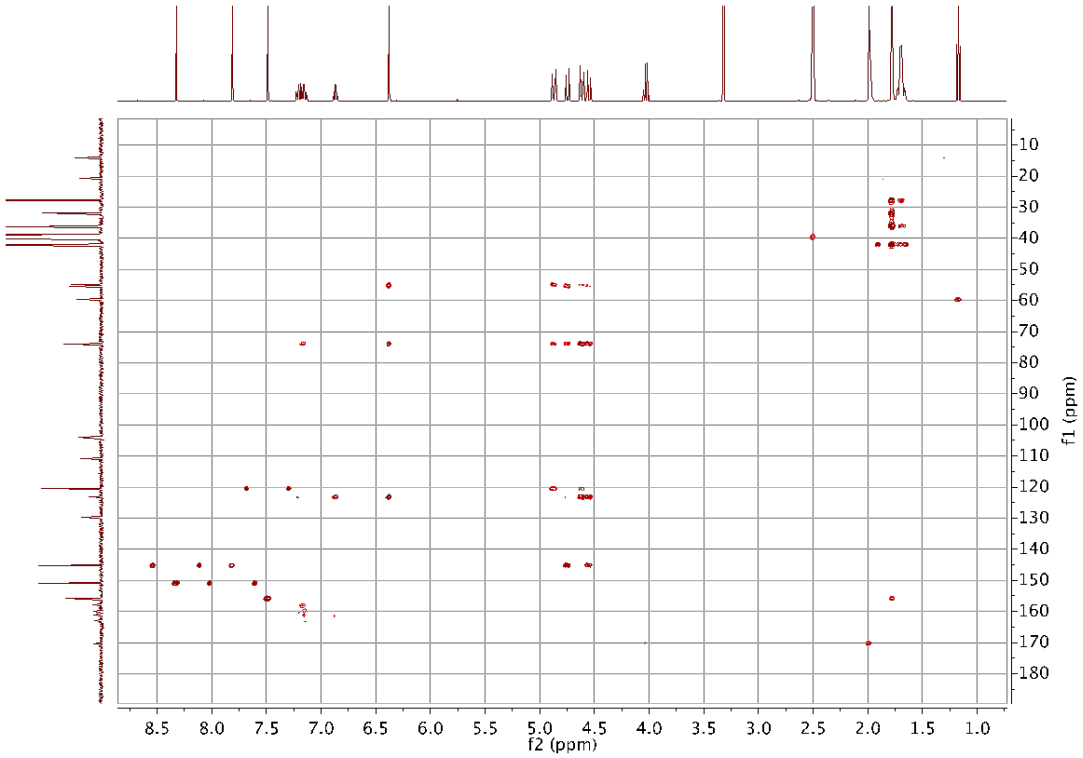

Figure S37 HMBC spectrum of **A4** in DMSO-D6

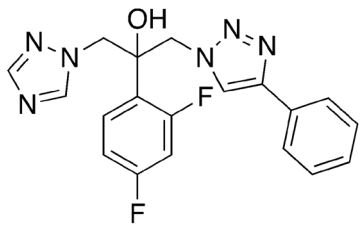

A5

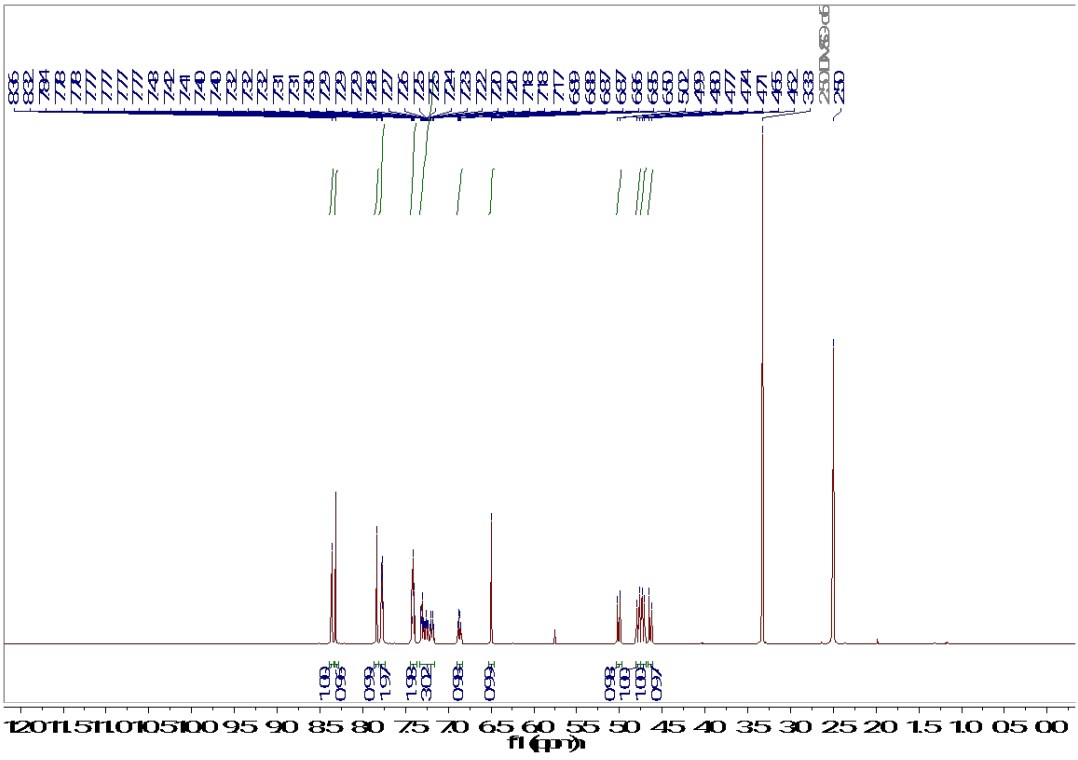

Figure S38 ^{1}H NMR spectrum of **A5**

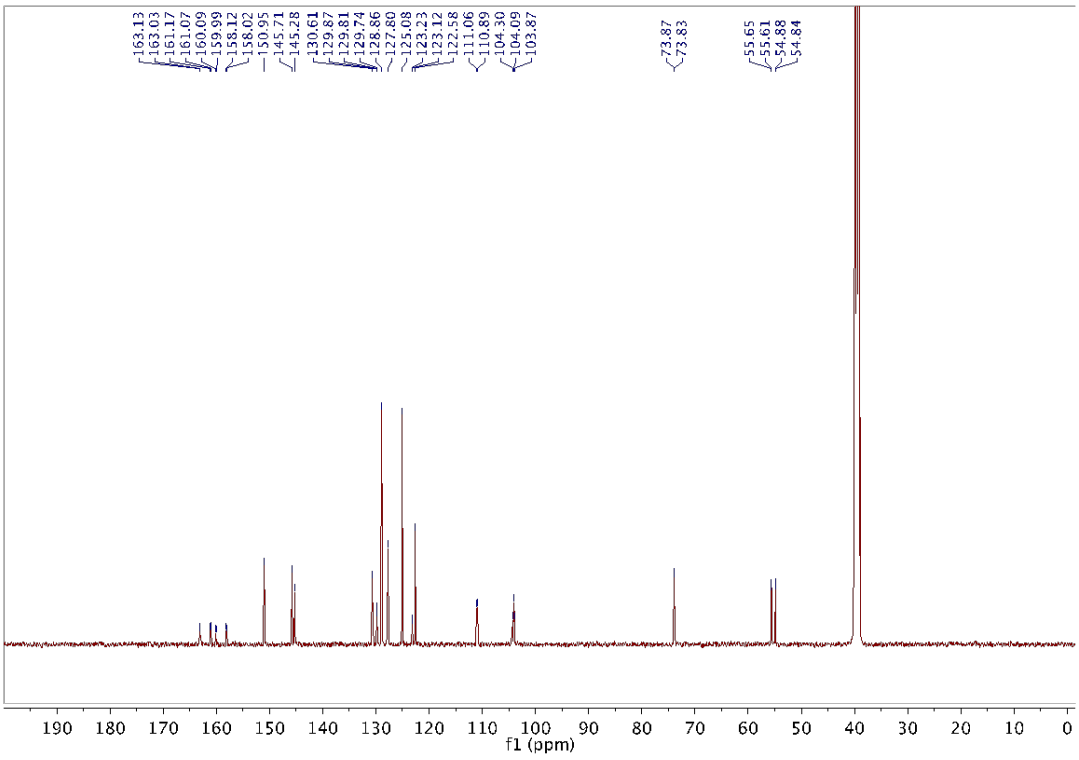

Figure S39 ^{13}C NMR spectrum of **A5**

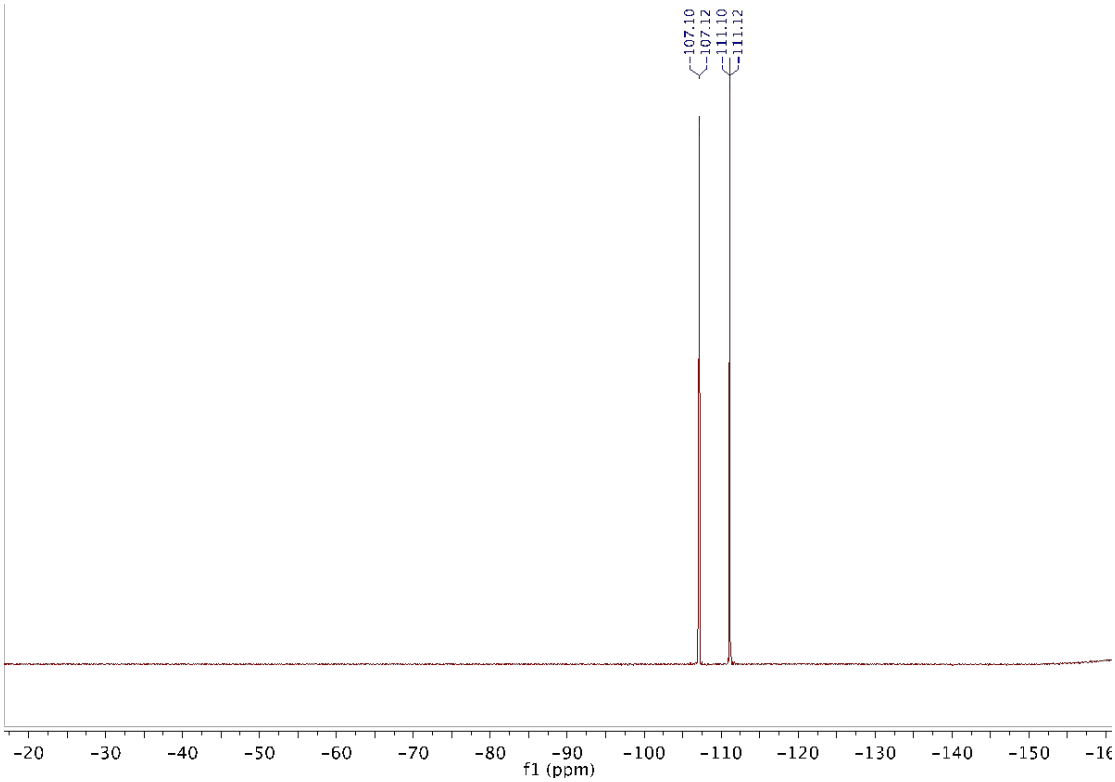

Figure S40 ^{19}F NMR spectrum of **A5**

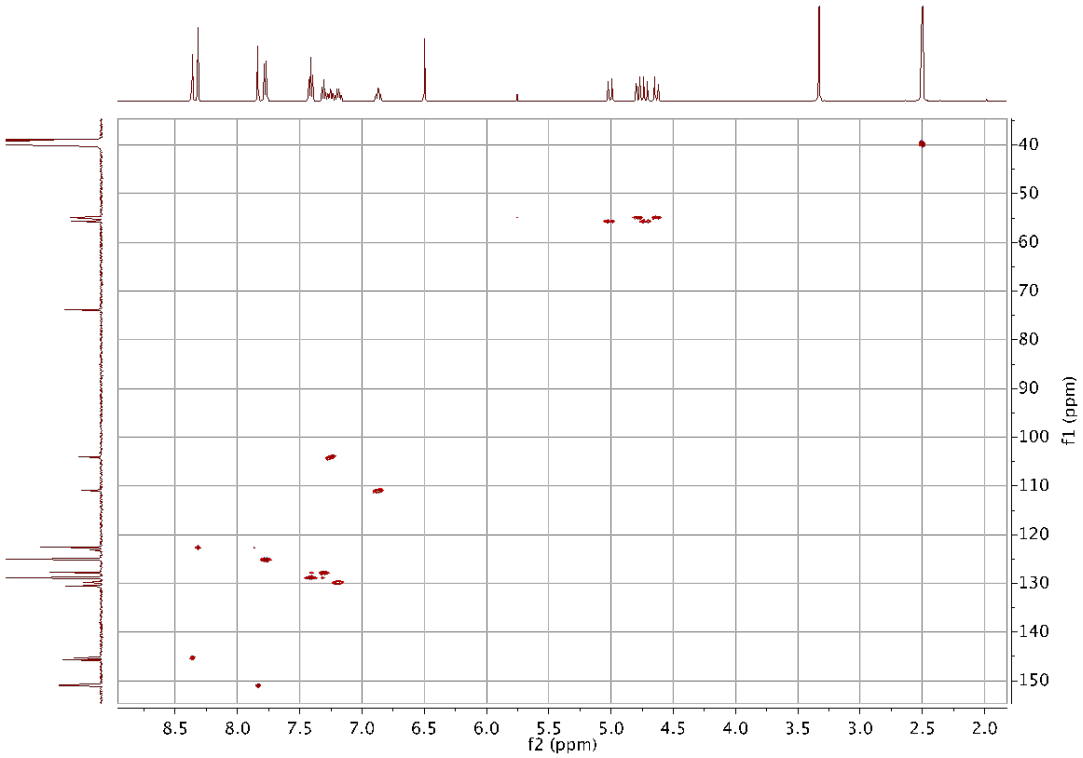

Figure S41 HSQC spectrum of **A5** in DMSO-D6

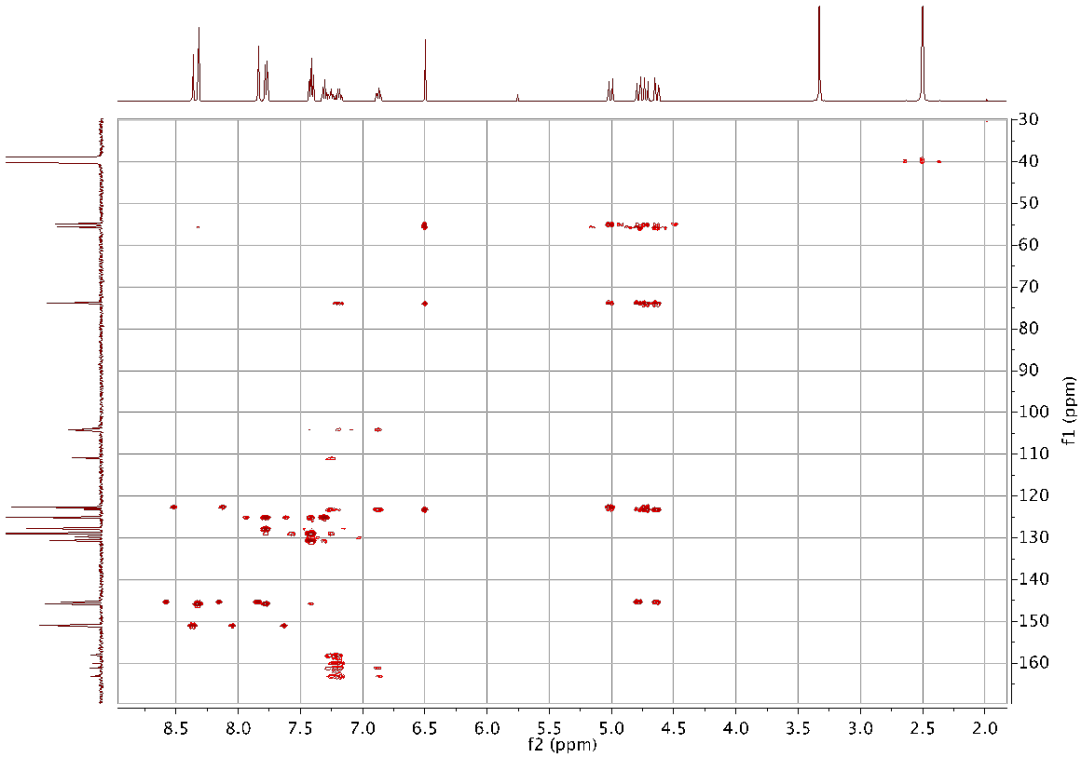

Figure S42 HMBC spectrum of **A5** in DMSO-D6

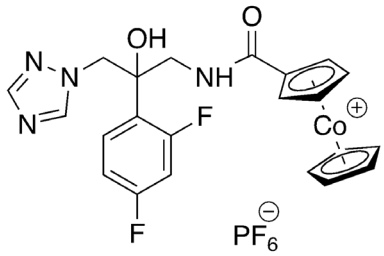

B1-PF$_6$

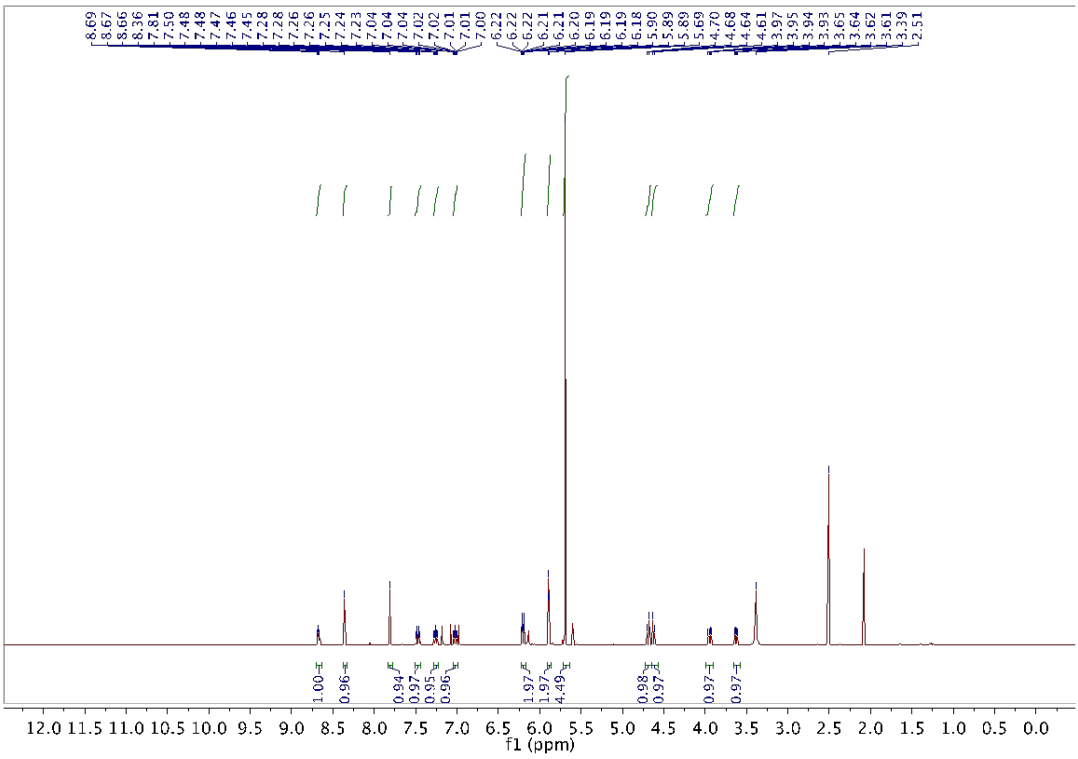

Figure S43 ^{1}H NMR spectrum of **B1-PF$_6$**

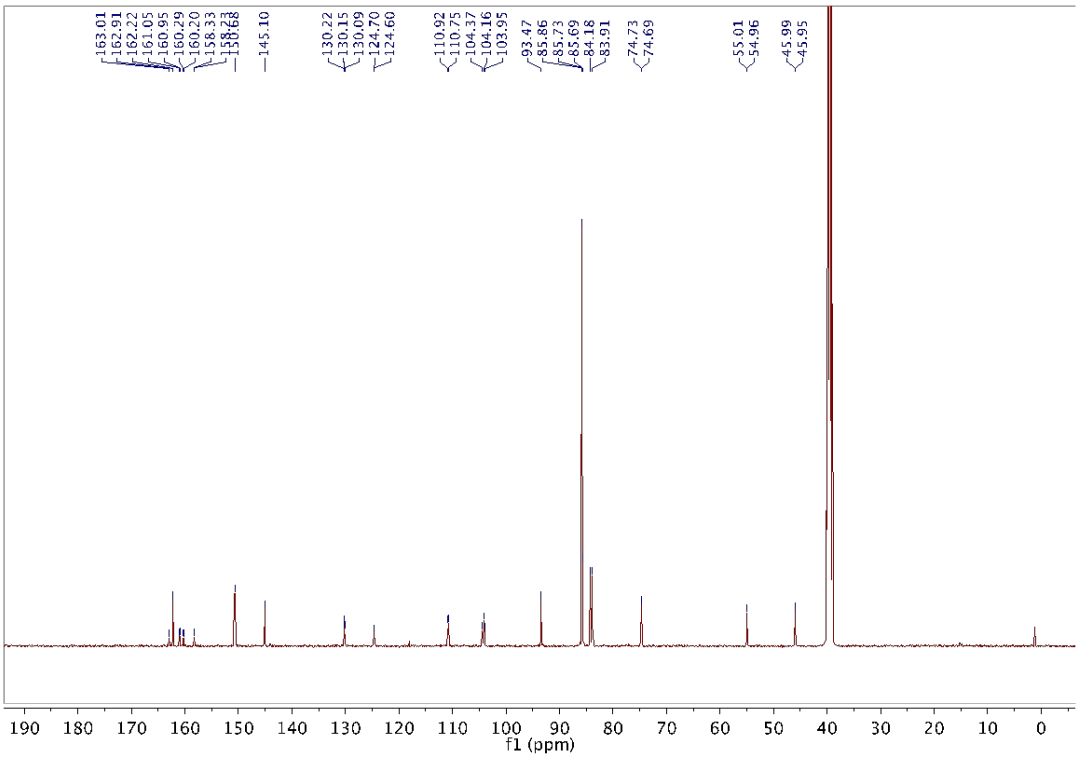

Figure S44 ^{13}C NMR spectrum of **B1-PF$_6$**

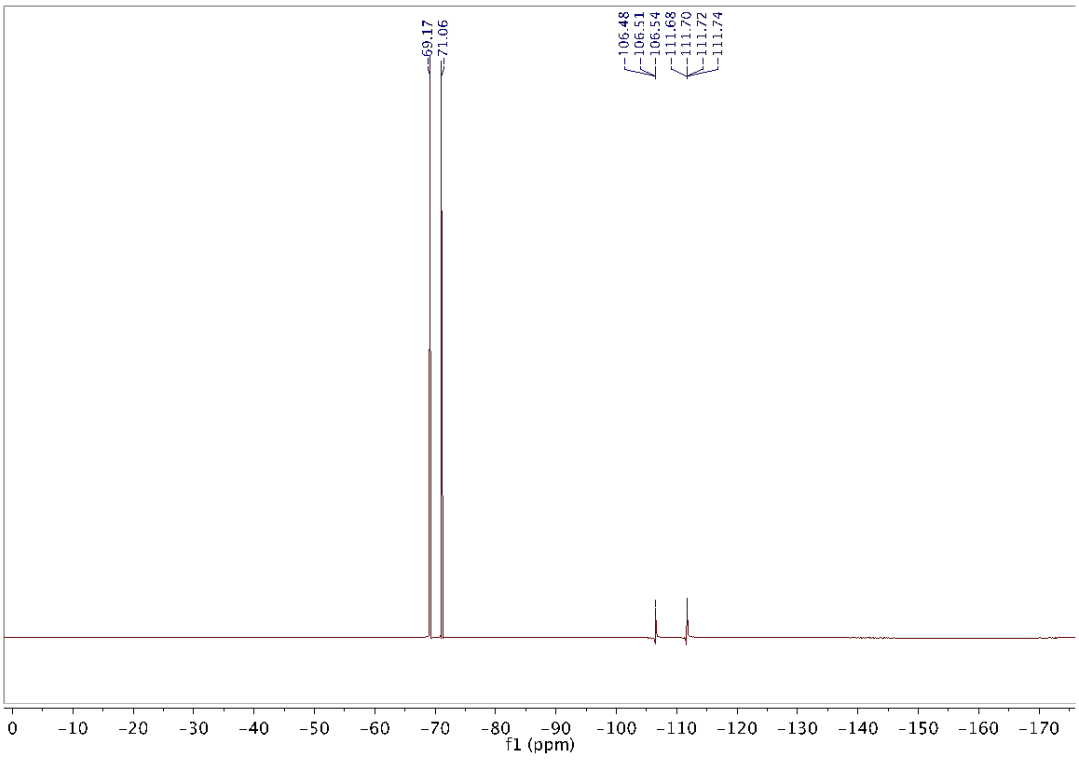

Figure S45 ^{19}F NMR spectrum of **B1-PF$_6$**

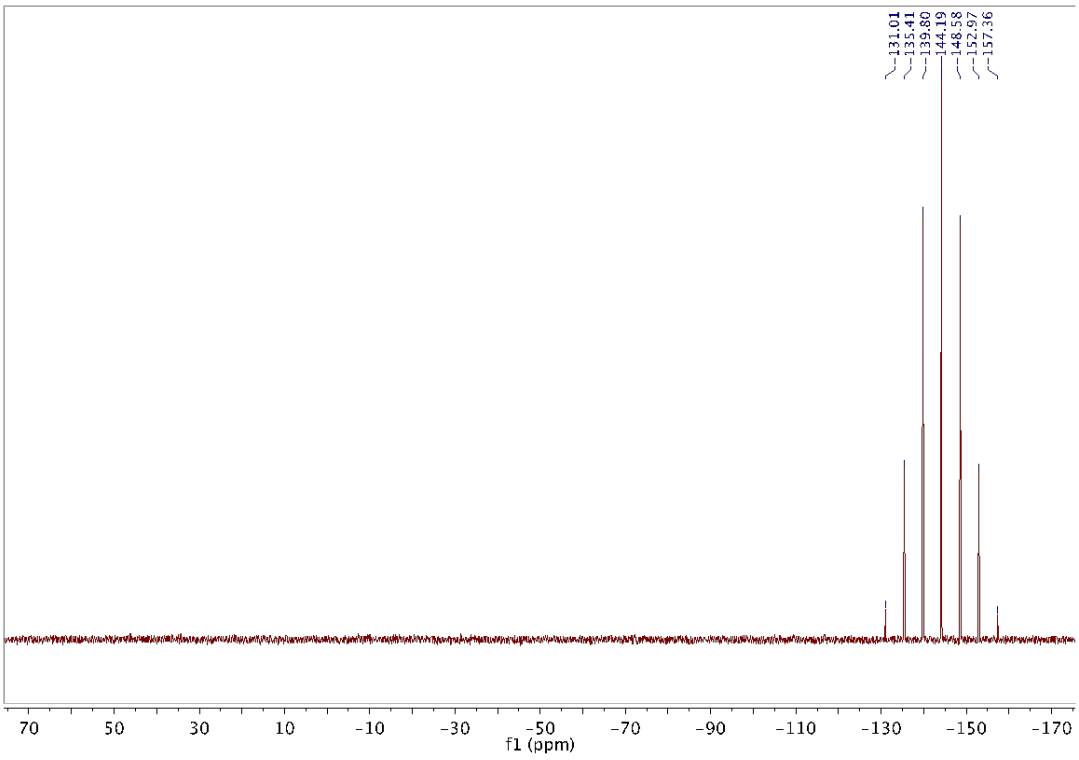

Figure S46 ^{31}P NMR spectrum of **B1-PF$_6$**

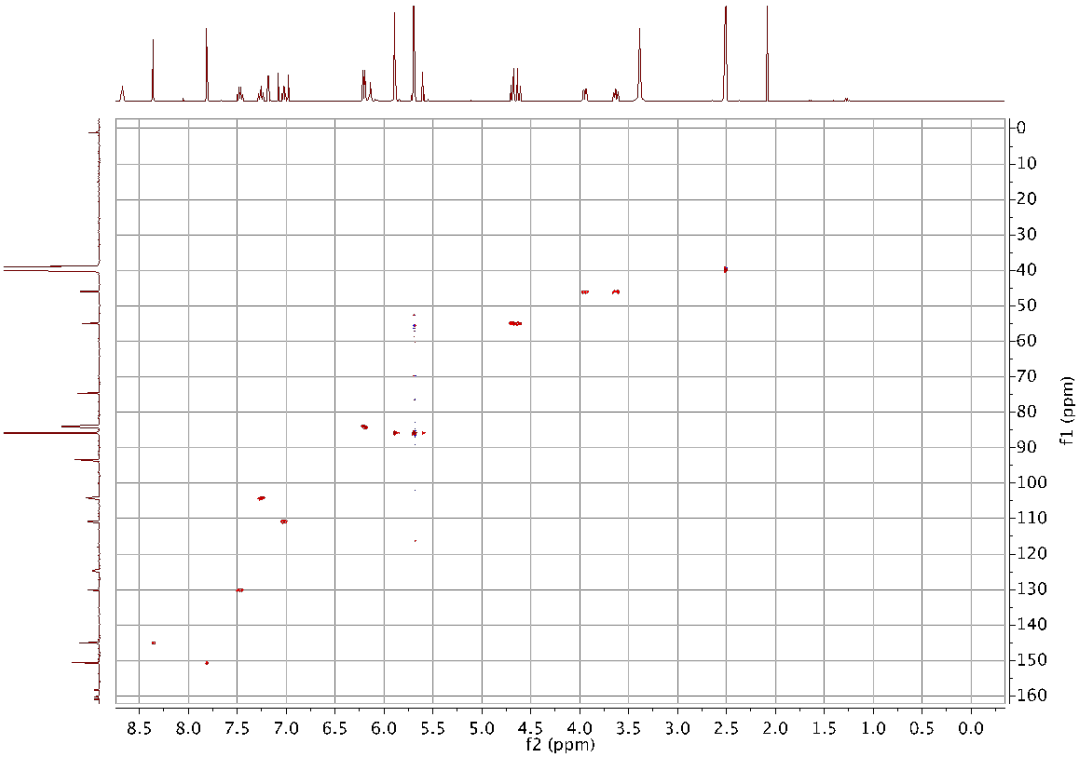

Figure S47 HSQC spectrum of **B1-PF$_6$** in DMSO-D6

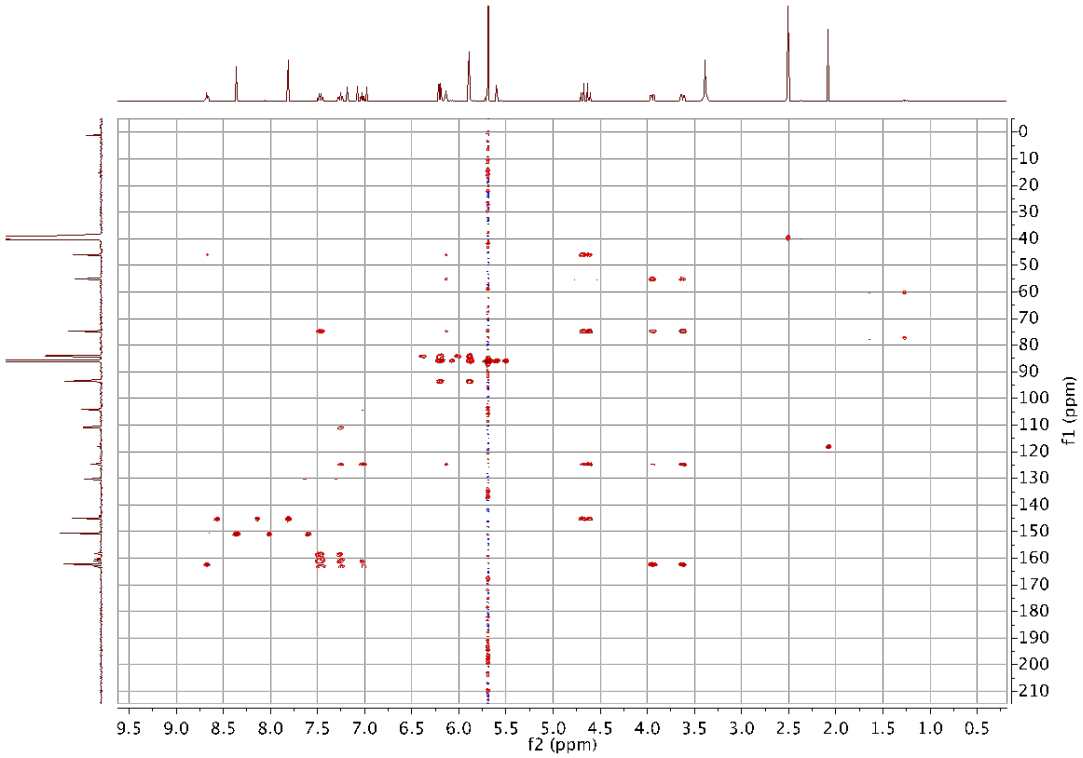

Figure S48 HMBC spectrum of **B1-PF_6** in DMSO-D6

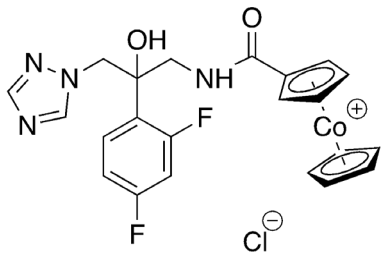

B1-Cl

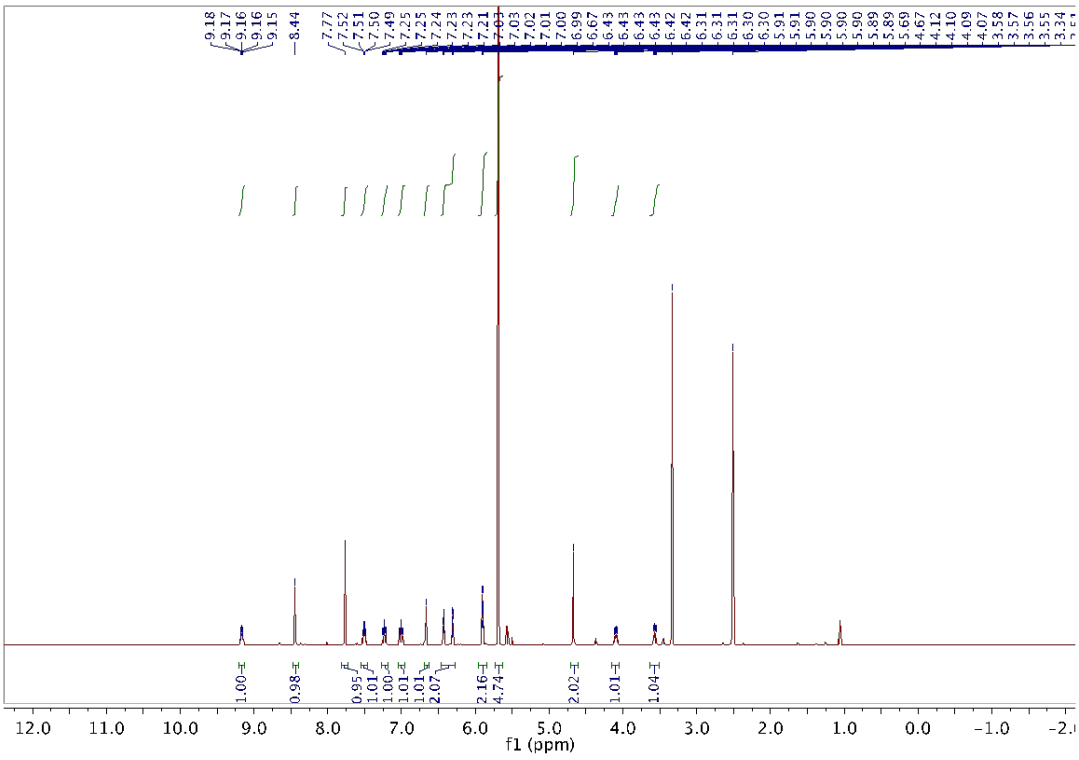

Figure S49 ^{1}H NMR spectrum of **B1-Cl**

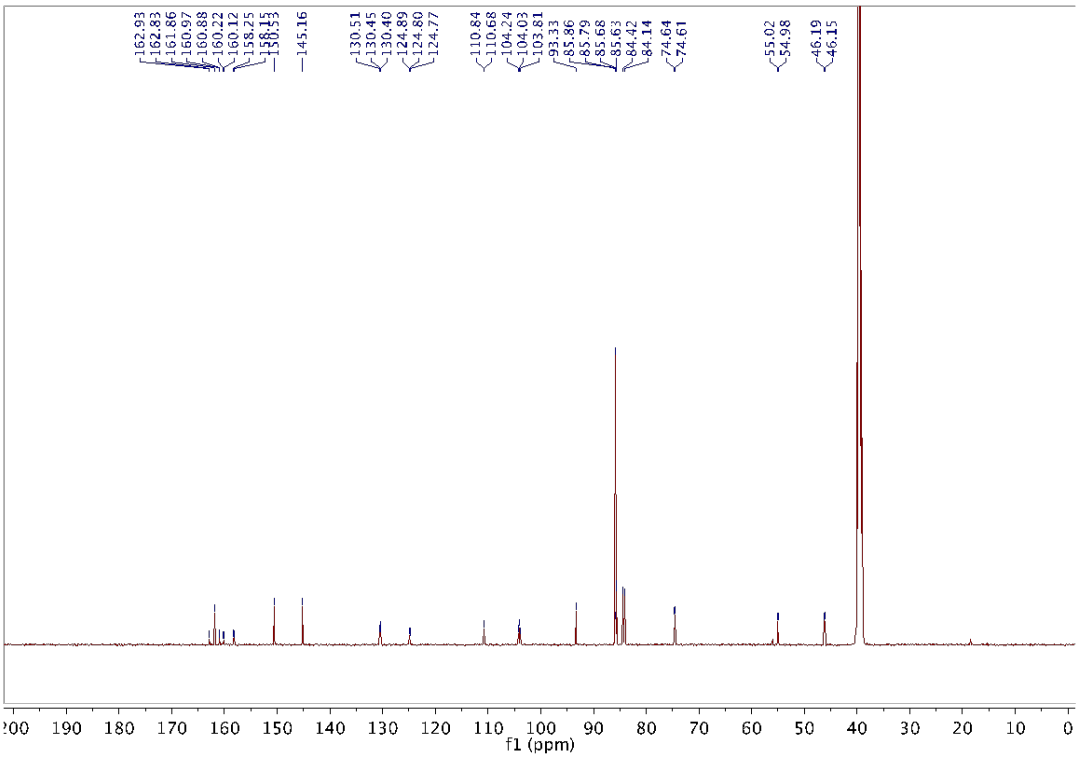

Figure S50 ^{13}C NMR spectrum of **B1-Cl**

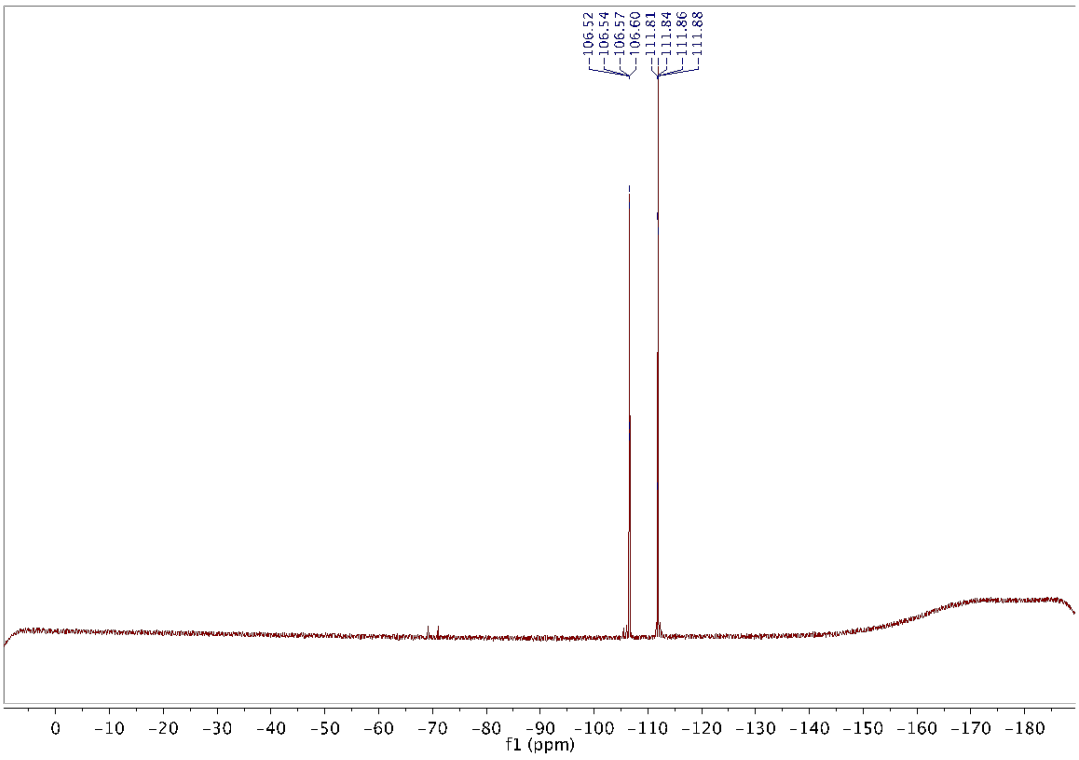

Figure S51 ^{19}F NMR spectrum of **B1-Cl**

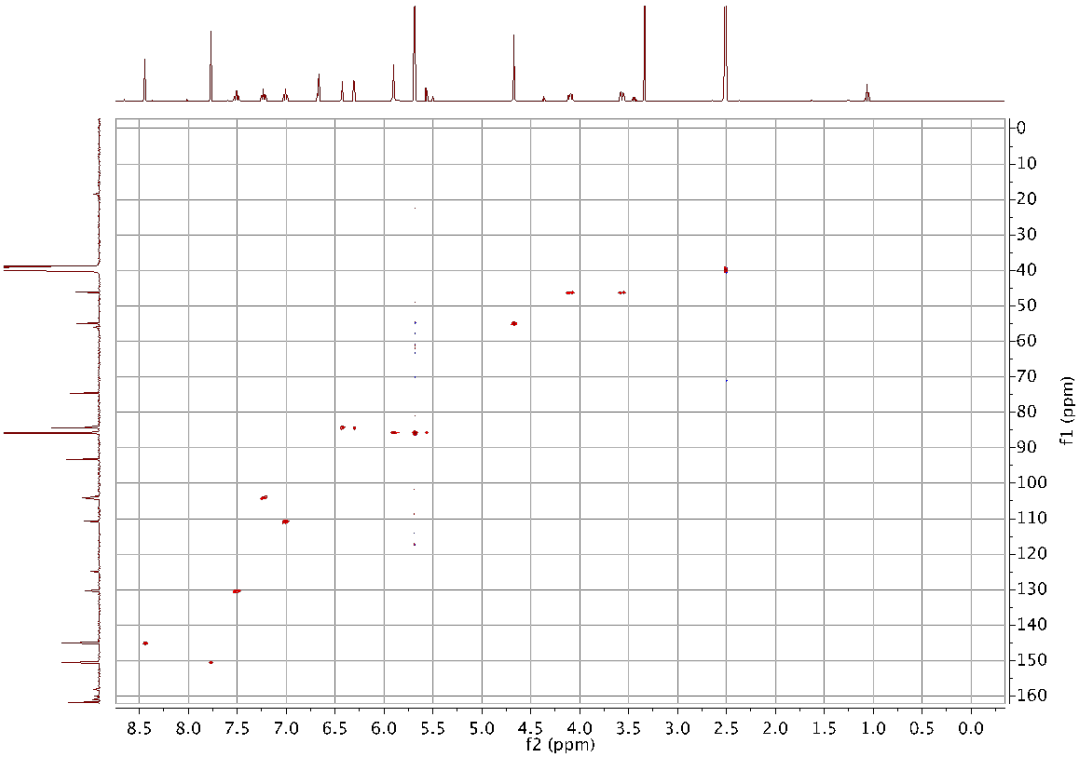

Figure S52 HSQC spectrum of **B1-Cl** in DMSO-D6

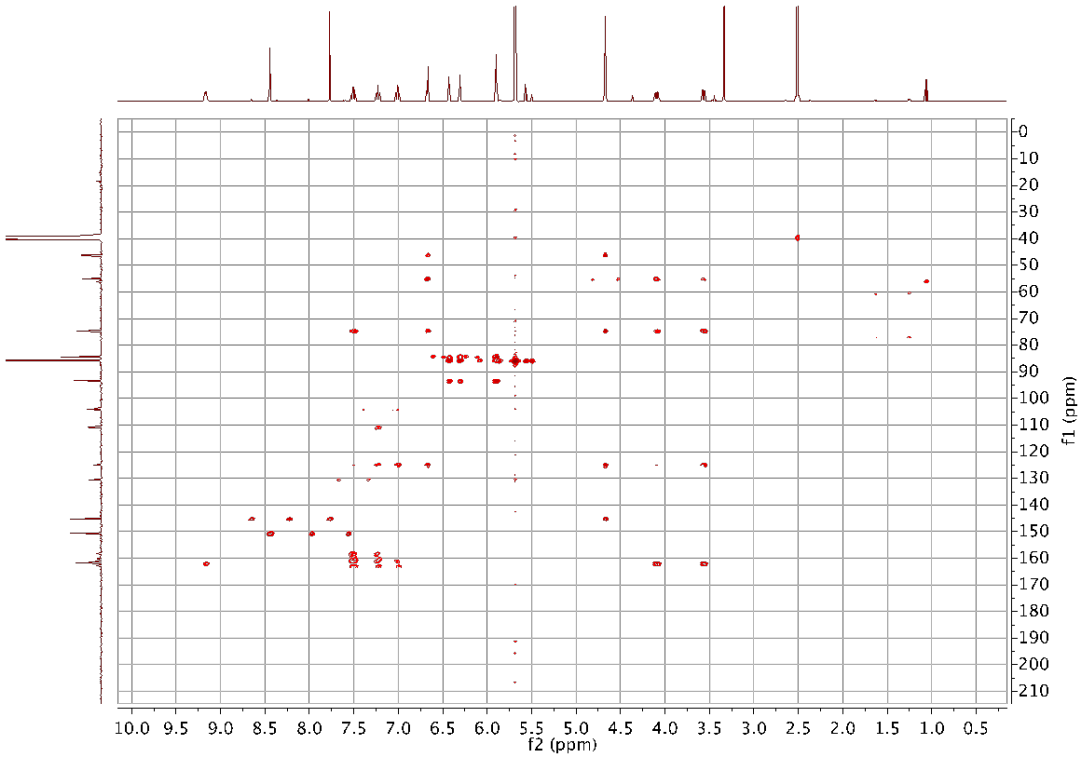

Figure S53 HMBC spectrum of **B1-Cl** in DMSO-D6

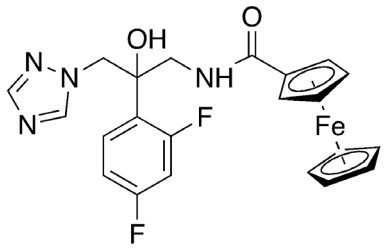

B2

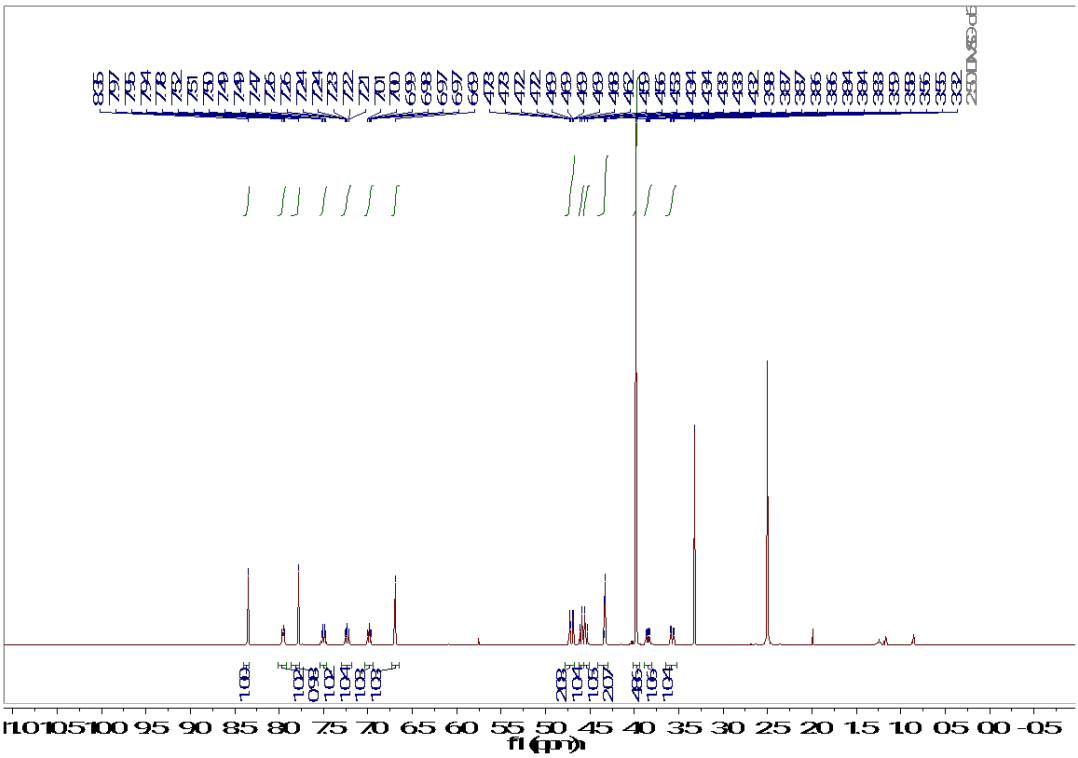

Figure S54 ^{1}H NMR spectrum of **B2**

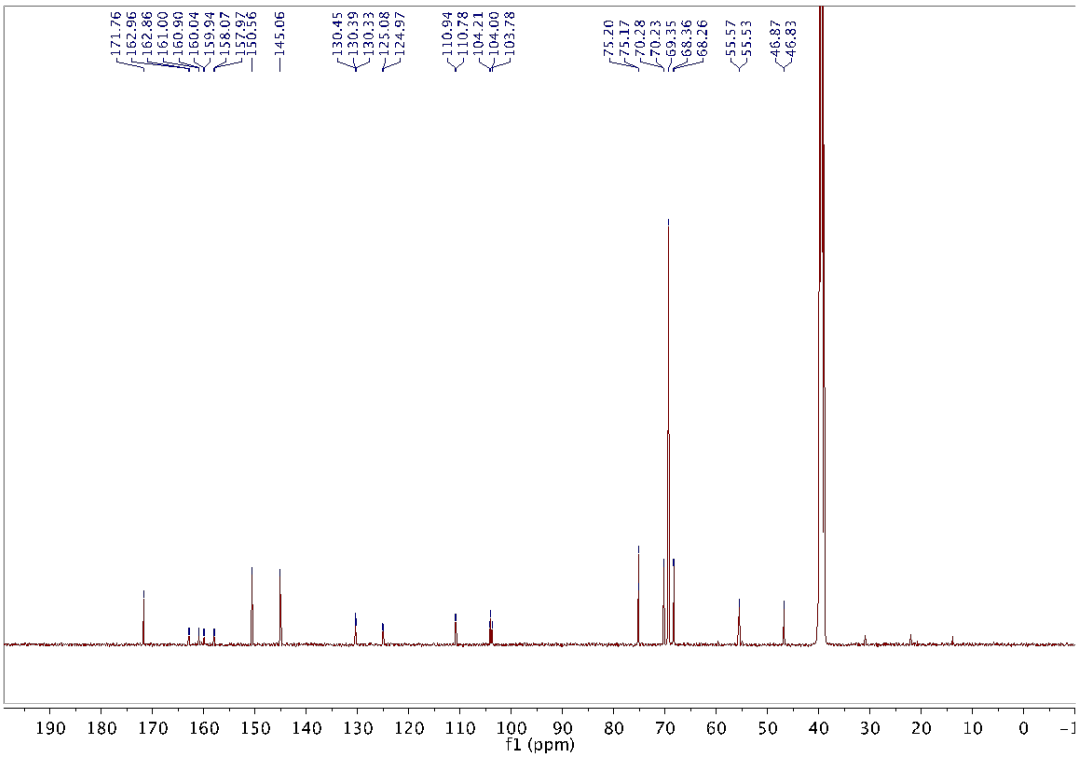

Figure S55 ^{13}C NMR spectrum of **B2**

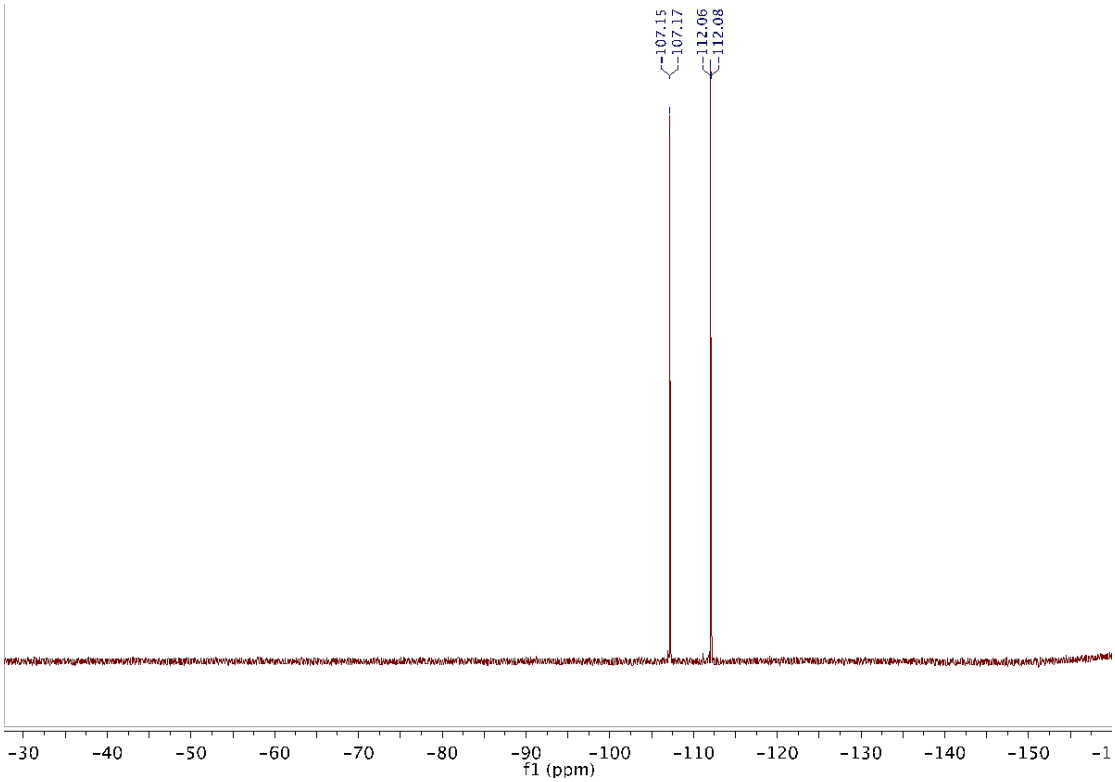

Figure S56 ^{19}F NMR spectrum of **B2**

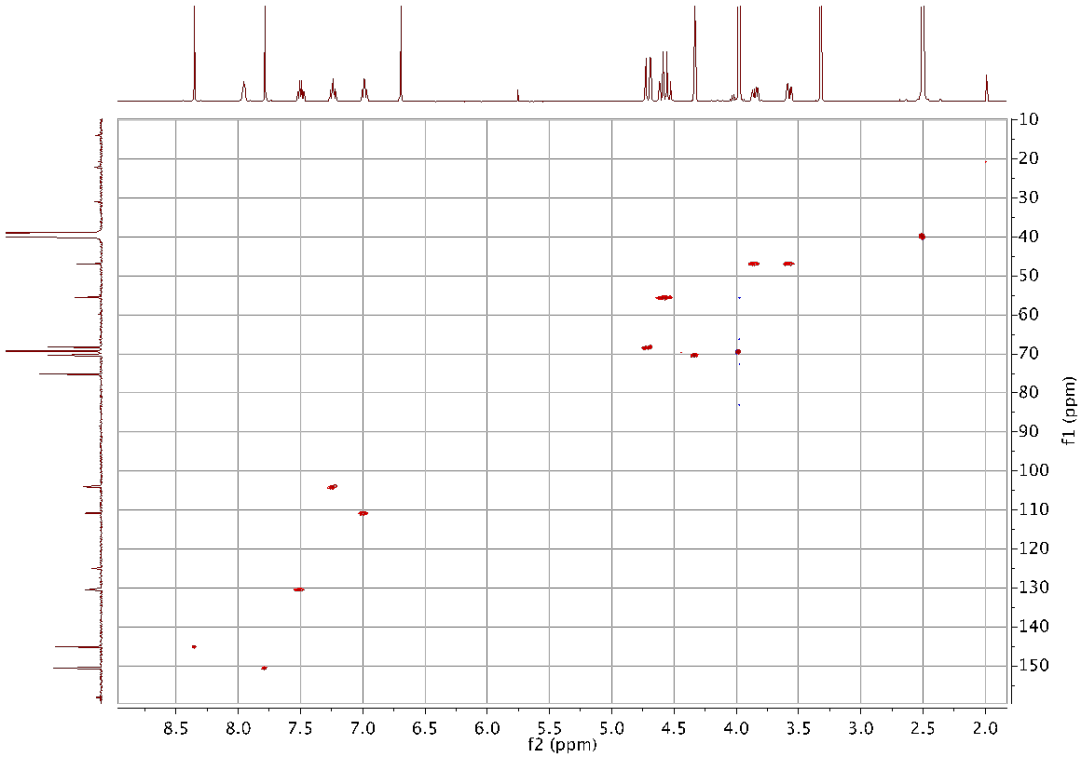

Figure S57 HSQC spectrum of **B2** in DMSO-D6

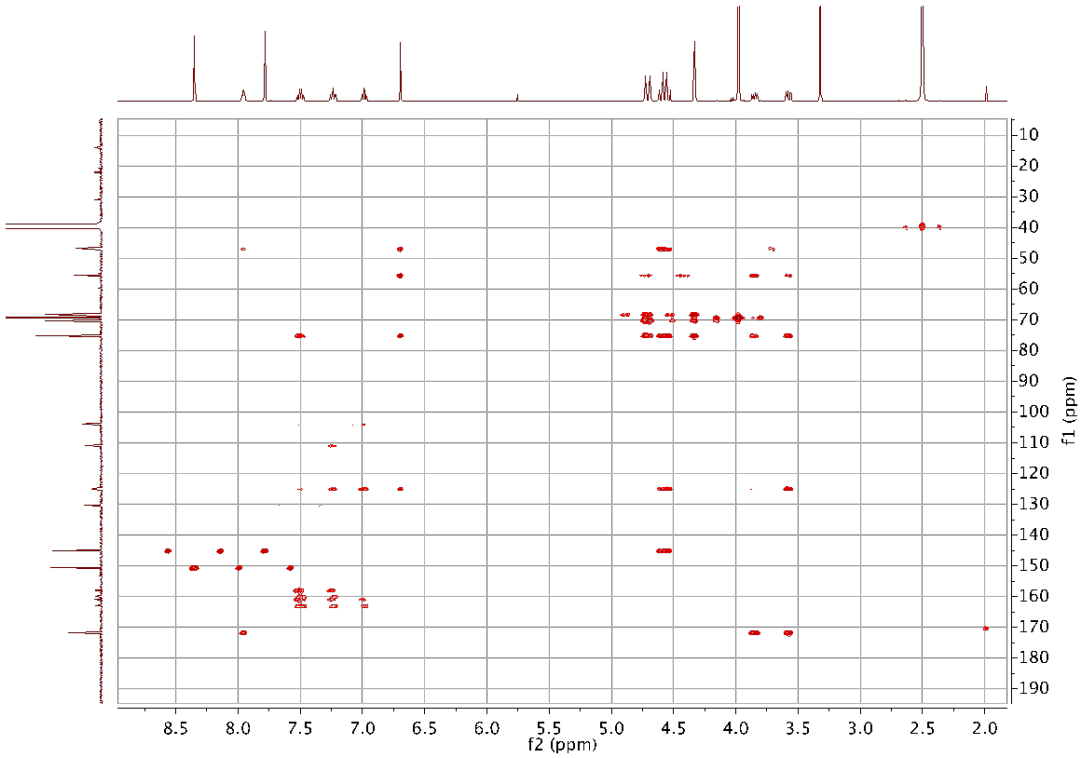

Figure S58 HMBC spectrum of **B2** in DMSO-D6

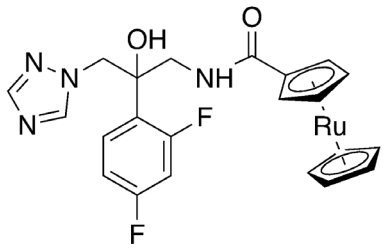

B3

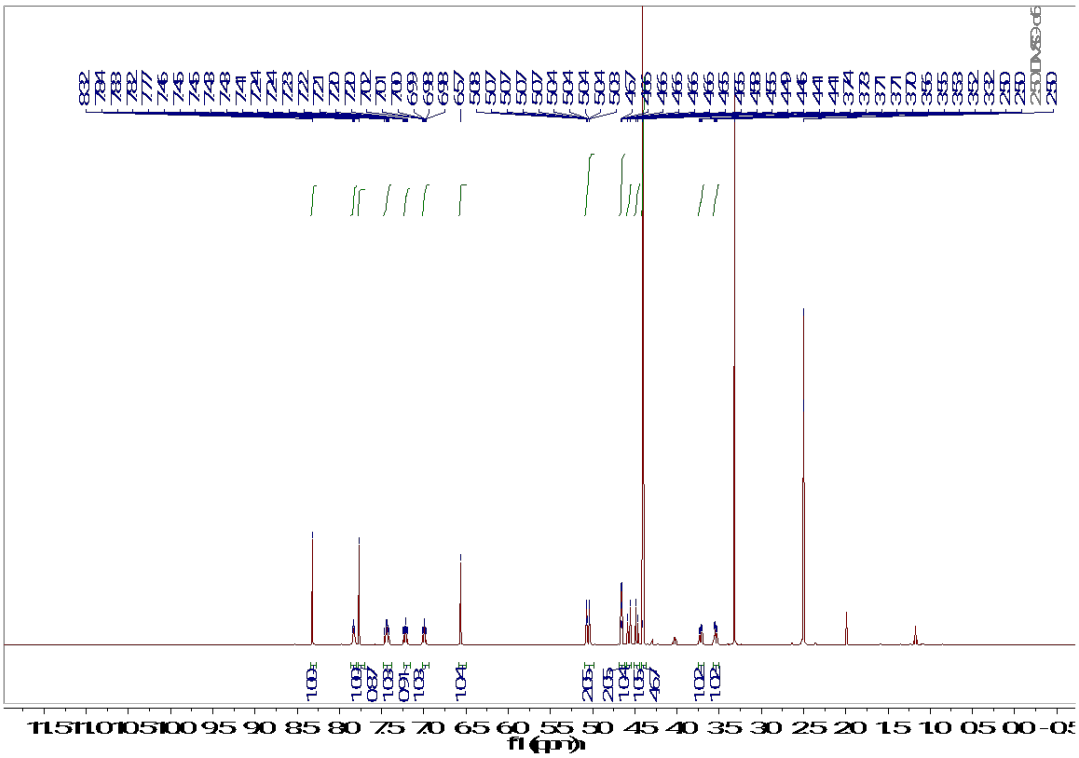

Figure S59 ^{1}H NMR spectrum of **B3**

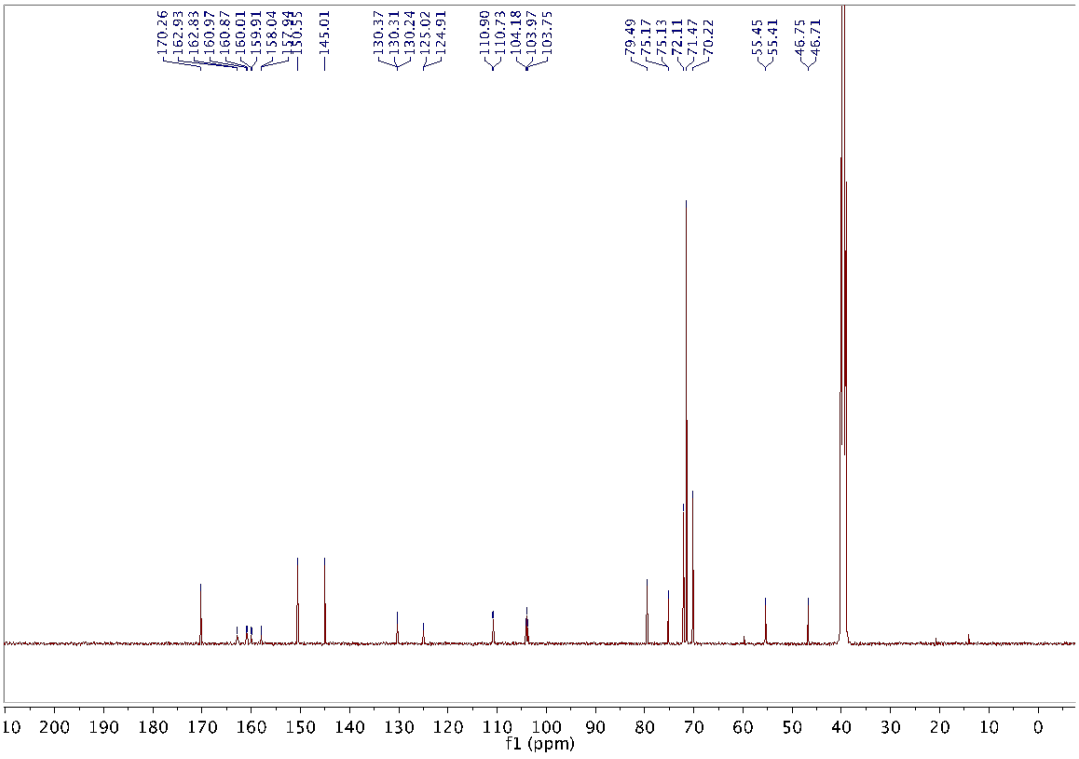

Figure S60 ^{13}C NMR spectrum of **B3**

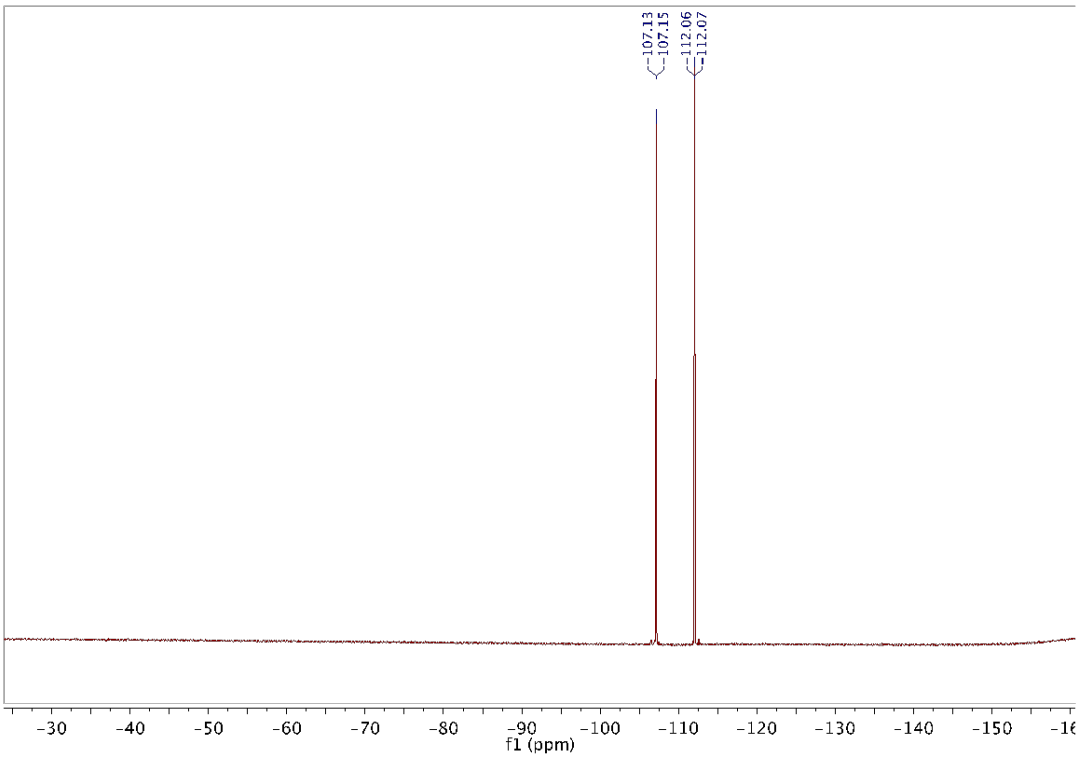

Figure S61 ^{19}F NMR spectrum of **B3**

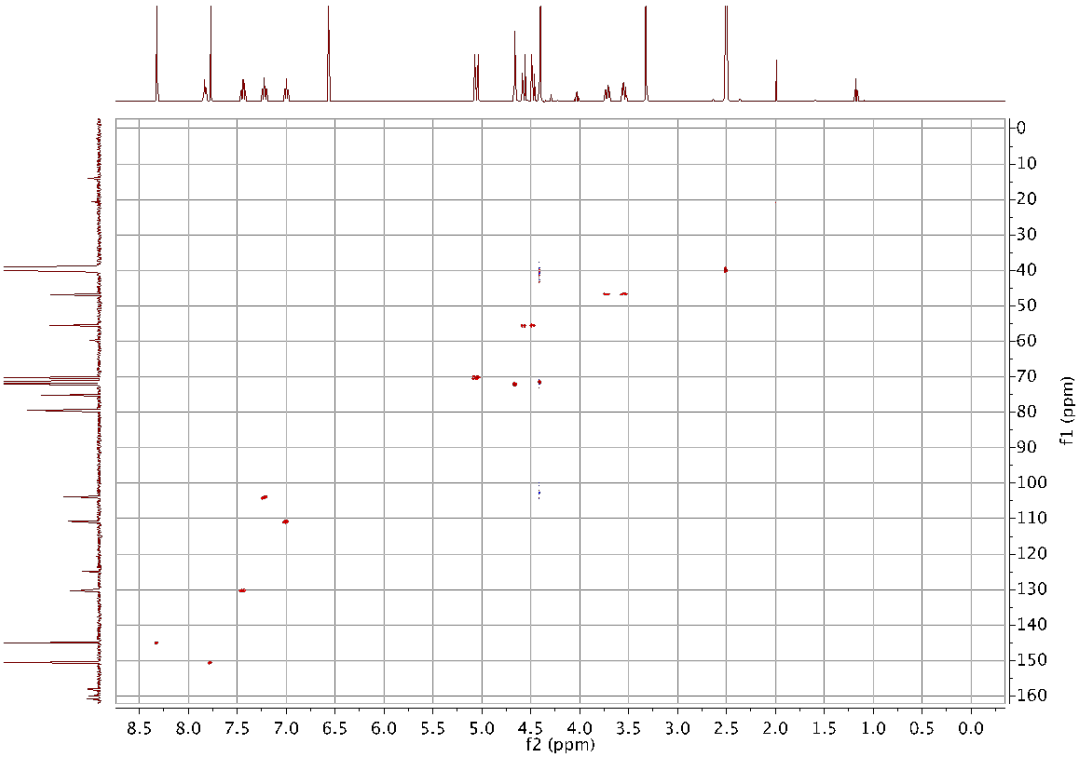

Figure S62 HSQC spectrum of **B3** in DMSO-D6

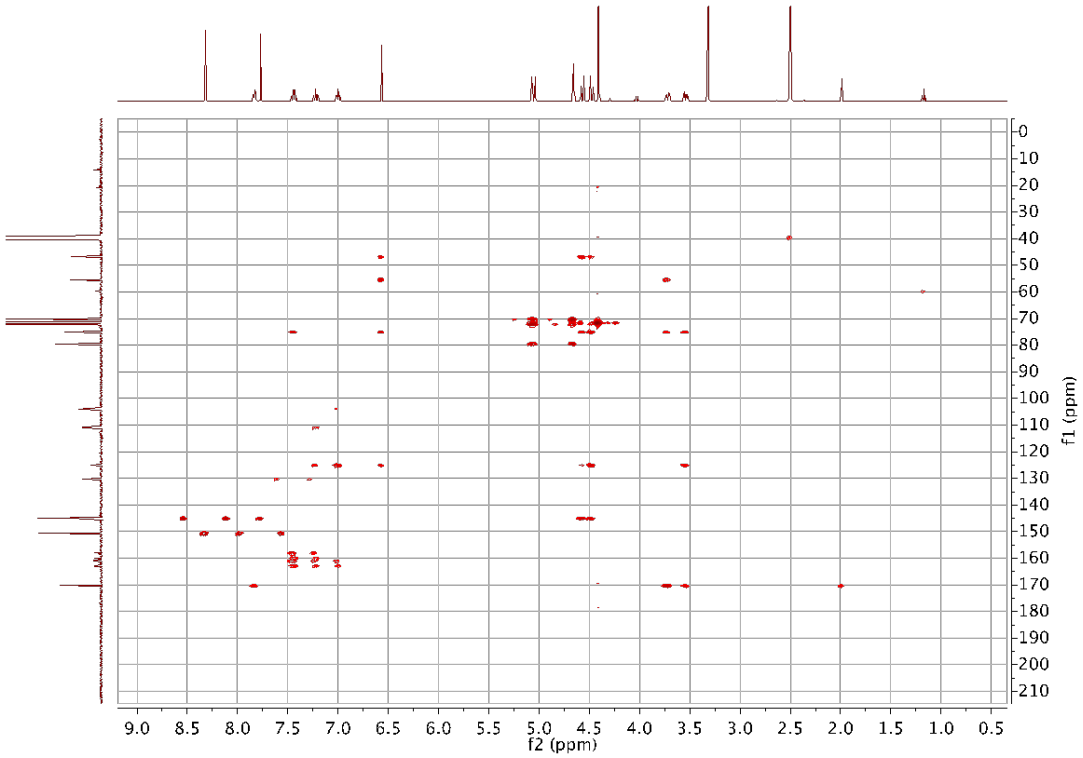

Figure S63 HMBC spectrum of **B3** in DMSO-D6

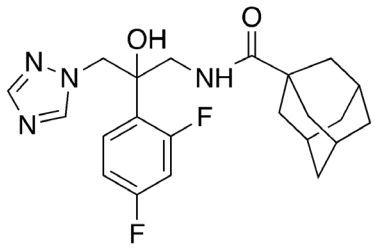

B4

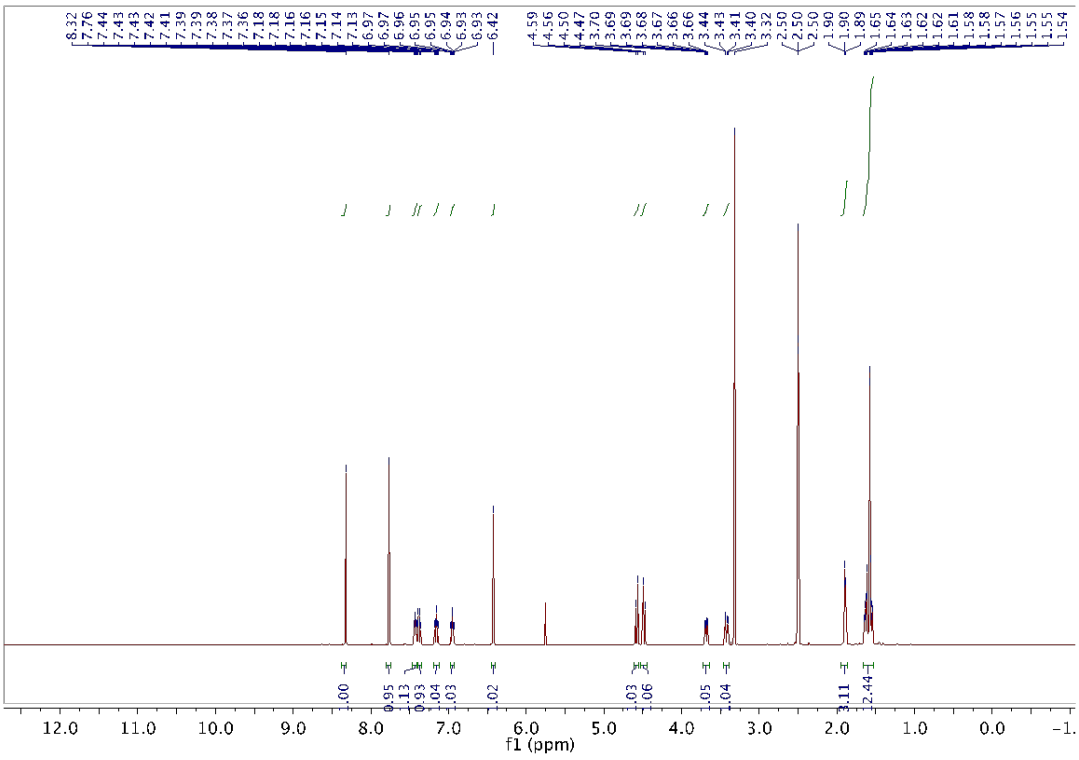

Figure S64 ^{1}H NMR spectrum of **B4**

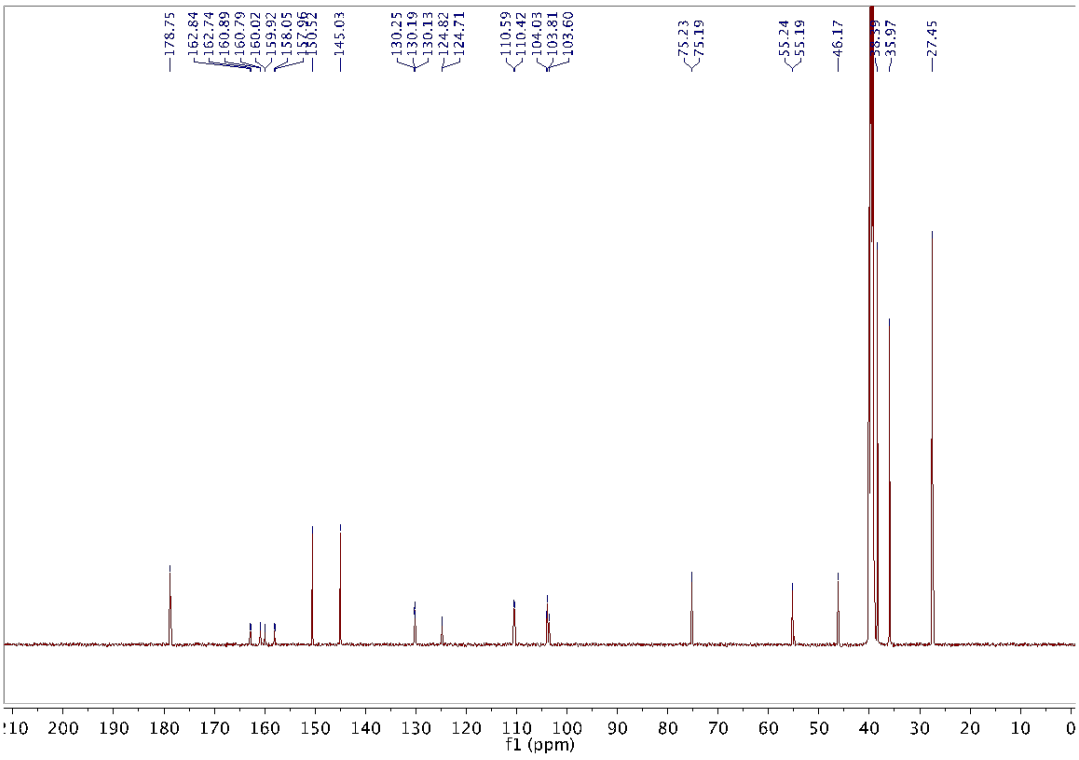

Figure S65 ^{13}C NMR spectrum of **B4**

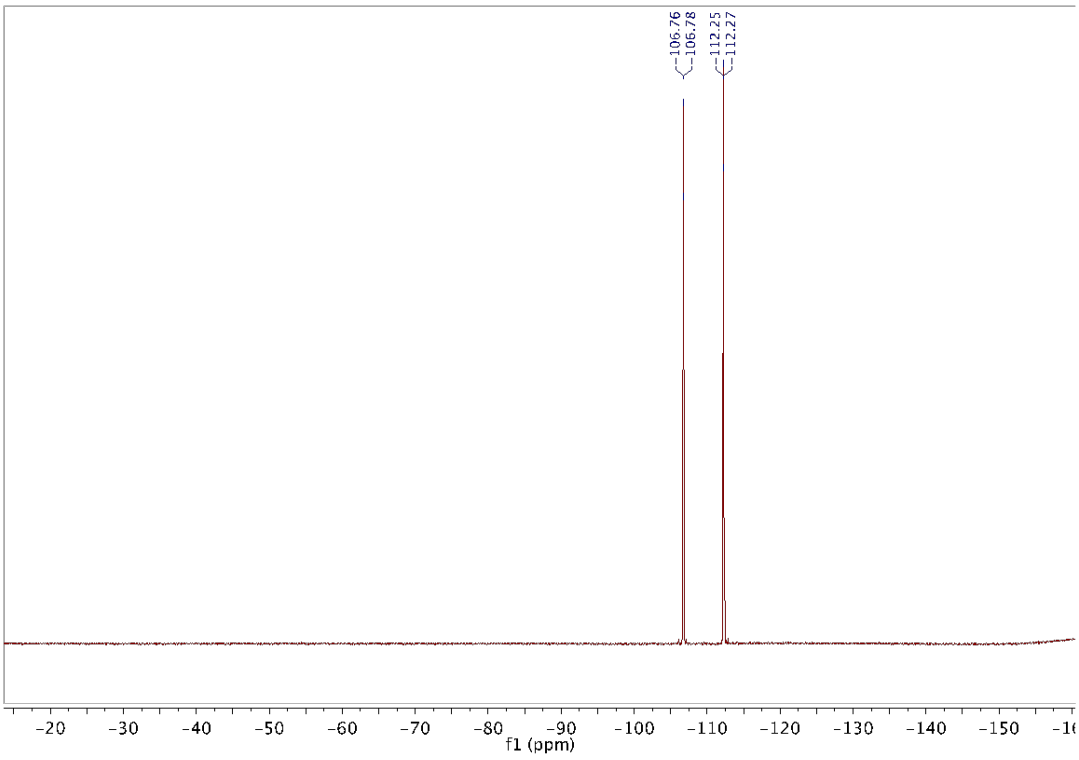

Figure S66 ^{19}F NMR spectrum of **B4**

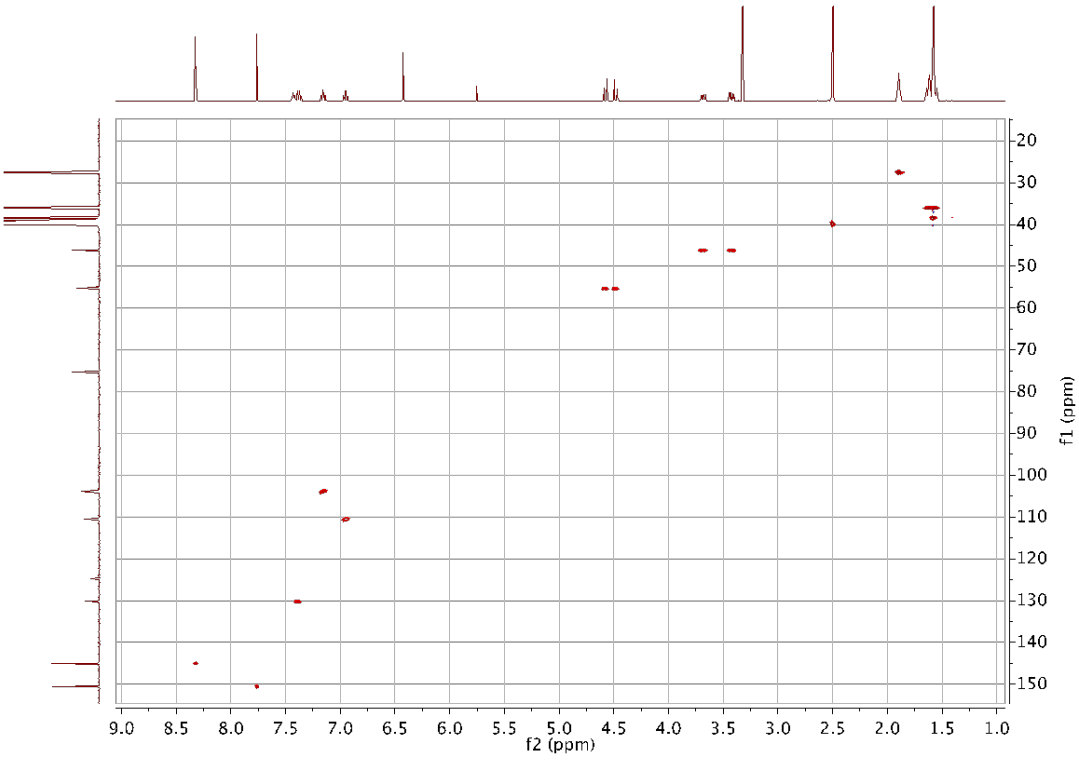

Figure S67 HSQC spectrum of **B4** in DMSO-D6

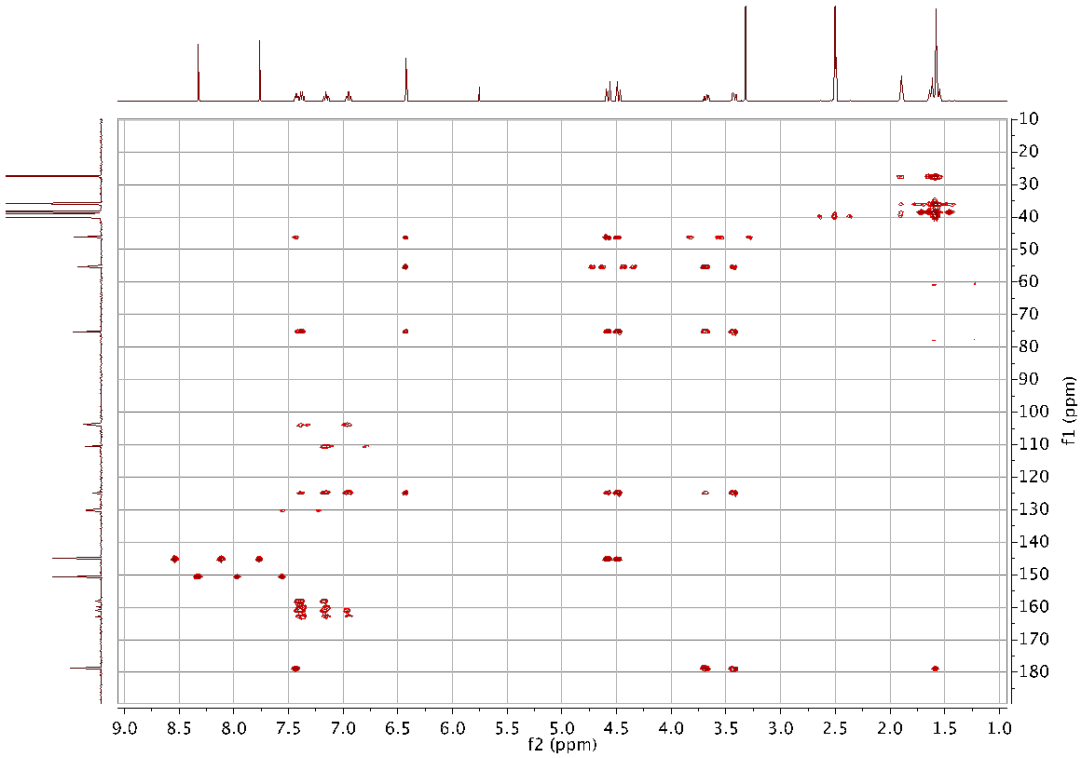

Figure S68 HMBC spectrum of **B4** in DMSO-D6

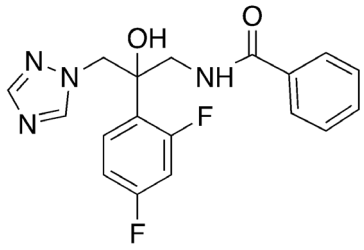

B5

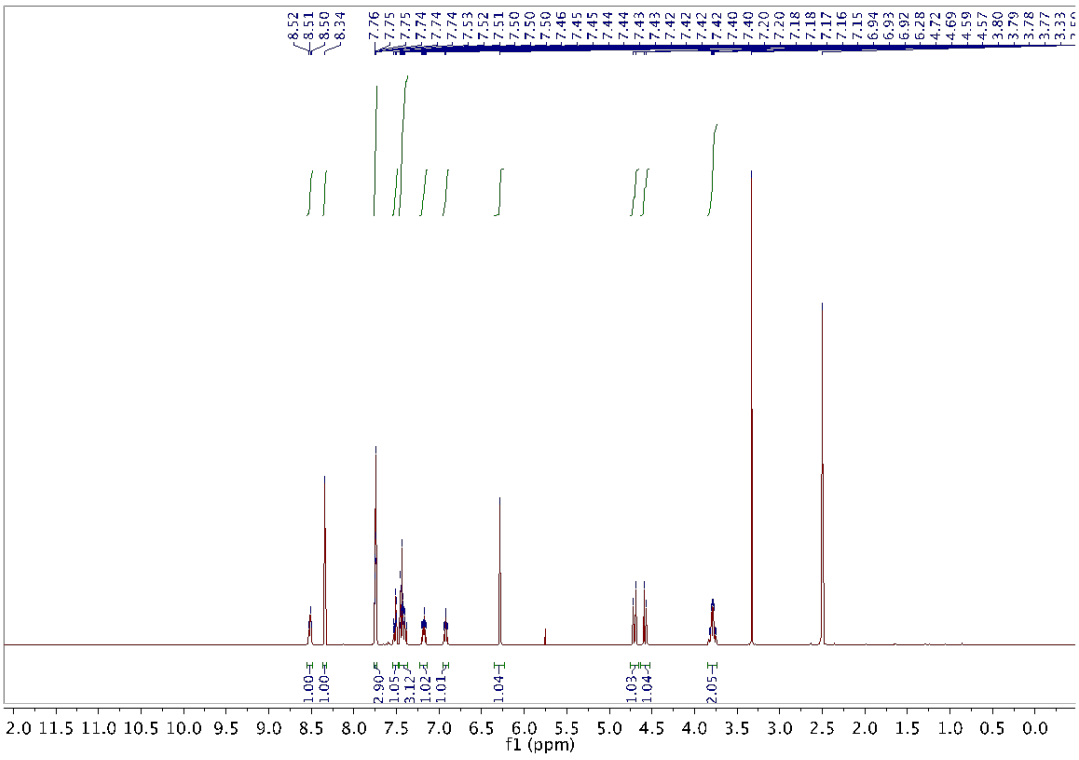

Figure S69 ^{1}H NMR spectrum of **B5**

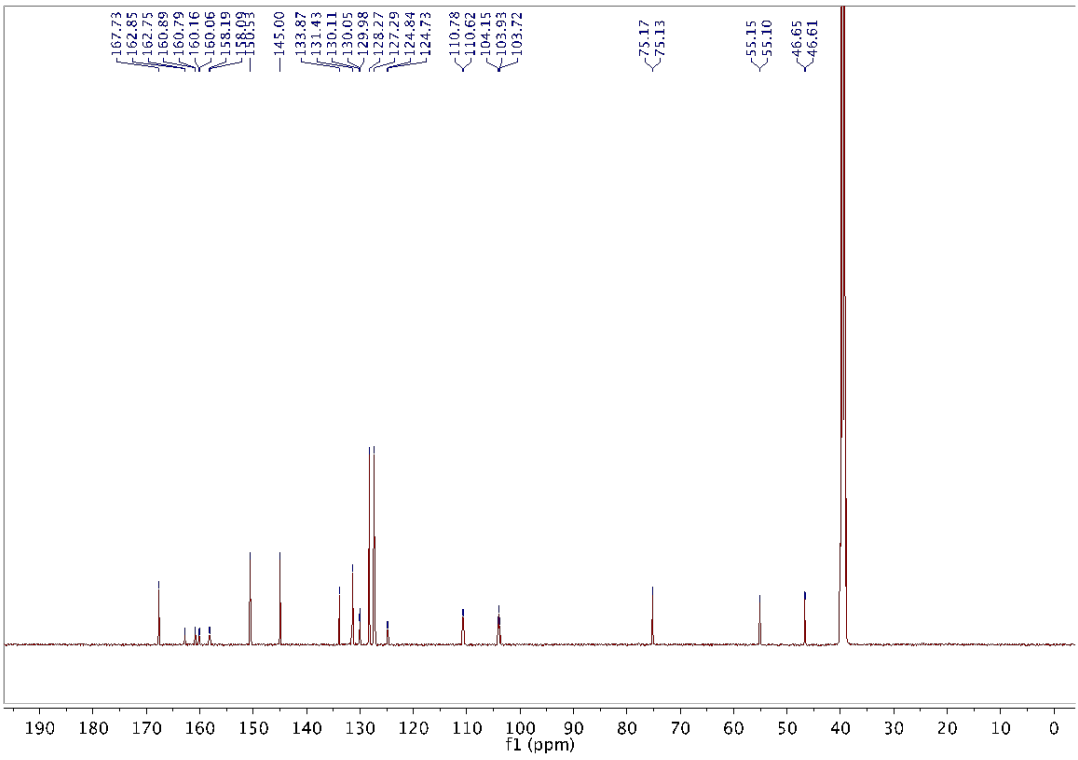

Figure S70 ^{13}C NMR spectrum of **B5**

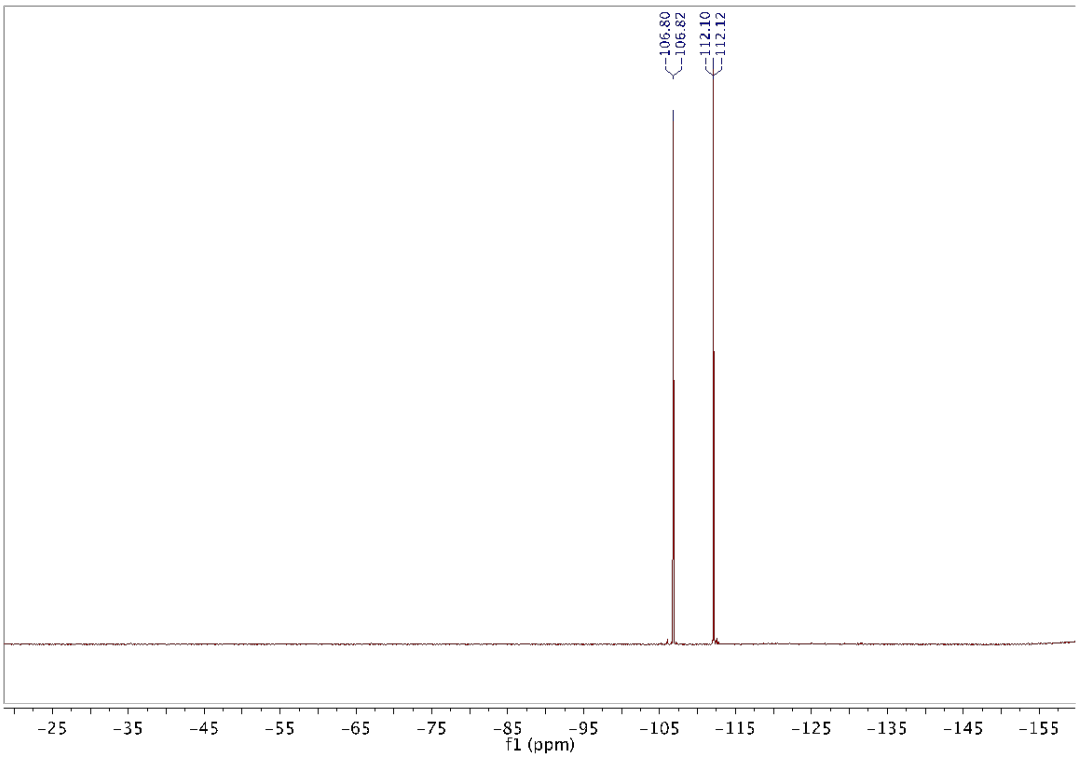

Figure S71 ^{19}F NMR spectrum of **B5**

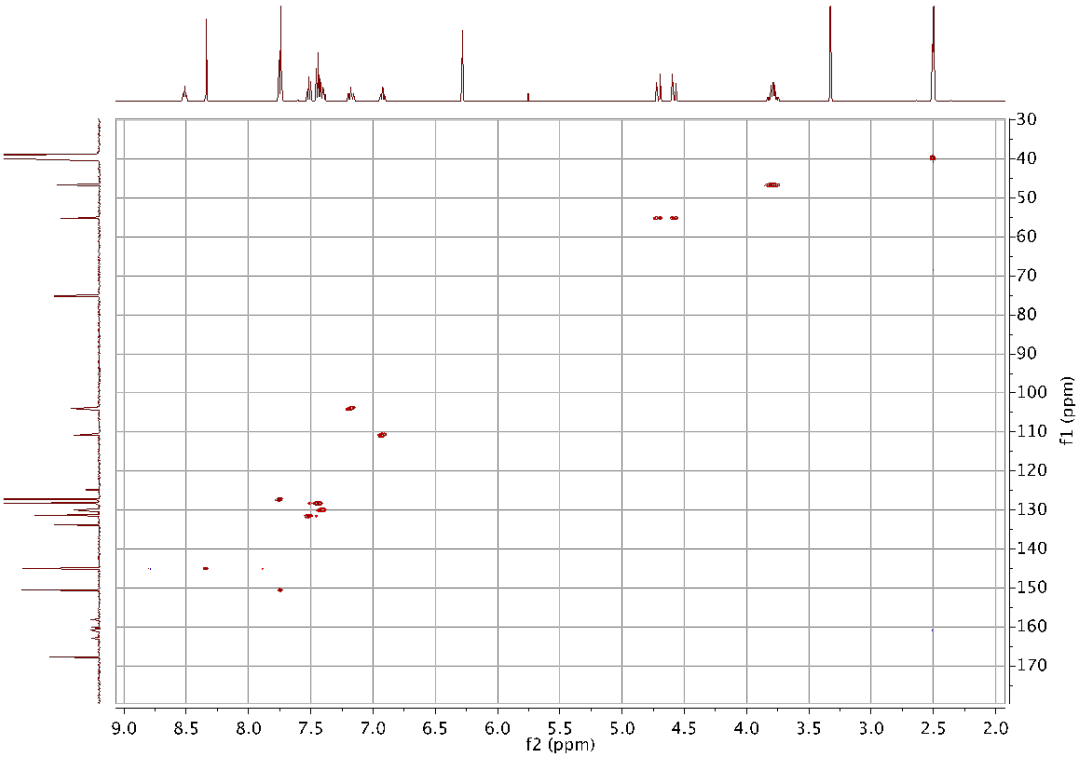

Figure S72 HSQC spectrum of **B5** in DMSO-D6

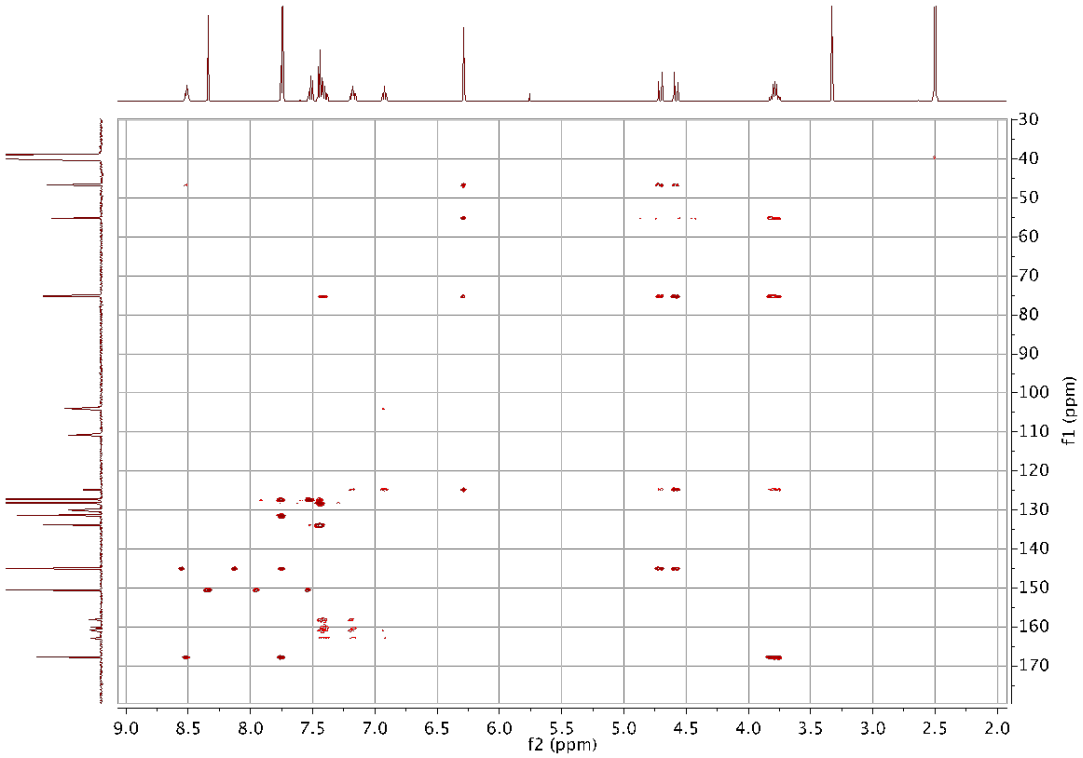

Figure S73 HMBC spectrum of **B5** in DMSO-D6

Infrared spectra

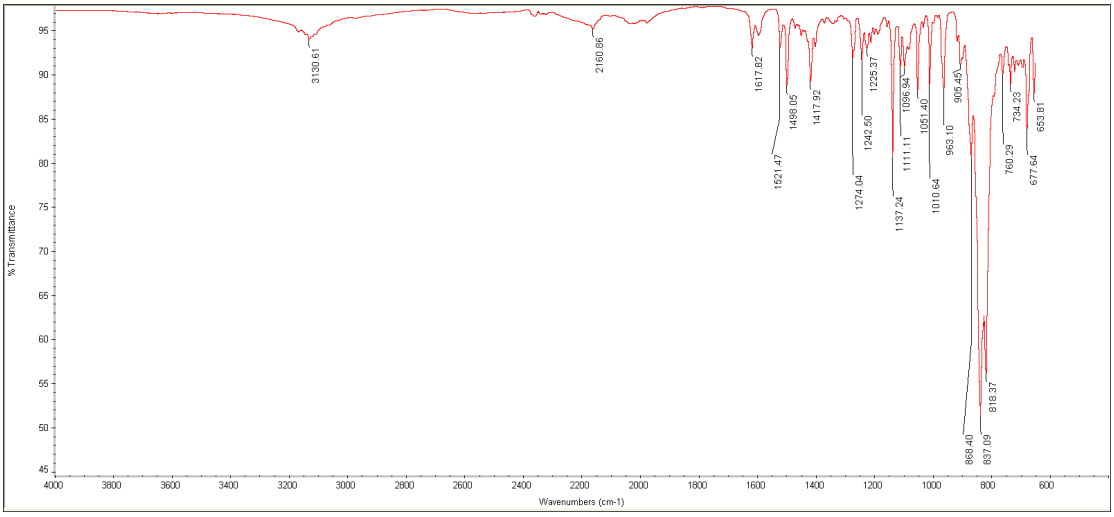

Figure S74 Infrared spectra of **A1-PF_6**

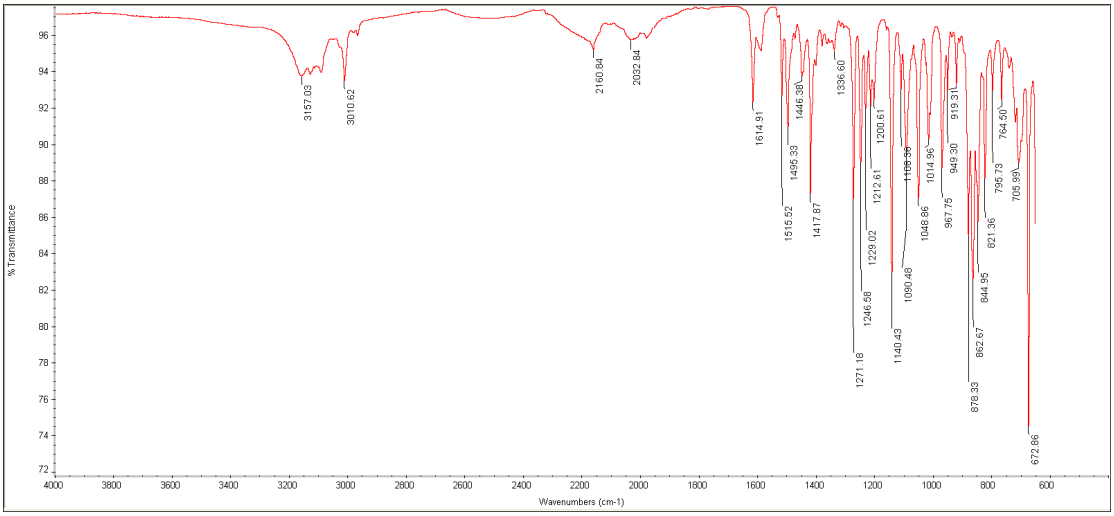

Figure S75 Infrared spectra of **A1-Cl**

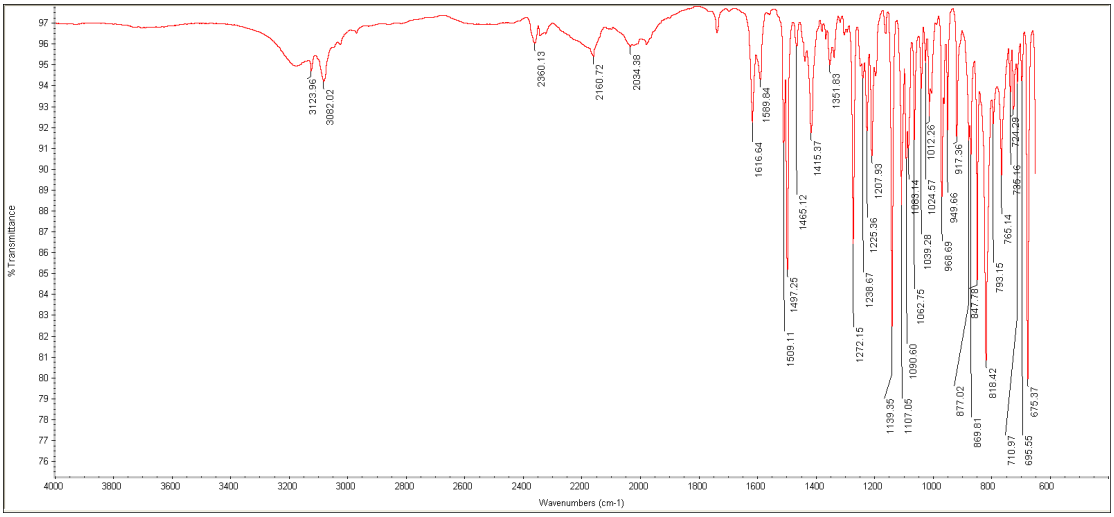

Figure S76 Infrared spectra of **A2**

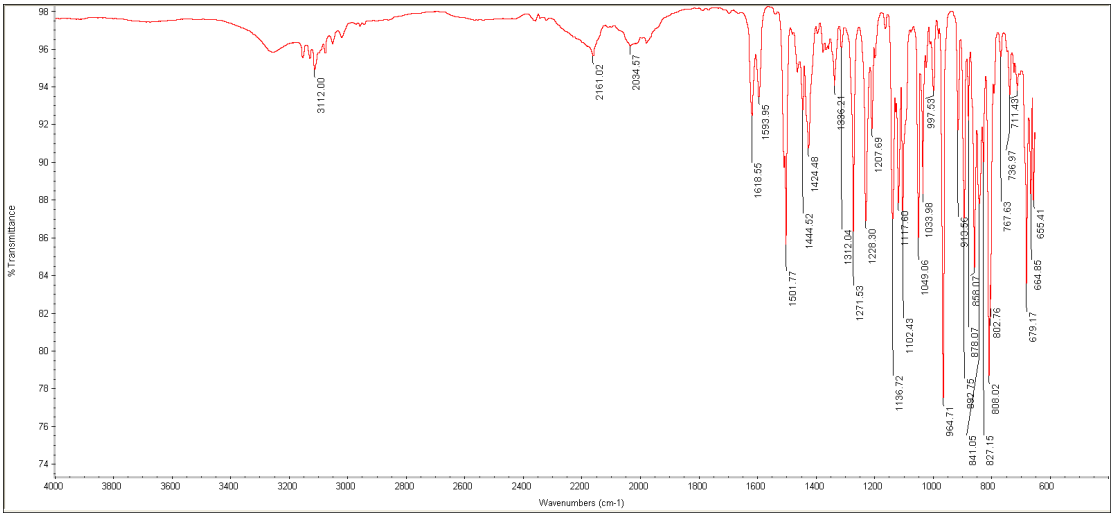

Figure S77 Infrared spectra of **A3**

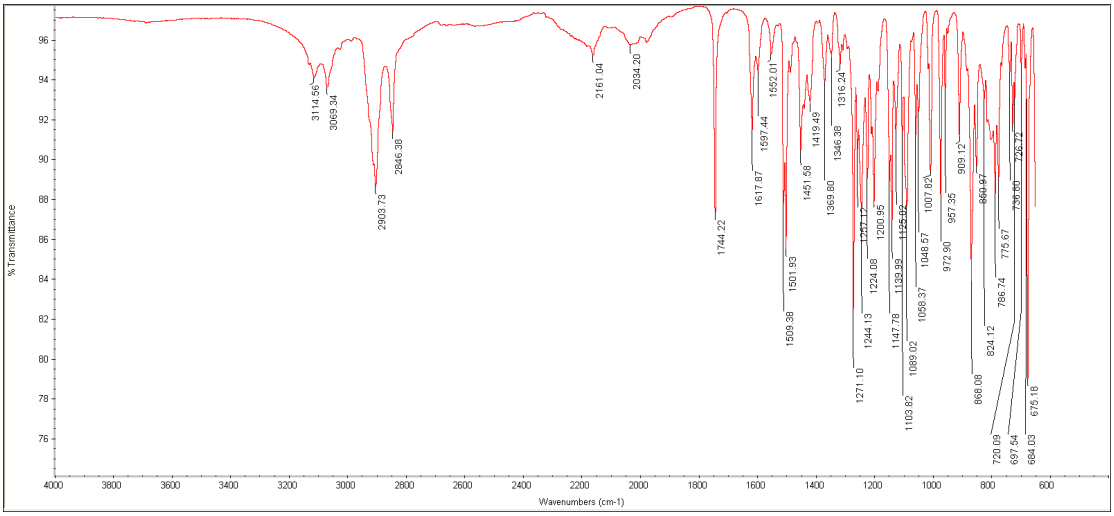

Figure S78 Infrared spectra of **A4**

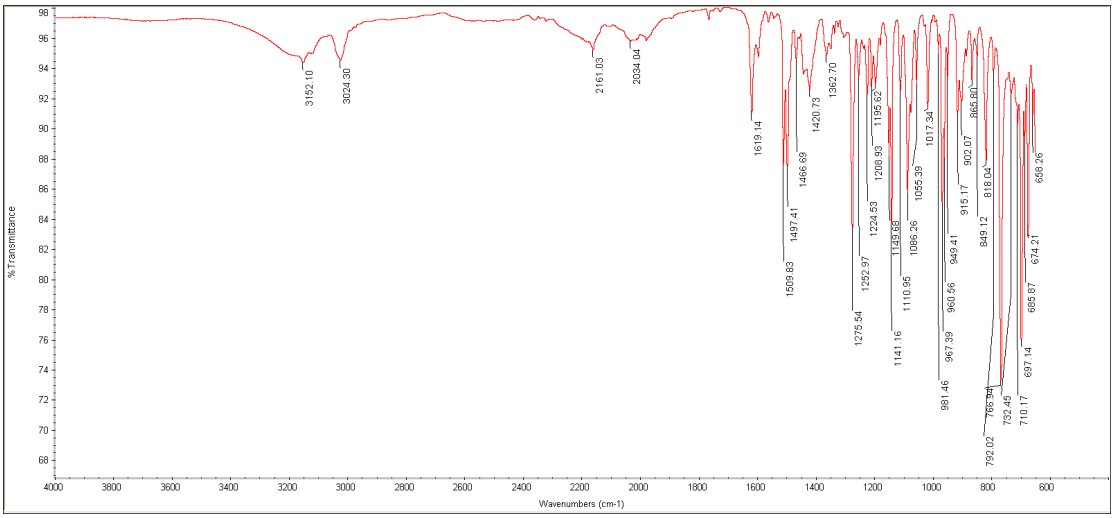

Figure S79 Infrared spectra of **A5**

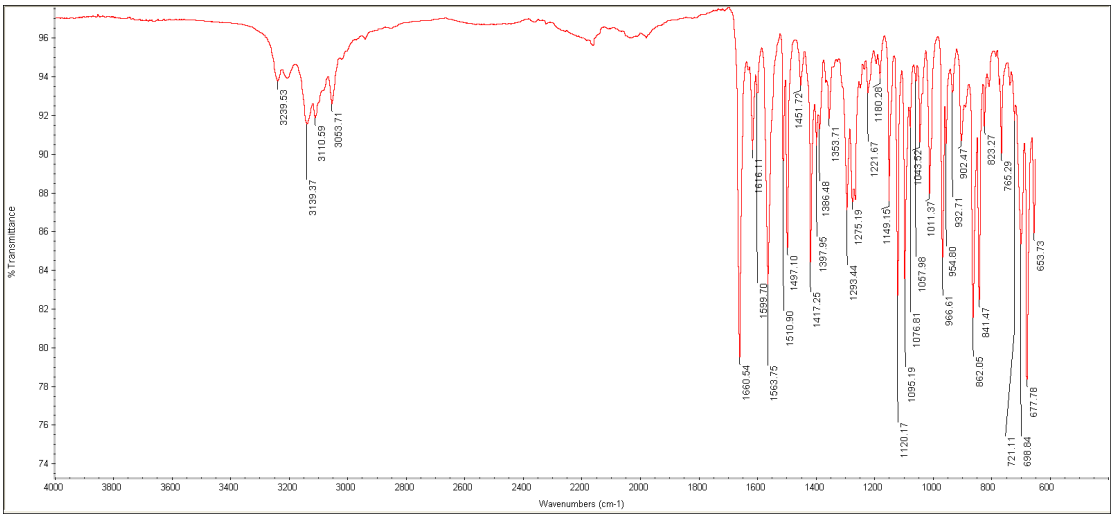

Figure S80 Infrared spectra of **B1-Cl**

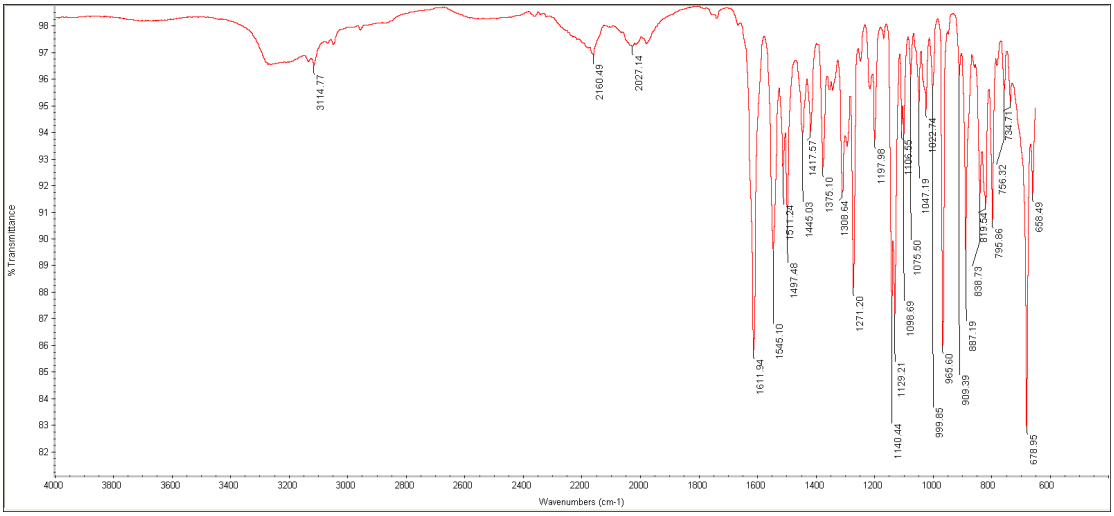

Figure S81 Infrared spectra of **B2**

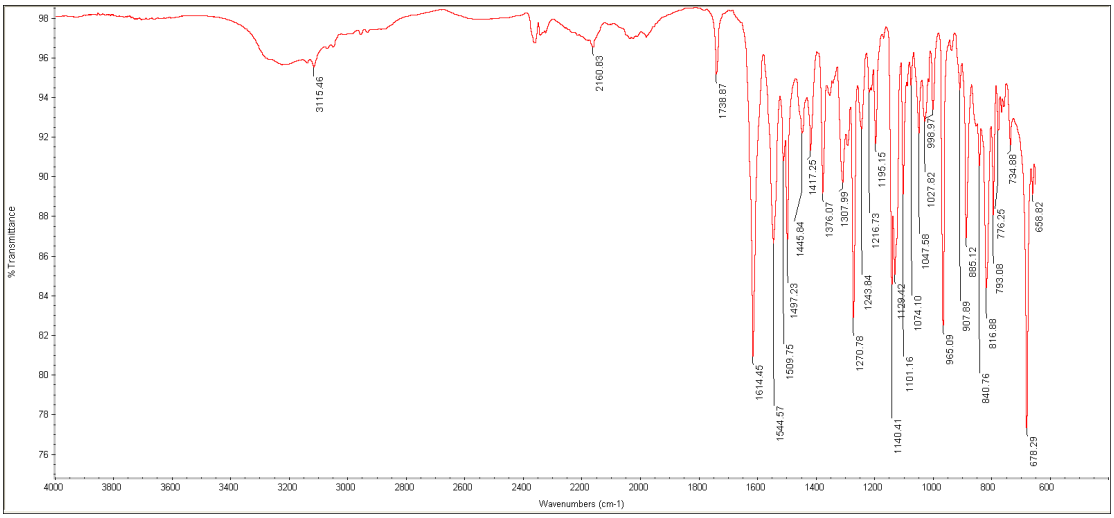

Figure S82 Infrared spectra of **B3**

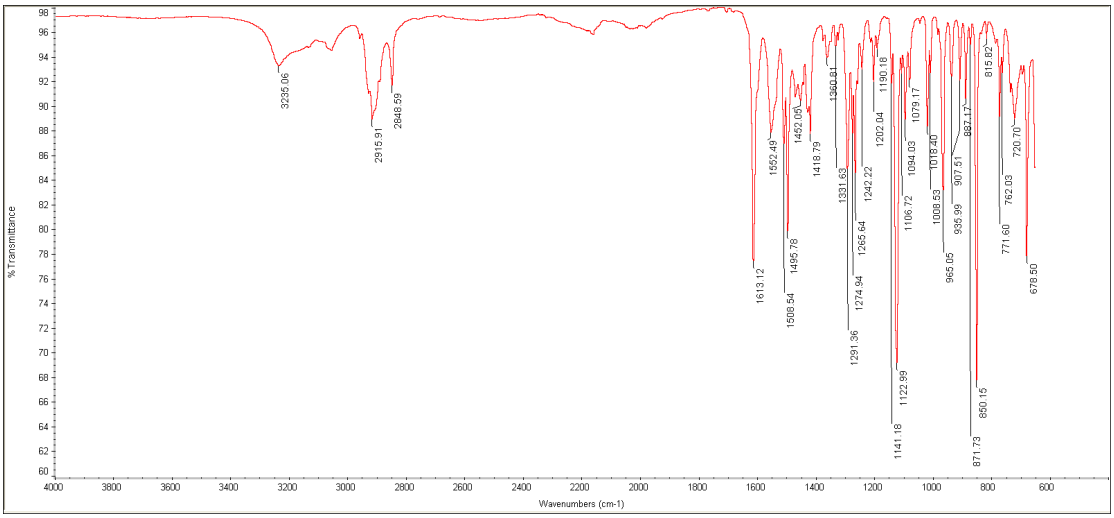

Figure S83 Infrared spectra of **B4**

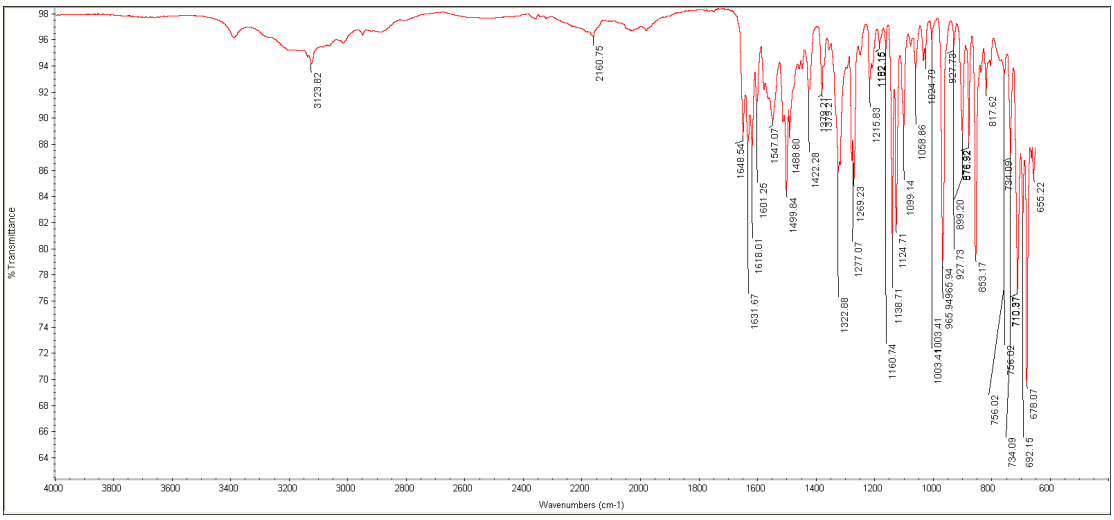

Figure S84 Infrared spectra of **B5**

1H NMR spectra for stability

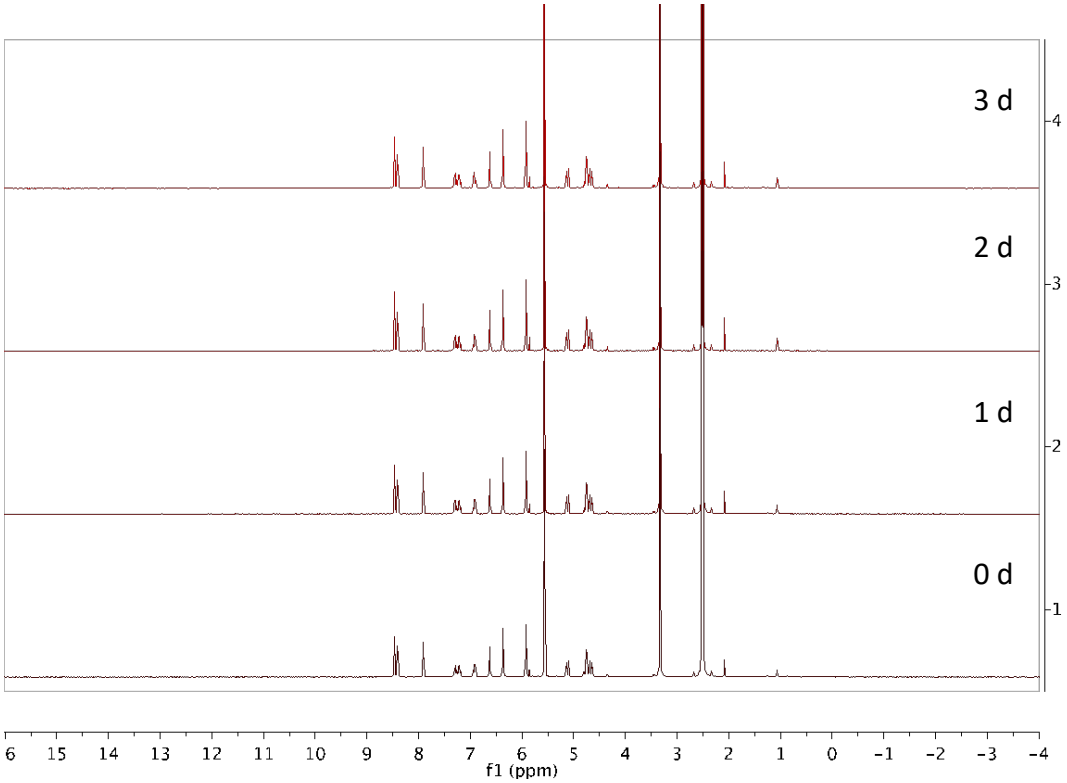

Figure S85. Stability of **A1-PF_6** in DMSO up to three days.

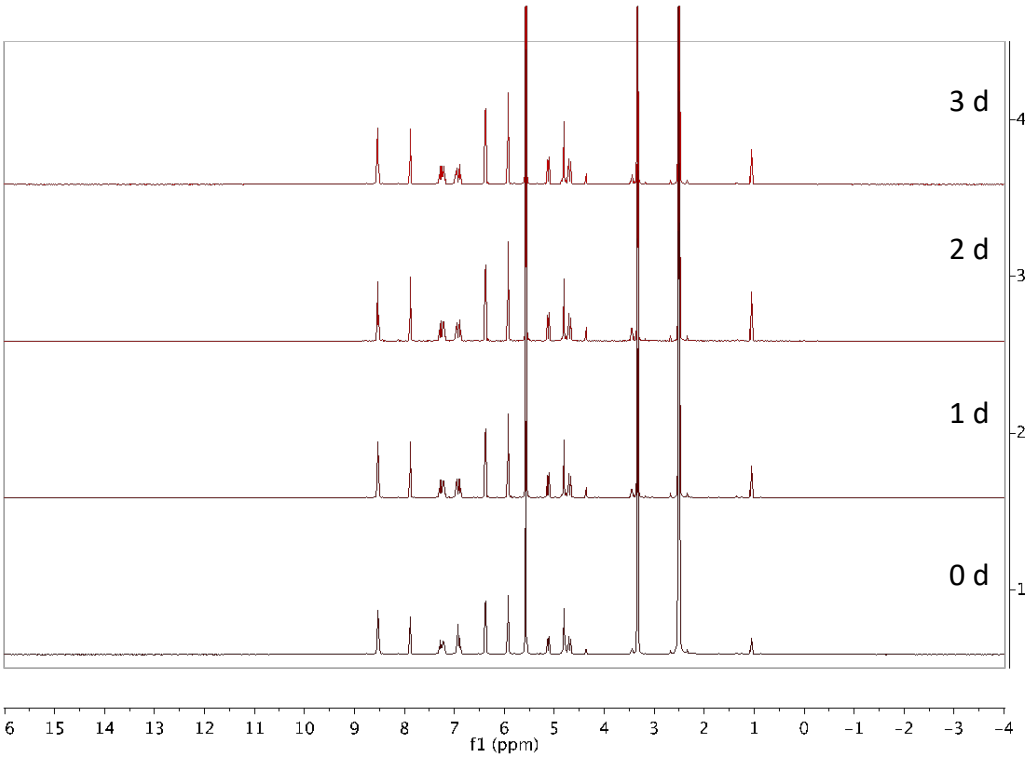

Figure S86. Stability of **A1-Cl** in DMSO up to three days.

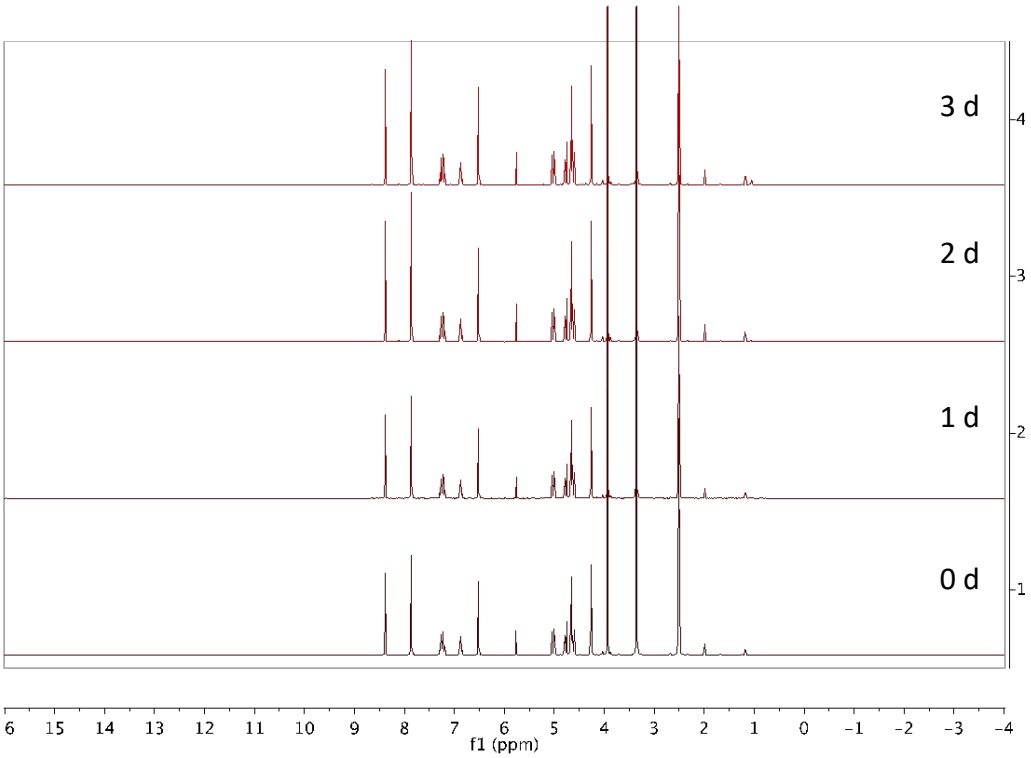

Figure 87. Stability of **A2** in DMSO up to three days.

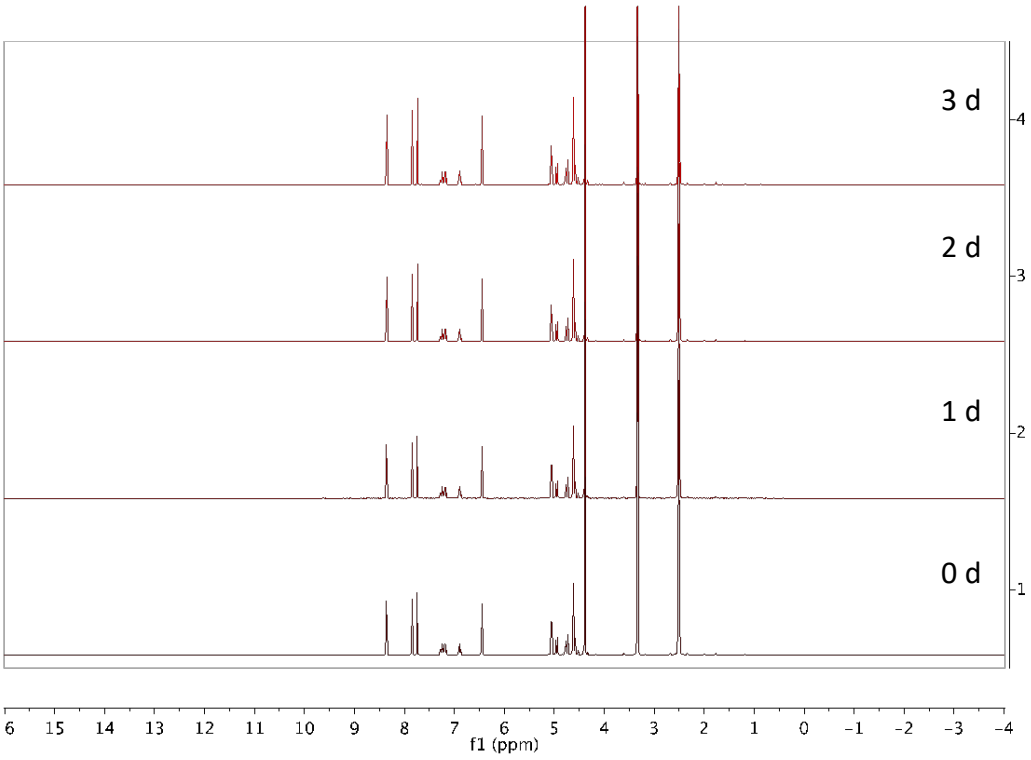

Figure S88. Stability of **A3** in DMSO up to three days.

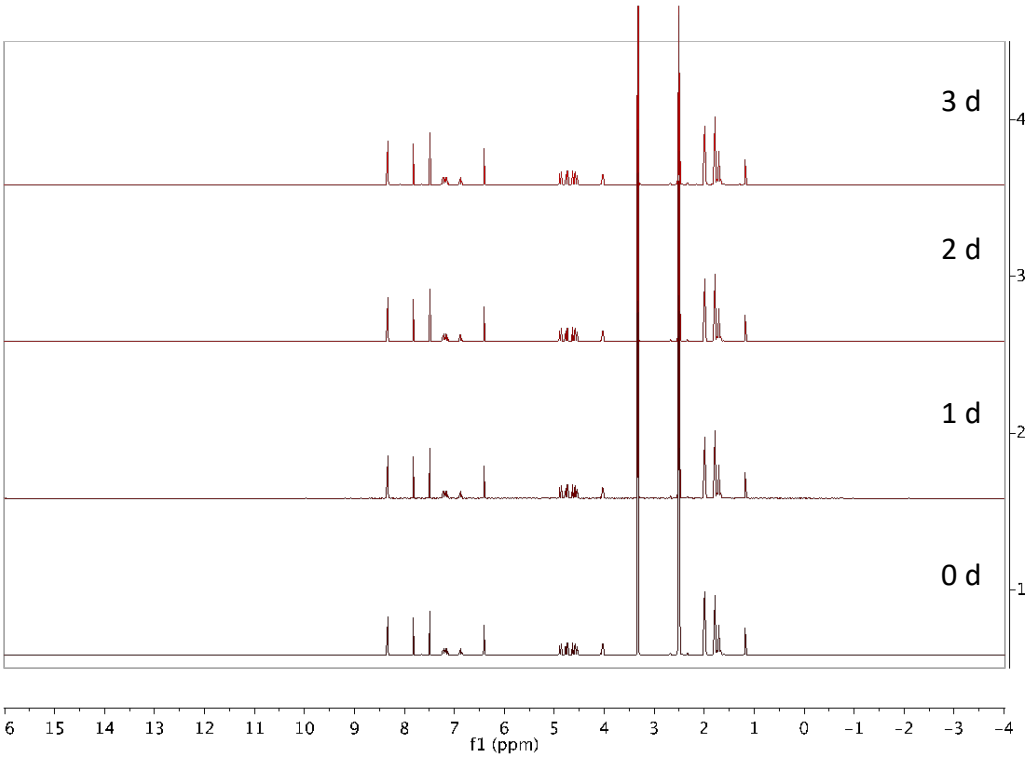

Figure S89. Stability of **A4** in DMSO up to three days.

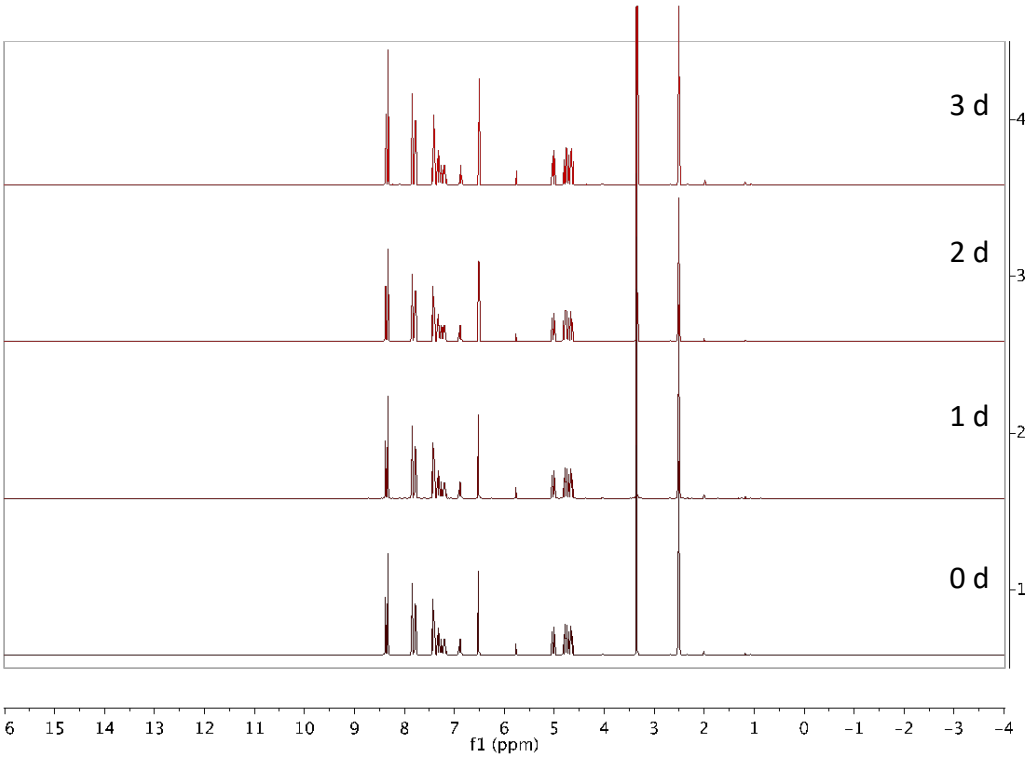

Figure S90. Stability of **A5** in DMSO up to three days.

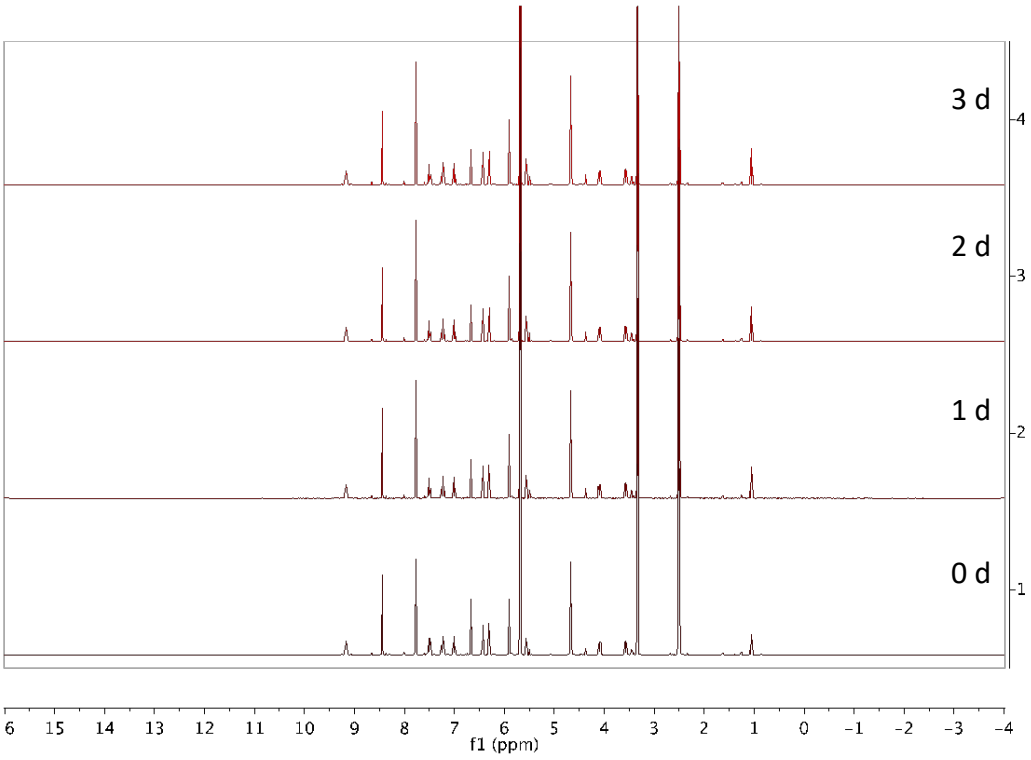

Figure S91. Stability of **B1-Cl** in DMSO up to three days.

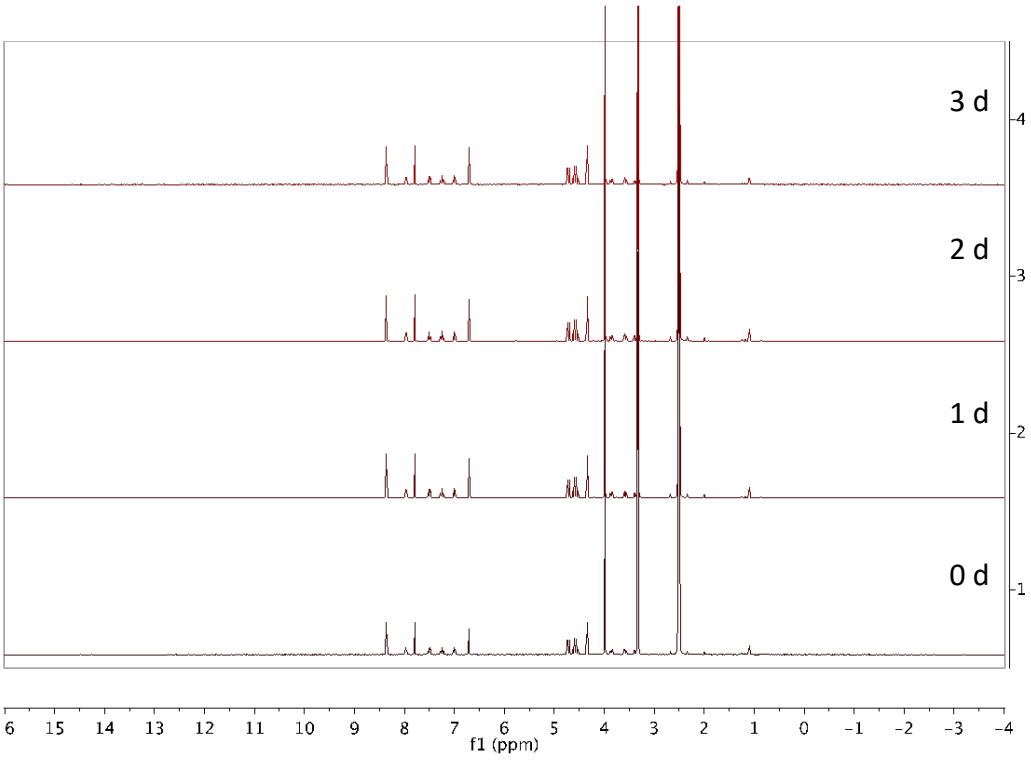

Figure S92. Stability of **B2** in DMSO up to three days.

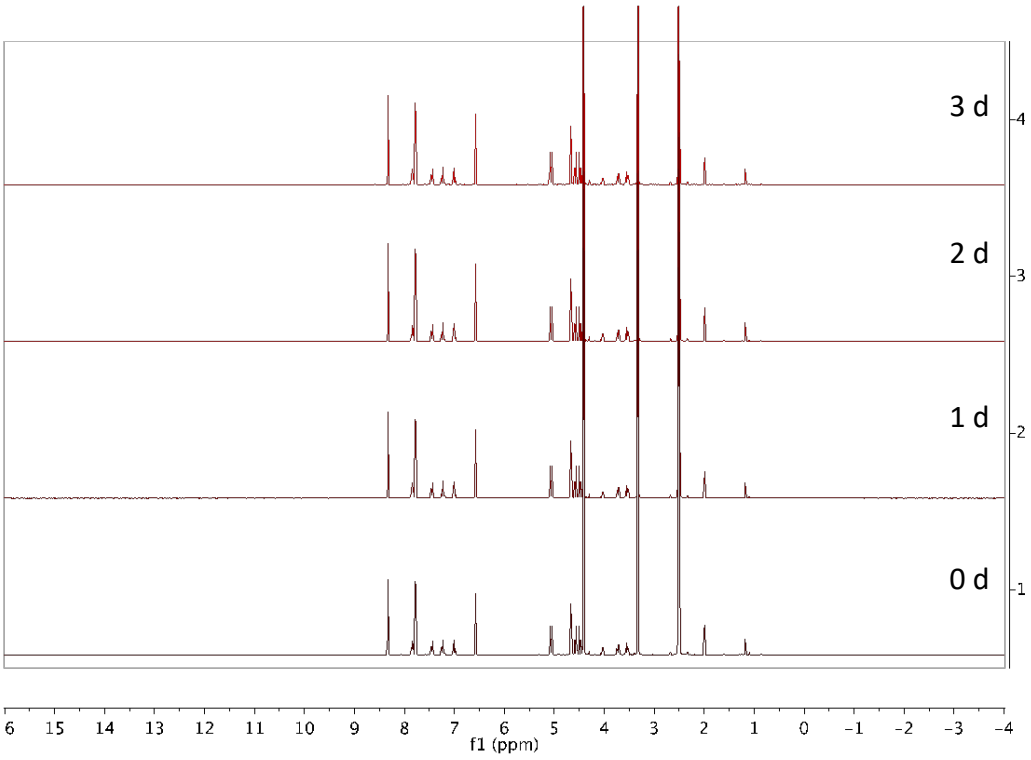

Figure S93. Stability of **B3** in DMSO up to three days.

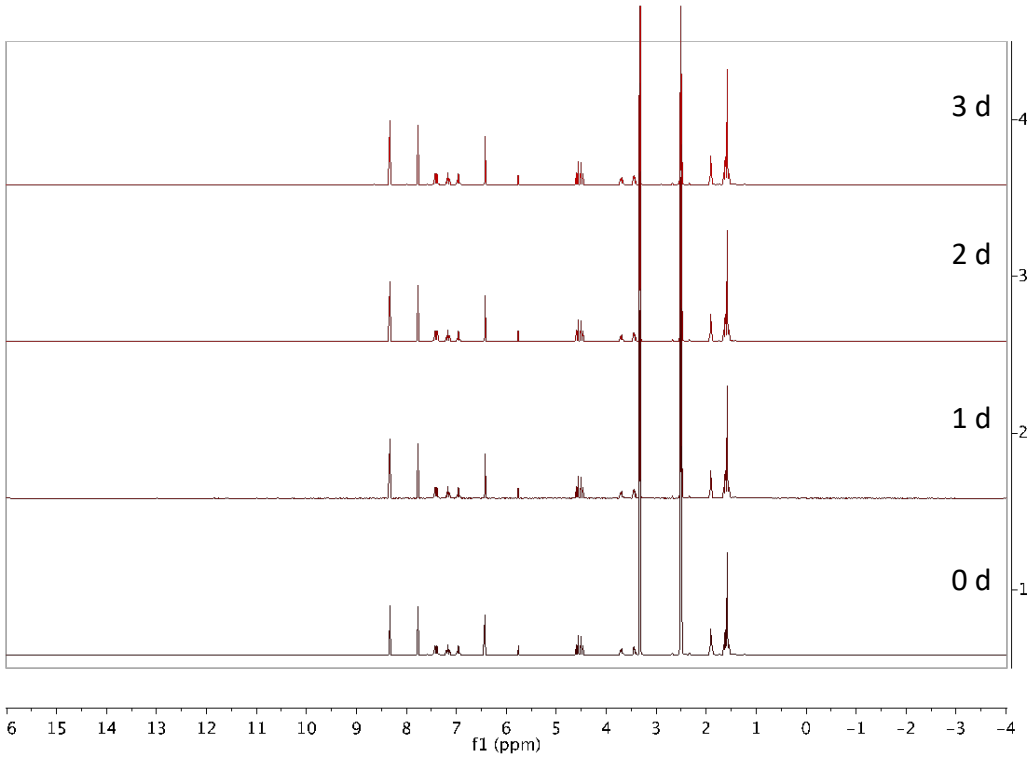

Figure S94. Stability of **B4** in DMSO up to three days.

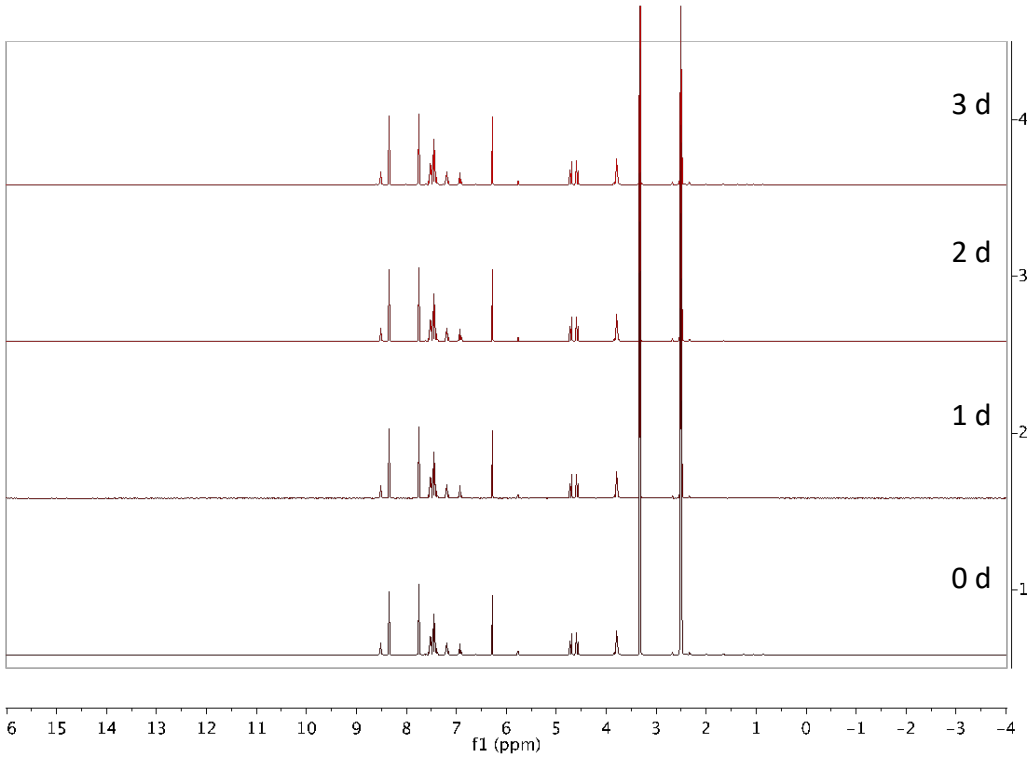

Figure S95. Stability of **B5** in DMSO up to three days.

Materials and Methods section for computational studies

Modelling of the fluconazole derivatives.

The modelling of fluconazole derivatives was necessary since even knowing their crystallographic structure, possible conformational changes may be essential to understand their binding modes.

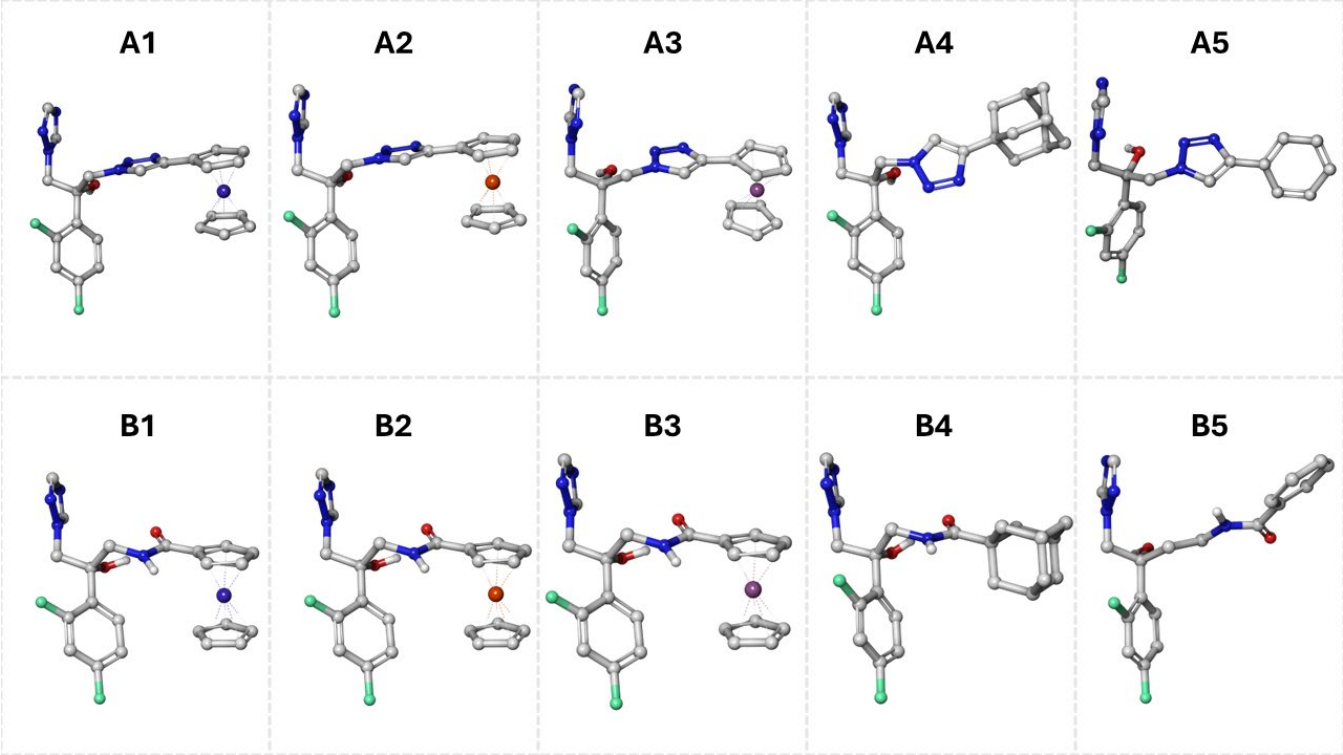

Figure S96. Structures of the modelled ligands in its minimal energy conformation.

Sequences and 3D protein alignment.

After alignment, the comparison of both *T. cruzi* and *H. sapiens* CYP51 resulted in an identity of 33% and a similarity of 53.8%. This value equals the number or residue matches between *H. sapiens* and *T. cruzi* CYP51 sequences and divided by the length of the *T. cruzi* sequence. Even this low rate of identity and similarity, the enzyme structures denote a high conservation in the secondary structures. A 3D superposition of structures is shown in the Figure S97. The aligned sequences are shown in Figure S98.

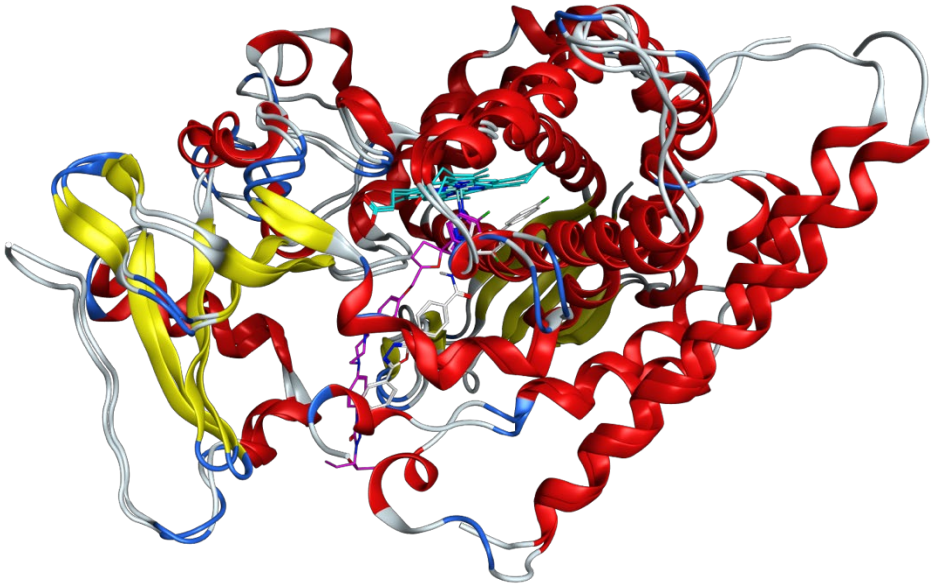

Figure S97. 3D structures of *T cruzi* and *H sapiens* CYP51 crystallographic data. Cyan rods: _HEME moieties. Magenta rods: posaconazole co-crystallized within *T cruzi* CYP51. Yellow rods: (*R*)-*N*-(1-(3,4'-difluorobiphenyl-4-yl)-2-(1*H*-imidazol-1-yl)ethyl)-4-(5-phenyl-1,3,4-oxadiazol-2-yl)benzamide (VFV) co-crystallized within *H sapiens* CYP51**.**

Figure S98: Aligned sequences of *T. cruzi* and *H. sapiens* species.

Site Finder*:*

The crystallographic structure of the CYP51 of *T. cruzi* in complex with posaconazole (PDB id 2KIO) was used for the Site Finder analysis. Thirty-one sites were detected being two bigger sites of 62 and 95 alpha spheres placed in the region of co-crystallized posaconazole molecule. The shape and composition of *T. cruzi* and *H. sapiens* (PDB id 4UHL with the co-crystallized ligand VFV) is shown in the Figure S99. Then, theses sequences were annotated as the "Site" for docking. Note that both sites contain the HEME molecule.

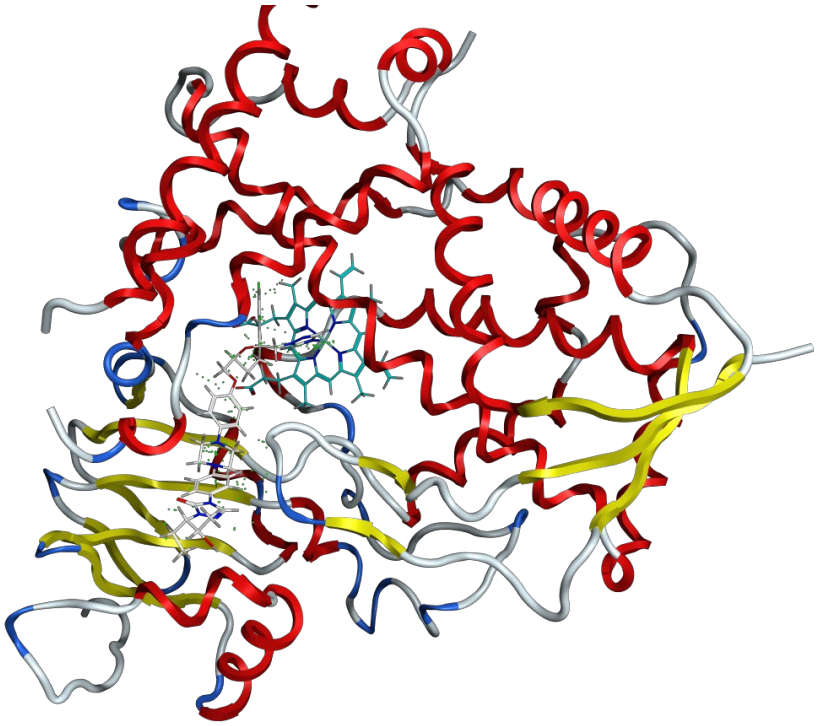

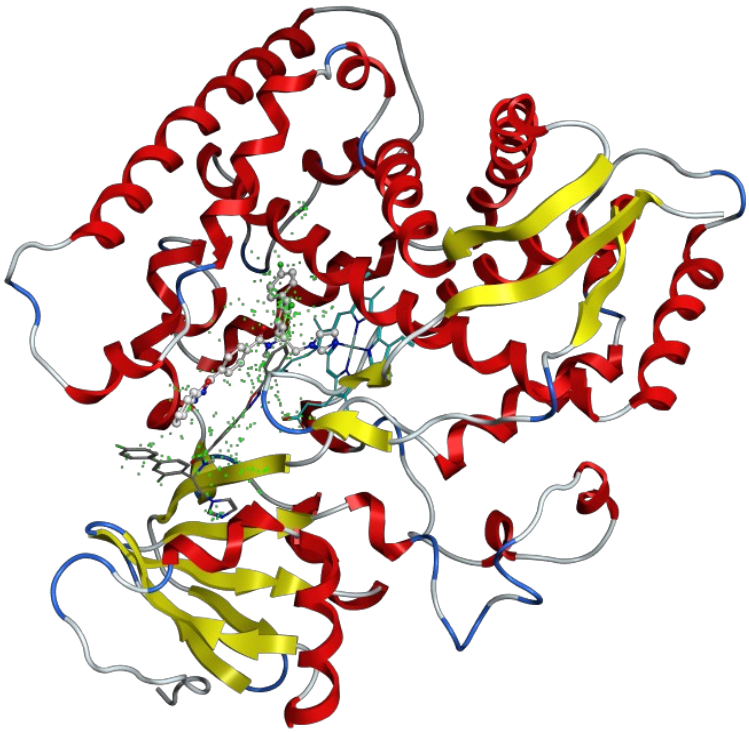

Figure S99. Main sites detected by Site Finder module in both (up) *T cruzi* and *H sapiens* (bottom) crystalographic structures. HEME molecule is drawn in cyan rods. The composition of two bigger sites of 62 and 95 alpha spheres placed in the region of co crystallyzed posaconazole molecule is for the case ot T cruzi: ILE45 PHE48 GLY49 LYS50 PRO52 ILE72 TYR103 ILE105 MET106 PHE110 ALA115 TYR116 LEU127 PRO210 ALA211 VAL213 PHE214 ALA287 ALA288 PHE290 ALA291 GLY292 GLN293 HIS294 THR295 LEU356 LEU357 MET358 MET360 TYR457 HIS458 THR459 MET460 VAL461 VAL462. (HEM488)

In the case of *H sapiens* structure, *j*ust one site was detected of 347 spheres, composed by: ILE75 PHE77 GLY78 LYS79 PRO81 PHE98 MET100 VAL101 LYS103 PHE105 TYR107 ASP129 VAL130 TYR131 LEU134 THR135 PHE139 VAL143 ALA144 TYR145 PHE152 GLN155 LEU159 PHE195 ILE203 ALA224 TYR227 ALA228 ASP231 GLY232 PHE234 SER235 HIS236 TRP239 GLY303 MET304 GLY307 LEU308 LEU310 ALA311 GLN313 HIS314 THR315 THR318 PRO376 ILE377 MET378 ILE379 MET380 MET381 MET383 GLN400 TYR484 THR485 THR486 MET487 ILE488 HIS489 THR490)2:(HEM540)

Docking

The docking was performed with AUTODOCK4.2 software.[29] Protein and compounds structures were prepared in AUTODOCK TOOLS.[30] Crystallographic structure of T. cruzi CYP51 (2WX2) co-crystallized with fluconazole was used to dock, taking the fluconazole pose as a reference. Docking protocol is described in.[30] Genetic Algorithm with 50 GA runs was used to found and perform the conformational search and selection of best docked poses. Default parameters for the studied putative ligands were used. Interaction energies were evaluated by the scoring AUTODOCK 4 scoring function.[31]

Docking analysis

After docking a clustering of all conformations was performed by AUTODOCK TOOLS and the more populated cluster was selected as the best.

Images of this selected pose inside the binding docked site were rendered using the academic licence of MAESTRO software.[32]

The results of docking are summarized in Table S7.

Table S7. *First column*: generic name of compounds. FCS: fluconazole. *Second column*: interaction free energy in kcal.mol^{-1} evaluated by the AUTODOCK scoring function for the T. cruzi. *Third column*: number of conformation in the most populated cluster over the maximum number of cluster conformations. Color codes in the first line: light green in hydrophobic residues and polar residues in light yellow.

	Score	C/T	Y103	M106	F110	A115	Y 116	L127	A287	F290	A291	T295	L356	L357	V359	M358	M 360	M460	HEMB480
FCS	-6,69	42/50	X				X		X	X	X	X							X
A1	-9,57	25/50	X				X			X			X		X	X	X	X	X
A2	-9,71	20/50	X		X		X		X		X	X	X			X	X	X	X
A3	-10,47	32/50	X				X				X	X	X	X		X	X	X	x
A4	-10,09	20/50	x		x	x	x	x	x		x	x	x			x		x	x
A5	-8,9	38/50	x		x		x					x	x			x			x
B1	-8,56	23/50	x	x		x	x	x	x	x	x	x	x			x		x	x
B2	-9,08	25/50	x	x		x	x	x	x		x	x	x			x		x	x
B3	-9,38	15/50	x	x			x	x		x	x	x	x			x		x	x
B4	-9,44	31/50	x				x				x	x	x		x	x		x	x
B5	-7,98	15/50	x	x	x		x		x	x	x		x		x	x			x

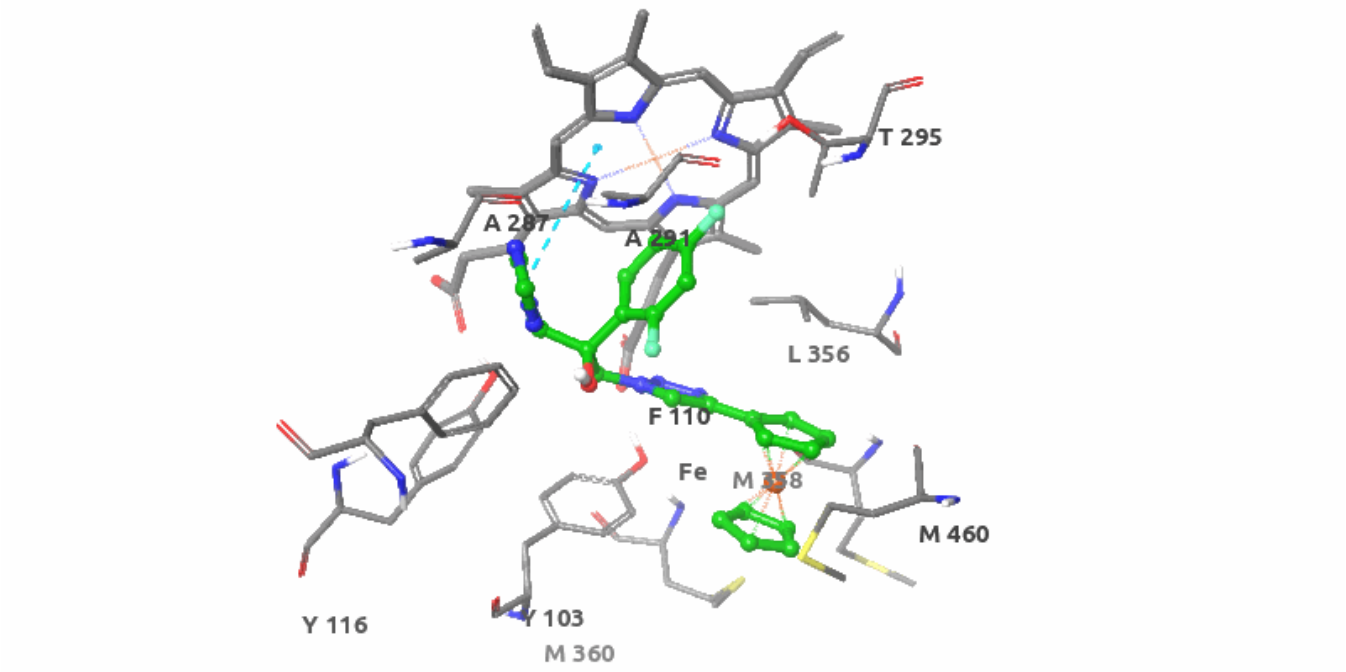

Figure S100. Animated version of the best docked conformation for the A2 molecule.

References

(1) Rubbiani, R.; Weil, T.; Tocci, N.; Mastrobuoni, L.; Jeger, S.; Moretto, M.; Ng, J.; Lin, Y.; Hess, J.; Ferrari, S.; Kaech, A.; Young, L.; Spencer, J.; Moore, A. L.; Cariou, K.; Renga, G.; Pariano, M.; Romani, L.; Gasser, G. *In Vivo* Active Organometallic-Containing Antimycotic Agents. *RSC Chem. Biol.* **2021**, *2* (4), 1263–1273. https://doi.org/10.1039/D1CB00123J.

(2) Wang, W.; Sheng, C.; Che, X.; Ji, H.; Miao, Z.; Yao, J.; Zhang, W. Design, Synthesis, and Antifungal Activity of Novel Conformationally Restricted Triazole Derivatives. *Arch. Pharm. Chem. Life Sci.* **2009**, *342* (12), 732–739. https://doi.org/10.1002/ardp.200900103.

(3) Vanicek, S.; Kopacka, H.; Wurst, K.; Müller, T.; Schottenberger, H.; Bildstein, B. Chemoselective, Practical Synthesis of Cobaltocenium Carboxylic Acid Hexafluorophosphate. *Organometallics* **2014**, *33* (5), 1152–1156. https://doi.org/10.1021/om401120h.

(4) Courtney, D.; John McAdam, C.; Manning, A. R.; Müller-Bunz, H.; Ortin, Y.; Simpson, J. The Preparation, Spectroscopy, Structure and Electrochemistry of Some [Co(H4-C4Ph4)(H5-C5H4CC–CHY)], [Fe(H5-C5H5)(H5-C5H4CC–CHY)], and Related Complexes. *Journal of Organometallic Chemistry* **2012**, *705*, 7–22. https://doi.org/10.1016/j.jorganchem.2011.12.012.

(5) Sanders, R.; Mueller-Westerhoff, U. T. The Lithiation of Ferrocene and Ruthenocene: A Retraction and an Improvement. *Journal of Organometallic Chemistry* **1996**, *512* (1–2), 219–224. https://doi.org/10.1016/0022-328X(95)05914-B.

(6) Pertici, P.; Vitulli, G.; Spink, W. C.; Rausch, M. D. Cycloolefin Complexes of Ruthenium. In *Inorganic Syntheses*; Holt, S. L., Ed.; John Wiley & Sons, Inc.: Hoboken, NJ, USA, 2007; pp 176–181. https://doi.org/10.1002/9780470132531.ch38.

(7) Alkan, A.; Gleede, T.; Wurm, F. R. Ruthenocenyl Glycidyl Ether: A Ruthenium-Containing Epoxide for Anionic Polymerization. *Organometallics* **2017**, *36* (16), 3023–3028. https://doi.org/10.1021/acs.organomet.7b00278.

(8) Hassenrück, C.; Mang, A.; Winter, R. F. Mixed-Valent Ruthenocene–Vinylruthenium Conjugates: Valence Delocalization Despite Chemically Different Redox Sites. *Inorg. Chem.* **2019**, *58* (4), 2695–2707. https://doi.org/10.1021/acs.inorgchem.8b03253.

(9) Ha, S.; Lee, Y.; Kwak, Y.; Mishra, A.; Yu, E.; Ryou, B.; Park, C.-M. Alkyne–Alkene [2 + 2] Cycloaddition Based on Visible Light Photocatalysis. *Nat Commun* **2020**, *11* (1), 2509. https://doi.org/10.1038/s41467-020-16283-9.

(10) Hellmuth, T.; Rieckhoff, S.; Weiss, M.; Dorst, K.; Frey, W.; Peters, R. Cooperative Bimetallic Asymmetric Catalysis: Comparison of a Planar Chiral Ruthenocene Bis-Palladacycle to the Corresponding Ferrocene. *ACS Catal.* **2014**, *4* (6), 1850–1858. https://doi.org/10.1021/cs500393x.

(11) MacLean, L. M.; Thomas, J.; Lewis, M. D.; Cotillo, I.; Gray, D. W.; De Rycker, M. Development of Trypanosoma Cruzi in Vitro Assays to Identify Compounds Suitable for Progression in Chagas' Disease Drug Discovery. *PLoS Negl Trop Dis* **2018**, *12* (7), e0006612. https://doi.org/10.1371/journal.pntd.0006612.

(12) Duran-Rehbein, G. A.; Vargas-Zambrano, J. C.; Cuéllar, A.; Puerta, C. J.; Gonzalez, J. M. Mammalian Cellular Culture Models of *Trypanosoma Cruzi* Infection: A Review of the Published Literature. *Parasite* **2014**, *21*, 38. https://doi.org/10.1051/parasite/2014040.

(13) Scalese, G.; Machado, I.; Fontana, C.; Risi, G.; Salinas, G.; Pérez-Díaz, L.; Gambino, D. New Heteroleptic Oxidovanadium(V) Complexes: Synthesis, Characterization and Biological Evaluation as Potential Agents against Trypanosoma Cruzi. *J Biol Inorg Chem* **2018**, *23* (8), 1265–1281. https://doi.org/10.1007/s00775-018-1613-1.

(14) Vieites, M.; Smircich, P.; Parajón-Costa, B.; Rodríguez, J.; Galaz, V.; Olea-Azar, C.; Otero, L.; Aguirre, G.; Cerecetto, H.; González, M.; Gómez-Barrio, A.; Garat, B.; Gambino, D. Potent in Vitro Anti-Trypanosoma Cruzi Activity of Pyridine-2-Thiol N-Oxide Metal Complexes Having an Inhibitory Effect on Parasite-Specific Fumarate Reductase. *J Biol Inorg Chem* **2008**, *13* (5), 723–735. https://doi.org/10.1007/s00775-008-0358-7.

(15) Scalese, G.; Machado, I.; Correia, I.; Pessoa, J. C.; Bilbao, L.; Pérez-Diaz, L.; Gambino, D. Exploring Oxidovanadium(Iv) Homoleptic Complexes with 8-Hydroxyquinoline Derivatives as Prospective Antitrypanosomal Agents. *New J. Chem.* **2019**, *43* (45), 17756–17773. https://doi.org/10.1039/C9NJ02589H.

(16) Scalese, G.; Machado, I.; Salinas, G.; Pérez-Diaz, L.; Gambino, D. Heteroleptic Oxidovanadium(V) Complexes Active against in-Fective and Non-Infective Stages of Trypanosoma Cruzi. *Submitted to Molecules 2021*.

(17) Marcellino, C.; Gut, J.; Lim, K. C.; Singh, R.; McKerrow, J.; Sakanari, J. WormAssay: A Novel Computer Application for Whole-Plate Motion-Based Screening of Macroscopic Parasites. *PLoS Negl Trop Dis* **2012**, *6* (1), e1494. https://doi.org/10.1371/journal.pntd.0001494.

(18) Bulman, C. A.; Bidlow, C. M.; Lustigman, S.; Cho-Ngwa, F.; Williams, D.; Rascón, Jr, A. A.; Tricoche, N.; Samje, M.; Bell, A.; Suzuki, B.; Lim, K. C.; Supakorndej, N.; Supakorndej, P.; Wolfe, A. R.; Knudsen, G. M.; Chen, S.; Wilson, C.; Ang, K.-H.; Arkin, M.; Gut, J.; Franklin, C.; Marcellino, C.; McKerrow, J. H.; Debnath, A.; Sakanari, J. A. Repurposing Auranofin as a Lead Candidate for Treatment of Lymphatic Filariasis and Onchocerciasis. *PLoS Negl Trop Dis* **2015**, *9* (2), e0003534. https://doi.org/10.1371/journal.pntd.0003534.

(19) Tyagi, R.; Elfawal, M. A.; Wildman, S. A.; Helander, J.; Bulman, C. A.; Sakanari, J.; Rosa, B. A.; Brindley, P. J.; Janetka, J. W.; Aroian, R. V.; Mitreva, M. Identification of Small Molecule Enzyme Inhibitors as Broad-Spectrum Anthelmintics. *Sci Rep* **2019**, *9* (1), 9085. https://doi.org/10.1038/s41598-019-45548-7.

(20) Brenner, S. THE GENETICS OF CAENORHABDITIS ELEGANS. *Genetics* **1974**, *77* (1), 71–94. https://doi.org/10.1093/genetics/77.1.71.

(21) Simonetta, S. H.; Golombek, D. A. An Automated Tracking System for Caenorhabditis Elegans Locomotor Behavior and Circadian Studies Application. *Journal of Neuroscience Methods* **2007**, *161* (2), 273–280. https://doi.org/10.1016/j.jneumeth.2006.11.015.

(22) Risi, G.; Aguilera, E.; Ladós, E.; Suárez, G.; Carrera, I.; Álvarez, G.; Salinas, G. Caenorhabditis Elegans Infrared-Based Motility Assay Identified New Hits for Nematicide Drug Development. *Veterinary Sciences* **2019**, *6* (1), 29. https://doi.org/10.3390/vetsci6010029.

(23) Clark, R. C.; Reid, J. S. The Analytical Calculation of Absorption in Multifaceted Crystals. *Acta Crystallogr A Found Crystallogr* **1995**, *51* (6), 887–897. https://doi.org/10.1107/S0108767395007367.

(24) CrysAlisPro(Version 1.171.41.1221), Rigaku Oxford Diffraction Ltd, Yarnton, Oxfordshire, England. **2019**.

(25) Dolomanov, O. V.; Bourhis, L. J.; Gildea, R. J.; Howard, J. A. K.; Puschmann, H. *OLEX2* : A Complete Structure Solution, Refinement and Analysis Program. *J Appl Crystallogr* **2009**, *42* (2), 339–341. https://doi.org/10.1107/S0021889808042726.

(26) Sheldrick, G. M. *SHELXT* – Integrated Space-Group and Crystal-Structure Determination. *Acta Crystallogr A Found Adv* **2015**, *71* (1), 3–8. https://doi.org/10.1107/S2053273314026370.

(27) Sheldrick, G. M. Crystal Structure Refinement with *SHELXL*. *Acta Crystallogr C Struct Chem* **2015**, *71* (1), 3–8. https://doi.org/10.1107/S2053229614024218.

(28) Spek, A. L. Structure Validation in Chemical Crystallography. *Acta Crystallogr D Biol Crystallogr* **2009**, *65* (2), 148–155. https://doi.org/10.1107/S090744490804362X.

(29) Morris, G. M.; Huey, R.; Lindstrom, W.; Sanner, M. F.; Belew, R. K.; Goodsell, D. S.; Olson, A. J. AutoDock4 and AutoDockTools4: Automated Docking with Selective Receptor Flexibility. *J Comput Chem* **2009**, *30* (16), 2785–2791. https://doi.org/10.1002/jcc.21256.

(30) Forli, S.; Huey, R.; Pique, M. E.; Sanner, M. F.; Goodsell, D. S.; Olson, A. J. Computational Protein–Ligand Docking and Virtual Drug Screening with the AutoDock Suite. *Nat Protoc* **2016**, *11* (5), 905–919. https://doi.org/10.1038/nprot.2016.051.

(31) Huey, R.; Morris, G. M.; Olson, A. J.; Goodsell, D. S. A Semiempirical Free Energy Force Field with Charge-based Desolvation. *J Comput Chem* **2007**, *28* (6), 1145–1152. https://doi.org/10.1002/jcc.20634.

(32) *Schrödinger Software Release 2023-3*: *Maestro, Schrödinger, LLC, New York, NY, 2023.*